
Article:
Aad, G. orcid.org/0000-0002-6665-4934, Aakvaag, E. orcid.org/0000-0001-7616-1554, Abbott, B. orcid.org/0000-0002-5888-2734 et al. (2934 more authors) (2025) Measurement of the associated production of a top-antitop-quark pair and a Higgs boson decaying into a bb pair in pp collisions at √s = 13 TeV using the ATLAS detector at the LHC. The European Physical Journal C, 85. 210. ISSN 1434-6044

https://doi.org/10.1140/epjc/s10052-025-13740-x

Eur. Phys. J. C (2025) 85:210
https://doi.org/10.1140/epjc/s10052-025-13740-x

THE EUROPEAN PHYSICAL JOURNAL C

Regular Article - Experimental Physics

Measurement of the associated production of a top-antitop-quark pair and a Higgs boson decaying into a $b\bar{b}$ pair in pp collisions at $\sqrt{s} = 13$ TeV using the ATLAS detector at the LHC

ATLAS Collaboration[*]

CERN,1211 Geneva 23, Switzerland

Received: 16 July 2024 / Accepted: 2 January 2025

Abstract This paper reports the measurement of Higgs boson production in association with a $t\bar{t}$ pair in the $H \to b\bar{b}$ decay channel. The analysis uses 140 fb^{-1} of 13 TeV proton–proton collision data collected with the ATLAS detector at the Large Hadron Collider. The final states with one or two electrons or muons are employed. An excess of events over the expected background is found with an observed (expected) significance of 4.6 (5.4) standard deviations. The $t\bar{t}H$ cross-section is $\sigma_{t\bar{t}H} = 411\,^{+101}_{-92}$ fb $= 411 \pm 54$(stat.) $^{+85}_{-75}$(syst.) fb for a Higgs boson mass of 125.09 GeV, consistent with the prediction of the Standard Model of 507^{+35}_{-50} fb. The cross-section is also measured differentially in bins of the Higgs boson transverse momentum within the simplified template cross-section framework.

Contents

1 Introduction

After the discovery of the Higgs boson [1–3] in 2012 by the ATLAS [4] and CMS [5] collaborations, attention has turned to detailed measurements of its properties and couplings as a means of testing the predictions of the Standard Model (SM) [6–8]. The Higgs boson coupling to the top quark, the heaviest particle in the SM, is of special interest as it could be very sensitive to effects of physics beyond the SM (BSM) [9]. It is indirectly constrained assuming no BSM contributions to loop-induced processes from measurements of gluon–gluon fusion Higgs boson production and decay into $\gamma\gamma$ [10,11]. The Higgs boson production in association with a pair of top quarks ($t\bar{t}H$), where the top quark couples to the Higgs boson at tree level, provides a possibility for a direct measurement of the top-quark's Yukawa coupling without assumptions about the potential presence of BSM physics [12–15]. It was observed by the ATLAS and CMS collaborations using several Higgs boson decay modes [16,17].

The decay into two b-quarks is predicted to have the largest branching fraction of about 58% [18] and has the advantage of allowing for the reconstruction of the Higgs boson four-momentum from the kinematics of its decay products. Furthermore, the $t\bar{t}H(b\bar{b})$ channel involves only fermionic Higgs boson couplings in the production and decay, leading to an enhanced sensitivity for probing them. However, this final state is affected by a large irreducible background arising from the $t\bar{t}$ production in associations with jets ($t\bar{t}$+jets), in particular when the jets originate from b- or c-quarks, which is challenging to predict theoretically.

The ATLAS Collaboration has measured the $t\bar{t}H(b\bar{b})$ production at $\sqrt{s} = 13$ TeV in the final state with at least one lepton using the full Run 2 dataset collected in proton–proton (pp) collisions at the Large Hadron Collider (LHC) [19] between 2015 and 2018, corresponding to an integrated luminosity of 139 fb^{-1} [20]. The measured signal strength, defined as the ratio of the measured cross-section to that predicted by the SM, was found to be $0.35^{+0.36}_{-0.34}$, and corresponds to an observed (expected) significance of 1.0 (2.7) standard deviations. The signal strength was also measured differen-

[*] e-mail: atlas.publications@cern.ch

Published online: 24 February 2025

tially in five intervals of the Higgs boson transverse momentum (p_{T}^{H}) in the simplified template cross-section framework (STXS) [18], probing potential p_{T}^{H}-dependent deviations from the SM expectation.

The CMS Collaboration also recently released a measurement of the $t\bar{t}H(b\bar{b})$ production using 138 fb^{-1} of data collected at $\sqrt{s} = 13$ TeV in 2016–2018 [21]. The analysis achieved an observed (expected) significance of 1.3 (4.1) standard deviation and measured a signal strength of 0.33 ± 0.26. Additionally, the $t\bar{t}H$ production rate was determined in intervals of p_{T}^{H}.

This paper presents a re-analysis of the full Run 2 dataset collected at $\sqrt{s} = 13$ TeV with the ATLAS detector in final states with one or two leptons, referred to in the following as single-lepton and dilepton channels, and supersedes the result of Ref. [20]. Compared with the previous result, this analysis has an increased acceptance by selecting events with less restrictive requirements on the number of jets identified as originating from b-hadrons (b-jets), resulting in an increased efficiency to select $t\bar{t}H$ signal. It utilises a revised treatment of the different flavour components of the $t\bar{t}$ + jets background, and in particular, of the $t\bar{t}$ production in association with b-jets, the main background and the dominant source of the systematic uncertainty in the previous $t\bar{t}H(b\bar{b})$ measurement. For the modelling of this background, a new sample of Monte Carlo (MC) simulated events with improved settings was produced, and a corresponding set of systematic uncertainties was developed [22,23]. This measurement also uses improved analysis techniques: an advanced b-jet identification and an improved event categorisation. In particular, unlike the previous result, where the event categorisation into the background-dominated and signal-rich categories was made based on the number of jets and the number of b-jets, this analysis uses a multiclass neural network to define regions enriched in different components of the main background, the $t\bar{t}$ + jets production processes, and the signal. A more powerful multivariate discriminant is also employed to separate the signal from background and to reconstruct p_{T}^{H}. These improvements lead to better overall sensitivity and allow for a measurement of the $t\bar{t}H(b\bar{b})$ production cross-section in six bins of p_{T}^{H}, 0–60 GeV, 60–120 GeV, 120–200 GeV, 200–300 GeV, 300–450 GeV, and ≥ 450 GeV, as obtained from the MC event record before the Higgs boson decays, in the STXS formalism.

2 ATLAS detector

The ATLAS experiment [24] at the LHC is a multipurpose particle detector with a forward–backward symmetric cylindrical geometry and a near 4π coverage in solid angle.[1] It consists of an inner tracking detector (ID) surrounded by a thin superconducting solenoid providing a 2 T axial magnetic field, electromagnetic and hadronic calorimeters, and a muon spectrometer. The inner tracking detector covers the pseudorapidity range $|\eta| < 2.5$. It consists of silicon pixel, silicon microstrip, and transition radiation tracking detectors. Lead/liquid-argon (LAr) sampling calorimeters provide electromagnetic (EM) energy measurements with high granularity within the region $|\eta| < 3.2$. A steel/scintillator-tile hadronic calorimeter covers the central pseudorapidity range ($|\eta| < 1.7$). The endcap and forward regions are instrumented with LAr calorimeters for EM and hadronic energy measurements up to $|\eta| = 4.9$. The muon spectrometer (MS) surrounds the calorimeters and is based on three large superconducting air-core toroidal magnets with eight coils each. The field integral of the toroids ranges between 2.0 and 6.0 Tm across most of the detector. The muon spectrometer includes a system of precision tracking chambers up to $|\eta| = 2.7$ and fast detectors for triggering up to $|\eta| = 2.4$. The luminosity is measured mainly by the LUCID-2 [25] detector, which is located close to the beampipe. A two-level trigger system is used to select events [26]. The first-level trigger is implemented in hardware and uses a subset of the detector information to accept events at a rate below 100 kHz. This is followed by a software-based trigger that reduces the accepted event rate to 1 kHz on average depending on the data-taking conditions. A software suite [27] is used in data simulation, in the reconstruction and analysis of real and simulated data, in detector operations, and in the trigger and data acquisition systems of the experiment.

3 Data and Monte Carlo simulation samples

This analysis was performed using the pp collision data collected by the ATLAS detector between 2015 and 2018 at $\sqrt{s} = 13$ TeV. After the application of data-quality requirements [28], the dataset corresponds to an integrated luminosity of 140 fb^{-1}. Samples of simulated events were produced to model the different signal and background processes. Additional samples were produced to estimate the modelling uncertainties for each process. The effects of the additional pp collisions in the same or a nearby bunch crossing (pile-up) were modelled by overlaying minimum bias events generated with Pythia8 [29] using the A3 set of tunable parameters [30] onto the simulated hard-scatter

[1] ATLAS uses a right-handed coordinate system with its origin at the nominal interaction point (IP) in the centre of the detector and the z-axis along the beam pipe. The x-axis points from the IP to the centre of the LHC ring, and the y-axis points upwards. Cylindrical coordinates (r, ϕ) are used in the transverse plane, ϕ being the azimuthal angle around the z-axis. The pseudorapidity is defined in terms of the polar angle θ as $\eta = -\ln\tan(\theta/2)$. Angular distance is measured in units of $\Delta R \equiv \sqrt{(\Delta\eta)^2 + (\Delta\phi)^2}$.

event. The MC events were weighted to reproduce the distribution of the average number of interactions per bunch crossing observed in the data. The MC samples were processed using the full ATLAS detector simulation [31] based on GEANT4 [32]. Some alternative samples used to evaluate the modelling uncertainties were produced using fast simulation, where the full GEANT4 simulation of the calorimeter response is replaced by a detailed parameterisation of the shower shapes. For the observables used in this analysis, both simulations were found to give similar modelling. All MC samples were reconstructed using the same software as for collider data. Corrections were applied to the simulated events so that the selection efficiencies, energy scales and energy resolutions of the physics objects closely match those determined from data control samples.

All samples generated with POWHEGBOX [33–36] and MADGRAPH5_AMC@NLO [37] were interfaced to PYTHIA8 [38] to simulate the parton shower (PS), fragmentation, and underlying event with the A14 tune [39] and the NNPDF2.3LO [40] parton distribution function (PDF) set. Some alternative samples use the HERWIG7 [41,42] PS model with the H7UE set of tuned parameters [42] and the MMHT2014LO PDF set [43]. Samples using PYTHIA8 and HERWIG7 have heavy-flavour hadron decays modelled by EvtGen [44]. The masses of the top quark, m_{top}, and of the Higgs boson, m_{H}, are set to 172.5 GeV and 125 GeV, respectively.

The nominal $t\bar{t}H$ signal sample was generated at next-to-leading order (NLO) in the five flavour scheme (5FS) using the POWHEGBOX [45] generator with the NNPDF3.0NLO [40] PDF set. The h_{damp} parameter[2] was set to $3/4 \cdot (m_t + m_{\bar{t}} + m_H) = 352.5$ GeV, and the functional form of the renormalisation and factorisation scales was set to $\sqrt[3]{m_{\text{T}}(t) \cdot m_{\text{T}}(\bar{t}) \cdot m_{\text{T}}(H)}$, where $m_{\text{T}} = \sqrt{m^2 + p_{\text{T}}^2}$ is the transverse mass of a generated particle, m is its mass, and p_{T} is its transverse momentum. It is normalised to the theoretical prediction of Ref. [18] computed at NLO in QCD.[3]

An alternative $t\bar{t}H$ sample generated with the same POWHEGBOX set-up, but interfaced to HERWIG7 is used to evaluate uncertainties due to the choice of parton shower, hadronisation and underlying event model. The uncertainty related to the matching between the matrix element (ME) generator and the PS is accessed by changing the definition of the hardness of the POWHEG emission calculated by PYTHIA8 via the parameter $p_{\text{T}}^{\text{hard}}$ from the value provided by POWHEG to the p_{T} of the POWHEG emission following Refs. [47,48].

Several MC samples with different accuracy in ME generator and with different PS models are used in this analysis to model the main $t\bar{t}$ + jets background. This background is categorised according to the flavour of the additional jets in the event, excluding jets from top-quark or W boson decays, using the same procedure as described in Ref. [49]. Generator-level particle jets are reconstructed from stable particles (mean lifetime $\tau > 3 \times 10^{-11}$ s, excluding muons and neutrinos) using the anti-k_t algorithm [50] with a radius parameter $R = 0.4$, and are required to have transverse momentum $p_{\text{T}} > 15$ GeV and $|\eta| < 2.5$. The flavour of a jet is determined by counting b- or c-hadrons within $\Delta R < 0.4$ of the jet axis. Jets matched to exactly one b-hadron, with p_{T} above 5 GeV, are labelled single-b-jets, while those matched to two or more b-hadrons are labelled B-jets (with no p_{T} requirement on the second b-hadron); single-c- and C-jets are defined analogously, only considering jets not already defined as single-b- or B-jets. Events that have a single-b- or B-jet, are labelled as $t\bar{t}+1b$ and $t\bar{t}+1B$ respectively, events with two or more b-jets are labelled as $t\bar{t}+\geq 2b$. These three categories together are collectively referred to as $t\bar{t}+\geq 1b$. Events with no single-b- or B-jet but at least one single-c- or C-jet are labelled as $t\bar{t}+\geq 1c$. Finally, events not containing any heavy-flavour jets aside from those from top-quark or W boson decays are labelled as $t\bar{t}$ + light.

The $t\bar{t}$ + light and $t\bar{t}+\geq 1c$ contributions are modelled by a MC sample produced with the HVQ programme [34] in the POWHEGBOX generator at NLO in QCD in the five flavour scheme (5FS) with the NNPDF3.0NLO PDF set. The h_{damp} parameter was set to 1.5 m_{top} [39,51]. An additional sample was generated with the h_{damp} parameter increased by a factor of two to evaluate the uncertainty in the modelling of $t\bar{t}$ + light and $t\bar{t}+\geq 1c$ stemming from the choice of the h_{damp} value.

To predict the $t\bar{t}+\geq 1b$ background with the highest available precision, the $t\bar{t}b\bar{b}$ MC sample is generated at NLO, where the additional b-quarks are included in the ME. The four flavour scheme (4FS) was used for this sample. It was produced with the POWHEGBOXRES [52] generator and OPENLOOPS [53–55], using the implementation of this process in POWHEGBOXRES [56], with the NNPDF3.1NNLONF4 [69] PDF set interfaced to PYTHIA8. Based on the studies of Ref. [22], the factorisation scale is set to $\frac{1}{2}\sum_{i=t,\bar{t},b,\bar{b},j} m_{\text{T},i}$, the renormalisation scale is set to $\frac{1}{2} \cdot \sqrt[4]{m_{\text{T}}(t) \cdot m_{\text{T}}(\bar{t}) \cdot m_{\text{T}}(b) \cdot m_{\text{T}}(\bar{b})}$, and the h_{damp} parameter is set to $H_{\text{T}}/2$. The POWHEG internal parameter h_{bzd} that regulates the damping function together with the parameter h_{damp}, was set to 5. The choice of model used for the recoil in the initial state parton shower was found to impact significantly the $t\bar{t}+\geq 1b$ background predictions [23]. The corresponding uncertainty is evaluated by changing the PYTHIA8 parameter from a global recoil to a dipole recoil while keep-

[2] The h_{damp} parameter controls the transverse momentum p_{T} of the first additional emission beyond the leading-order Feynman diagram in the PS and therefore regulates the high-p_{T} emission against which the $t\bar{t}$ system recoils.

[3] A new theoretical computation of the $t\bar{t}H$ production at next-to-next-to-leading order in QCD was published recently in Ref. [46].

ing the rest of the settings identical to the nominal $t\bar{t}b\bar{b}$ sample.

Similar to the $t\bar{t}H$ signal sample, alternative samples were generated to assess the PS and matching uncertainties in the modelling of $t\bar{t}+$light, $t\bar{t}+\geq 1c$ and $t\bar{t}+\geq 1b$ by replacing in the corresponding nominal set-ups the PYTHIA8 shower model by HERWIG and producing samples with a varied $p_{\mathrm{T}}^{\mathrm{hard}}$ parameter.

For an independent pseudo-data test, additional samples of $t\bar{t}$ events were produced to model $t\bar{t}+$light and $t\bar{t}+\geq 1c$ events with the SHERPA [57] generator. The NLO-accurate matrix elements for up to one additional parton, and LO-accurate matrix elements for up to four additional partons were calculated with the COMIX [58] and OPENLOOPS libraries. They were matched with the SHERPA PS [59] with the default set of tuned parameters using the MEPS@NLO prescription [60–63] with a matching scale of 30 GeV. Furthermore, $t\bar{t}+\geq 1b$ events were simulated using SHERPA and OPENLOOPSwith $t\bar{t}b\bar{b}$ ME calculated at NLO accuracy using COMIX in the 4FS using the same functional form of the factorisation and renormalisation scales as in the nominal $t\bar{t}b\bar{b}$ set-up.

Single-top-quark production processes, i.e. tW associated production, t-channel and s-channel production, were modelled using the POWHEGBOX [64–66] generator at NLO in QCD. The t-channel process was generated in the 4FS with the NNPDF3.0NLONF4 PDF set, while for tW and s-channel processes the 5FS NNPDF3.0NLO PDF was used. The tW MC sample was generated using the factorisation and renormalisation scales set to $H_{\mathrm{T}}/2$ with H_{T} defined as a sum of the transverse mass of the W boson, the top quark and the transverse momentum of an additional parton. The overlap between tW and $t\bar{t}$ production [66] was removed using the diagram-removal scheme [67]. An alternative tW MC sample implementing the diagram subtraction scheme [66] was produced to evaluate the systematic uncertainty due to the tW and $t\bar{t}$ interference treatment.

The events in the nominal $t\bar{t}W$ sample were simulated using the SHERPA [68] generator with the NNPDF3.0NNLO PDF set. The ME was calculated for up to one additional parton at NLO and up to two partons at LO using COMIX and OPENLOOPS, and merged with the SHERPA PS using the MEPS@NLO prescription with a merging scale of 30 GeV. The alternative sample was generated with MADGRAPH5_AMC@NLO with up to one additional parton in the final state at NLO accuracy in the strong coupling, using the NNPDF3.1NNLO [69] PDF set. The different jet multiplicities were merged using the FxFx NLO ME and PS merging prescription [70] with a merging scale of 30 GeV. Background events from $t\bar{t}Z/\gamma^*$ and the rare processes $tZq, tWZ, tHjb$, tWH and $t\bar{t}t\bar{t}$ were simulated at NLO in QCD using the MADGRAPH5_AMC@NLO generator. The alternative sample used to evaluate the PS uncertainty in the $t\bar{t}Z$ background was generated with the same set-up as the nominal but interfaced to HERWIG7.

The production of $V+$jets events (where $V = W$ or Z) was simulated with the SHERPA generator using NLO-accurate matrix elements for up to two partons and LO-accurate matrix elements for up to four partons. Samples of diboson final states (VV) were also simulated with the SHERPA generator.

All MC samples corresponding to small backgrounds were normalised to the most precise available theoretical predictions closely following Ref. [20]. The normalisation of the $t\bar{t}W$ background was updated to the most recent prediction of Ref. [71]. The $t\bar{t}+$ light and $t\bar{t}+\geq 1c$ components were normalised to the $t\bar{t}$ cross-section computed at next-to-next-to-leading order (NNLO) in QCD including the resummation of next-to-next-to-leading-logarithmic (NNLL) soft-gluon terms [72] while the $t\bar{t}+\geq 1b$ normalisation is taken from the $t\bar{t}b\bar{b}$ MC simulation.

4 Objects and event selection

Events are selected using single-lepton triggers with variable electron and muon transverse momentum thresholds, and various identification and isolation criteria depending on the lepton flavour and the data-taking period [73,74]. The lowest p_{T} threshold at trigger level used for muons is 20 GeV (26 GeV), while for electrons the threshold is 24 GeV (26 GeV) in 2015 (2016–2018). Events are required to have at least one vertex with at least two associated ID tracks with $p_{\mathrm{T}} > 0.5$ GeV. In each event, the primary vertex is defined as the reconstructed vertex having the highest scalar sum of squared p_{T} of associated tracks [75] among the vertices consistent with the average beam-spot position.

Electron candidates are reconstructed from energy deposits in the electromagnetic calorimeter matched to tracks reconstructed in the ID system and are required to satisfy the *MediumLH* identification criterion [76]. They are required to have $p_{\mathrm{T}} > 10$ GeV and $|\eta| < 2.47$, excluding the calorimeter barrel-endcap transition region ($1.37 < |\eta| < 1.52$). Muon candidates are reconstructed from tracks in the MS that are associated with tracks from the ID and are required to satisfy the *Loose* identification criterion [77] and to have $p_{\mathrm{T}} > 10$ GeV, $|\eta| < 2.5$. Electron (muon) candidates must be associated with the primary vertex of the event: the transverse impact parameter divided by its estimated uncertainty, $|d_0|/\sigma(d_0)$, is required to be less than five (three) for electron (muon) candidates. The longitudinal impact parameter must satisfy $|z_0 \sin(\theta)| < 0.5$ mm for both lepton flavours.

Jets are reconstructed from particle flow objects [78] using the anti-k_t jet clustering algorithm in the FASTJET implementation [79] with a radius parameter $R = 0.4$. Jets are required to satisfy the *Tight* criterion of the *jet vertex tagger* (JVT)

algorithm [80] to mitigate the contribution from pile-up jets, and to have $p_{\mathrm{T}} > 25$ GeV and $|\eta| < 2.5$. The jet energy scale (JES) and resolution are calibrated using simulations with in situ corrections obtained from data [81]. Events containing jets originating from non-collision sources or detector noise are removed.

Jets containing b-hadrons, referred to as b-jets, are identified using the DL1r b-tagging algorithm [82] that uses a neural network based on the distinctive features of b-hadron decays, primarily the impact parameters of tracks and the displaced vertices reconstructed in the ID. Additional input to this network is provided by discriminating variables constructed by a recurrent neural network that exploits the spatial and kinematic correlations between tracks originating from the same b-hadron. A multivariate b-tagging discriminant value is calculated for each jet. The b-tagged jets are required to satisfy the working point (WP) corresponding to an efficiency of 70% or 85% for identifying b-quark initiated jets in $t\bar{t}$ simulated events for the single-lepton and dilepton channels, respectively. For the 70% (85%) WP the rejection factors against light-quark/gluon jets and c-quark jets are 625 and 12 (40 and 3), respectively. To fully exploit the b-tagging information of an event, each jet is assigned a b-tagging score that defines if a jet satisfies a given WP but fails to satisfy the adjacent tighter one. In addition to the standard JES calibration, b-tagged jets satisfying the 85% WP receive additional flavour-specific corrections to their four-vectors to improve their energy measurement (scale and resolution) following the *muon-in-jet* procedure described in Ref. [83].

Hadronically decaying τ-leptons (τ_{had}) are distinguished from jets using their track multiplicity and a multivariate discriminant based on their shower shapes in calorimeter and on tracking information [84]. They are required to have $p_{\mathrm{T}} > 25$ GeV and $|\eta| < 2.5$, and to pass the *Medium* τ-lepton identification working point.

The missing transverse momentum vector, with magnitude $E_{\mathrm{T}}^{\mathrm{miss}}$, is defined as the negative sum of the transverse momenta of the reconstructed and calibrated physical objects, plus a 'soft term' built from all other tracks associated with the primary vertex [85] and not matched to a reconstructed object.

Targeting event topologies with a Higgs boson decaying into collimated hadronic final states, reclustered (RC) jets [86] are reconstructed from the selected jets, using the anti-k_t jet clustering algorithm with a radius parameter $R = 1.0$. RC jets are required to have an invariant mass $M > 50$ GeV, $p_{\mathrm{T}} > 200$ GeV, $|\eta| < 2.0$, have at least two constituent small-R jets (subjets) and have an angular distance $\Delta R > 1.0$ from all electrons.

An overlap removal procedure is applied to avoid the double counting of detector signatures. Electron candidates sharing a track with a muon candidate are first removed. Jets found within a $\Delta R = 0.2$ cone of an electron are removed and electrons within a $\Delta R = 0.4$ cone of a remaining jet are rejected. Jets with less than three associated tracks and within $\Delta R = 0.2$ of a muon and muons within $\Delta R = 0.4$ of a jet with more than two associated tracks are rejected. A τ_{had} candidate is rejected if it is separated by $\Delta R < 0.2$ from any selected electron or muon. No overlap removal is performed between jets and τ_{had} candidates.

Events are selected if they contain exactly one lepton candidate in the single-lepton channel and exactly two lepton candidates with opposite electric charges in the dilepton channel. At least one lepton should have $p_{\mathrm{T}} > 27$ GeV and be matched to the corresponding object at the trigger level. In the events with two electrons, the second lepton is required to have $p_{\mathrm{T}} > 15$ GeV while in the other two dilepton channels, $e\mu$ and $\mu\mu$, it must have $p_{\mathrm{T}} > 10$ GeV. In events with two electrons or two muons, the dilepton invariant mass is required to be above 15 GeV, to suppress contribution from the decays of heavy-flavour resonances and low-mass Drell–Yan processes, and be outside a window of $\pm$ 8 GeV centred at the Z boson mass. To maintain orthogonality with other $t\bar{t}H$ decay channels, events are vetoed if they contain one or more (two or more) τ_{had} candidates in the dilepton (single-lepton) channel.

To reduce the non-prompt and mis-identified lepton background contribution, additional lepton identification and isolation requirements are applied. Electrons (muons) are required to satisfy the *TightLH* (*Medium*) identification criteria and the tight isolation criteria based on the calorimeter and tracking information for electrons [76] and on tracking information only for muons [77]. Events for which the leptons fail to meet these requirements are removed.

In the single-lepton channel two event categories are defined, referred in the following as resolved and boosted categories. The latter is designed to select events in which the Higgs boson is produced with high transverse momentum as a collimated large-R jet. Events that do not satisfy the boosted category selection are assigned to the resolved one. In the single-lepton resolved channel, events are selected if they contain at least five jets, at least three of which satisfy the 70% b-tagging WP. In the single-lepton boosted channel, events are required to have at least one large-R jet and at least four small-R jets, including those contained within the large-R jet, at least three of which must satisfy the 85% b-tagging WP. In the dilepton channel, events are selected if they contain at least three jets satisfying the 85% b-tagging WP, and among these at least two jets that satisfy the 70% b-tagging WP. These requirements are henceforth referred to as "preselection" and have an acceptance of 6.3% for selecting $t\bar{t}H$ events with $H \to b\bar{b}$ decay, an acceptance that is more than a factor of three larger than in the previous analysis [20]. The corresponding acceptance in the signal regions is 2.1%.

5 Background modelling

The largest background from $t\bar{t}$+jets production is modelled by MC simulation with the data-driven corrections described in Sect. 5.1. Small backgrounds include single top production, $t\bar{t}W$, $t\bar{t}Z$, $t\bar{t}t\bar{t}$, rare top-quark processes and non-top-quark processes such as V+jets and diboson production. All of them are estimated from simulations. The contribution from the background arising from non-prompt or mis-identified leptons is determined from data in the single-lepton channel (see Sect. 5.2), and from MC simulation in the dilepton channel, where this background arises primarily from $t\bar{t}$ events with one prompt lepton and is very small.

5.1 Modelling of $t\bar{t}$ + jets background

The $t\bar{t}$ sample used to model the $t\bar{t}$ + light and $t\bar{t} + \geq 1c$ contributions is generated at NLO as described in Sect. 3, with up to one additional parton from the ME calculation. All jets not originating from the decay chain of one of the top quarks, i.e. additional jets, are produced by the parton shower. The dedicated measurement [87] demonstrated deficiencies in modelling the number of additional jets in the $t\bar{t}$ events and the scalar sum of the transverse momenta of the top quarks. Moreover, the rate of $t\bar{t}$ production in association with c- and b-jets was observed to be underestimated in the previous analysis [20]. The new $t\bar{t}b\bar{b}$ MC sample produced for this analysis with lower value of the renormalisation scale than the one used in Ref. [20] predicts larger inclusive $t\bar{t} + \geq 1b$ cross-section, which is expected to match data well. Nevertheless, the rate of the components of the $t\bar{t} + \geq 1b$ background defined in Sect. 3, $t\bar{t} + 1B$, $t\bar{t} + 1b$ and $t\bar{t} + \geq 2b$, could still be mismodelled. Thus, to obtain a reliable estimate of the $t\bar{t}$ + jets background, the $t\bar{t}$ MC events are reweighted using data. The corrections applied include a rescaling of the $t\bar{t}$ + jets flavour components followed by a kinematic reweighting and are described in the next paragraph. Any possible residual mismodelling is accounted for by the systematic uncertainties in the profile-likelihood fit used for the extraction of the signal strength which is described in Sect. 6.

Initial scaling factors for the five $t\bar{t}$ + jets flavour components, $t\bar{t}$ + light, $t\bar{t} + \geq 1c$, $t\bar{t} + 1B$, $t\bar{t} + 1b$ and $t\bar{t} + \geq 2b$, are obtained separately for the single-lepton and dilepton channels from the profile-likelihood fit to data. The fit is performed in background-dominated control regions including all systematic uncertainties (see Sect. 7) prior to the signal extraction fit described in Sect. 6. These scaling factors have similar values to those shown in Table 5. Following the flavour components rescaling, a reweighting is used to mitigate the kinematic mismodelling of the scalar sum of the p_{T}'s of the reconstructed leptons and jets, H_{T}, observed for the $t\bar{t}$ + light and $t\bar{t} + \geq 1c$ components of the inclusive $t\bar{t}$ + jets POWHEG + PYTHIA8 sample. The $t\bar{t} + \geq 1b$ component is excluded from the reweighting since it is simulated by a dedicated $t\bar{t}b\bar{b}$ MC sample. Thus the reweighting derived in the regions dominated by $t\bar{t}$ + light and $t\bar{t} + \geq 1c$ might not be applicable to $t\bar{t} + \geq 1b$. A dedicated reweighting was investigated for the $t\bar{t} + \geq 1b$ component but found to have a negligible effect and is not used in the analysis.

The reweighting corrects the distributions of H_{T} in exclusive jet multiplicity bins from $N_{\mathrm{jets}} = 5$ to $N_{\mathrm{jets}} \geq 8$ in the single-lepton channel and from $N_{\mathrm{jets}} = 3$ to $N_{\mathrm{jets}} \geq 6$ in the dilepton channel. It is derived in $t\bar{t}$ enriched regions selected by using looser b-tagging requirements after subtracting from data all contributions except for $t\bar{t}$ + light and $t\bar{t} + \geq 1c$ and taking the ratio of data to the sum of $t\bar{t}$ + light and $t\bar{t} + \geq 1c$ yields predicted by MC in each H_{T} bin. These regions are orthogonal to the signal and control regions of the analysis and contain less that 0.2% of signal.

The reweighting factors are also derived in the same way for each systematic variation affecting the $t\bar{t}$ + light and $t\bar{t} + \geq 1c$ predictions, such that all systematic variations match the H_{T} distribution in data.

5.2 Non-prompt or mis-identified lepton background

A data-driven method, referred to as "fake factor" method [88], based on the measurement of lepton selection efficiencies using different identification and isolation criteria, is used to estimate the non-prompt or mis-identified (fake) lepton background in the single-lepton channel.

The fake rate is measured in a fake-dominated region selected by requiring exactly one lepton with loose identification and isolation criteria, at least two jets, at least two b-tagged jets satisfying the 70% WP, and a scalar sum of missing transverse energy and the leptonically-decaying W boson mass below 60 GeV. It is parameterised as a function of the leading jet p_{T} and the lepton $|\eta|$. The expected number of events arising from the fake lepton background is determined by applying the measured lepton fake rate to data events satisfying the selection requirements of each analysis region except that the lepton is required to pass loose identification and isolation criteria and to fail the tighter requirements.

6 Signal extraction

After the preselection, events are classified into non-overlapping background-dominated or control regions (CR) and signal-enriched regions (SR) with higher signal-to-background ratios. The CRs provide stringent constraints on the normalisation of the backgrounds and the systematic uncertainties in a combined fit with the signal regions.

To define the regions in the single-lepton and dilepton channels, a multiclass classification neural network based

on the permutation-invariant transformer architecture with attention mechanism [89] is trained to predict the probability of an event to be from the $t\bar{t}H$ signal or from one of the five $t\bar{t}$+jets background categories introduced in Sect. 3: $t\bar{t}+1b$, $t\bar{t}+1B$, $t\bar{t}+\geq 2b$, $t\bar{t}+\geq 1c$, $t\bar{t}+$light jets. The probability p_i of a network class i is converted into a discriminant d_i in order to maximise the separation between the class and all the other classes ($i \neq j$), to yield a similar number of events in the $t\bar{t}+1b$, $t\bar{t}+1B$, and inclusive $t\bar{t}+\geq 2b$ control regions, and to maximise sensitivity. They are defined as

$$d_i = \frac{p_i}{\sum_{j\neq i} p_j \cdot \hat{N}_{ij}}. \quad (1)$$

Here, the denominator of each discriminant is a weighted average of all the remaining class probabilities $p_{j\neq i}$. The weights $\hat{N}_{ij} = N_j/\sum_{k\neq i} N_k$ are the respective fractions of event yields N_j relative to the total yield of all the remaining classes $k \neq i$. These yields are determined from MC simulation after the preselection and incorporate the $t\bar{t}+$ jets scaling factors described in Sect. 5.1.

In the single-lepton (dilepton) channel, events fulfilling $d_{t\bar{t}H} > 4.072$ ($d_{t\bar{t}H} > 9.031$) are assigned to the signal region. The thresholds are defined to maximize the ratio of signal to the square root of the background in the inclusive signal regions. All other events are assigned to the $t\bar{t}+$ jets background category with the highest value of the discriminant. By far the dominant Higgs boson decay mode in the signal region is $H \to b\bar{b}$ with a fraction of more than 97% (94%) of the $t\bar{t}H$ events in the single-lepton (dilepton) channel followed by the $H \to WW$ decay. This motivates the training of a second neural network, based on the same architecture, to identify the two jets most likely originating from the Higgs boson decay, to reconstruct p_{T}^H that is used to further classify the signal region events into the six reconstructed STXS regions. The performance of this reconstruction network to correctly identify both Higgs boson decay products decreases with increasing jet multiplicity and generally increases with increasing true p_{T}^H. Both Higgs boson decay products are correctly identified for 51% (58%) of $t\bar{t}H(b\bar{b})$ events in the single-lepton resolved (dilepton) channel. The boundaries of the regions are optimised to maximise fraction of the events with the corresponding truth p_{T}^H, listed in Fig. 1, separately per $t\bar{t}$ decay channel to capture potential differences due to the final states and separate neural networks. This optimisation leads, in particular, to improved purity in the highest truth p_{T}^H bins, the region of the phase space where this analysis provides a particularly valuable contribution to the global Higgs boson combination. The optimal reconstructed p_{T}^H boundaries are found to be [0, 60, 114, 186, 270, 402, ∞] GeV in the dilepton channel and [0, 60, 114, 192, 282, 408, ∞] GeV in the single-lepton resolved channel. They are referred to in the following as STXS 1–6 regions.

The inclusive control region dominated by the $t\bar{t}+\geq 2b$ background in the single-lepton channel is further split into three categories encompassing STXS regions 1–2, 3–4, and 5–6, to ensure a good control of the $t\bar{t}+\geq 2b$ background modelling over the bins of reconstructed Higgs boson p_{T}. These regions are henceforth referred to as $t\bar{t}+\geq 2b$ CR 1, CR 2, and CR 3. The split is not applied in the dilepton channel due to limited statistics.

Events fulfilling the boosted selection criteria are assigned to dedicated boosted signal and control regions. RC jets are used as input to a multiclass deep neural network (DNN), trained to distinguish high-p_{T} Higgs boson candidates decaying into collimated final states from top quarks and multijet backgrounds following the same strategy as in the previous analysis [20]. An event is flagged as containing a boosted Higgs boson candidate if one of the RC jets has a high probability of originating from a Higgs boson, as estimated by the DNN. Boosted Higgs boson candidates are required to have $p_{\mathrm{T}} \geq 300$ GeV, a mass consistent with the Higgs boson mass window of 100–140 GeV, contain at least two subjets, of which exactly two are required to satisfy the b-tagging 85% WP, and have a DNN score above 0.4. At least two small-R jets that do not form the Higgs boson candidate are required to satisfy the b-tagging 77% WP. The flowchart in Fig. 1 summarises the event classification strategy.

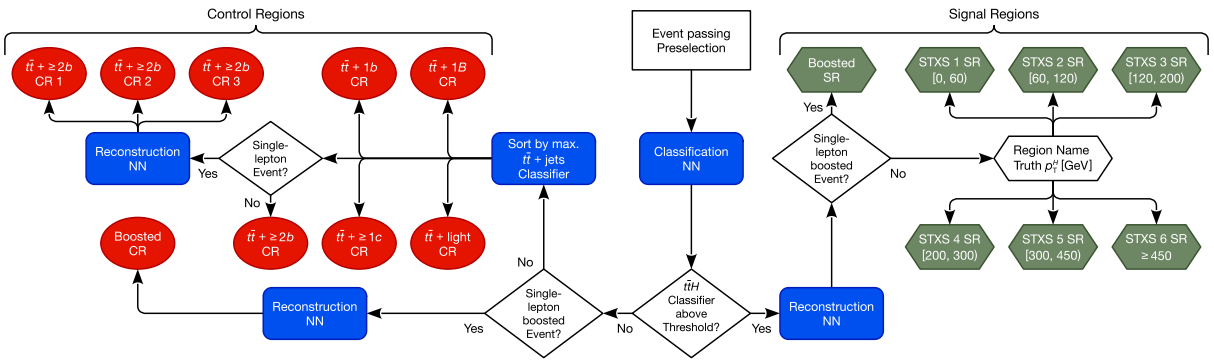

Fig. 1 Flowchart depicting the event classification and Higgs boson p_{T} reconstruction strategy used in the analysis

The transformer networks are trained using low-level features of the reconstructed jets, electrons, muons, and the missing transverse momentum of the event. For each reconstructed object, the kinematic features used are the x-, y- and z-component of the momentum (p_x, p_y, p_z), the energy, the p_{T}, the mass, the pseudorapidity, the azimuthal angle and its sine and cosine. Supplying redundant four-vector information is observed to improve network performance. Additionally, the DL1r pseudo-continuous b-tagging score is included for jets, and the electric charge and a variable indicating if it is an electron or a muon is included for leptons.

The multiclass event-classification network is trained using events sampled from the nominal and alternative $t\bar{t}H$ and $t\bar{t}+$jets background samples to profit from an increased number of events in training. The classification network yields an area under the receiver-operator characteristic curve (AUC) of 0.753 (0.774) for discriminating between $t\bar{t}H$ and the $t\bar{t}+\geq 1b$ background for events satisfying the preselection in the single-lepton resolved (dilepton) channel. The Higgs boson p_{T} reconstruction network is trained using only the $t\bar{t}H$ samples. Figure 2 shows for each bin of truth p_{T}^{H} the fraction of $t\bar{t}H$ events assigned to each of the STXS signal regions.

In the single-lepton channel, a total of 15 analysis regions are defined, including six STXS signal regions, two boosted regions (signal and control) and seven control regions targeting the different components of the $t\bar{t}+$jets background. In the dilepton channel, a total of 11 analysis regions are defined, including the six STXS signal regions and five $t\bar{t}+$jets control regions. The expected yields in the single-lepton (dilepton) signal and control regions are summarised in Tables 1 and 2 (3 and 4) after applying the data-driven corrections to the $t\bar{t}+$jets background discussed in Sect. 5.1.

The $t\bar{t}H$ inclusive signal strength, $\mu_{t\bar{t}H}$, defined as the ratio of the measured $t\bar{t}H$ cross-section including all Higgs boson decay modes to the corresponding SM prediction, or the signal strengths in each of the six STXS bins, μ_i, and the normalisation factors of the components of the $t\bar{t}+$jets background are determined via a binned likelihood fit to the distributions in all signal and control regions defined above. The $t\bar{t}H$ signal sample is split up according to the true p_{T}^{H} in each event, and the μ_i act on the respective component. In the resolved signal and control regions, the corresponding discriminant distribution is used in the likelihood fit, while in the boosted regions, event yields in two bins of the reconstructed p_{T}^{H} distribution, 300–450 GeV and ≥ 450 GeV, are used in the fit.

The $t\bar{t}+1b$, $t\bar{t}+\geq 1c$ and $t\bar{t}+$light normalisation factors are chosen to float independently in the single-lepton and dilepton channels, while the normalisations of the $t\bar{t}+\geq 2b$ and $t\bar{t}+1B$ backgrounds are scaled in a correlated way between the two channels. This choice is made based on studies of the different correlation assumptions between the normalisation factors in the combined fit. The chosen configuration provides enough freedom for the fit model and minimises pulls and constraints of the nuisance parameters in the fit to data.

The inclusive measurement of the signal strength and cross-section is performed in the full phase space. The measurement of these parameters in STXS bins is carried out for $t\bar{t}H$ events with a Higgs boson produced centrally within $|y|\leq 2.5$ at truth level, while the remaining forward events are considered as background.

The statistical model is based on a likelihood function built with HistFactory [90] as the product over every bin of the Poisson probability for the observed data, given the SM prediction. The value of each nuisance parameter, describing the systematic uncertainties for both signal and background processes (see Sect. 7), is constrained by a Gaussian penalty term present in the likelihood function, while all normalisation factors are unconstrained. The statistical uncertainty arising from the limited number of simulated events is included in the likelihood in the form of additional nuisance parameters with Poisson constraint terms. The maximum-likelihood fit is performed with the RooFit package [91]. A test statistic based on the profile-likelihood ratio is used to assess the compatibility of the observed data with the background-only hypothesis ($\mu=0$) [92].

Tests of the statistical model fitted to pseudo-data constructed with the Sherpa $t\bar{t}+$jets samples were performed to help inform the choice of fit variables and uncertainty model, with the goal of minimising bias, maximising robustness and optimising sensitivity.

7 Systematic uncertainties

Multiple sources of systematic uncertainty, arising from detector effects, theoretical assumptions and the limited number of events in the MC simulations, are considered in the analysis. They affect the categorisation of events as well as the normalisation and shape of the distributions used in the signal extraction fit.

All the sources of experimental uncertainty, except the uncertainty in the integrated luminosity, affect both the normalisations and the shapes of the distributions in all simulated samples. The uncertainty in the integrated luminosity is 0.83% [93], obtained using the LUCID-2 detector [25] for the primary luminosity measurements, complemented by measurements using the inner detector and calorimeters. The uncertainty in the pile-up modelling is obtained by varying the pile-up reweighting in the simulation within its uncertainties.

The correction factors applied to the simulated samples to improve the description of the lepton reconstruction, identification and isolation efficiencies, momentum scale and res-

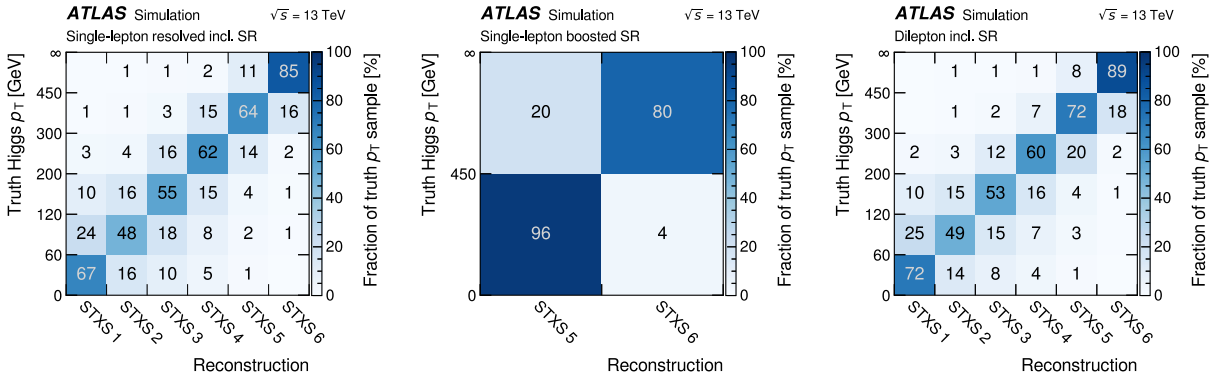

(a) (b) (c)

Fig. 2 STXS migration matrices for the $t\bar{t}H$ signal regions in (**a**) the single-lepton resolved, (**b**) the single-lepton boosted, and (**c**) the dilepton channel. The yield fractions of the predicted STXS bins are normalised per truth STXS sample

Table 1 Expected yields in the single-lepton signal regions before the fit to data. The data-driven corrections to the $t\bar{t}$ + jets background are applied and all uncertainties are included, except the ones associated with the $t\bar{t}$ + jets background normalisation factors, which are not defined pre-fit. The "Other" category includes the s- and t-channel single-top, tZq and tWZ processes. The $t\bar{t}H$ signal is normalised to the SM $t\bar{t}H$ cross-section. For presentation purposes, uncertainties are symmetrised

	STXS 1 SR	STXS 2 SR	STXS 3 SR	STXS 4 SR	STXS 5 SR	STXS 6 SR	Boosted SR
$t\bar{t}H$ truth p_T^H 0–60 GeV	77 ± 12	18.7 ± 3.2	11.1 ± 2.3	5.7 ± 1.0	1.66 ± 0.2	0.42 ± 0.09	0.58 ± 0.13
$t\bar{t}H$ truth p_T^H 60–120 GeV	49 ± 5	99 ± 13	37 ± 6	15.5 ± 2.2	4.4 ± 0.5	1.25 ± 0.19	1.54 ± 0.25
$t\bar{t}H$ truth p_T^H 120–200 GeV	22.7 ± 2.2	37 ± 4	125 ± 16	34 ± 5	8.1 ± 1.3	2.0 ± 0.4	2.31 ± 0.28
$t\bar{t}H$ truth p_T^H 200–300 GeV	4.0 ± 0.5	5.5 ± 0.7	22.5 ± 2.9	88 ± 12	19.4 ± 3.0	2.7 ± 0.4	3.3 ± 0.6
$t\bar{t}H$ truth p_T^H 300–450 GeV	0.39 ± 0.11	0.64 ± 0.16	1.4 ± 0.4	7.6 ± 1.3	32 ± 5	8.0 ± 1.3	20 ± 3
$t\bar{t}H$ truth p_T^H ≥450 GeV	<0.1	<0.1	0.14 ± 0.06	0.21 ± 0.09	1.30 ± 0.31	9.8 ± 1.8	6.9 ± 1.3
$t\bar{t}H$ $\|y\| > 2.5$	0.16 ± 0.06	0.10 ± 0.04	<0.1	<0.1	<0.1	<0.1	<0.1
$t\bar{t}+\geq 2b$	870 ± 80	870 ± 90	980 ± 100	640 ± 60	270 ± 40	92 ± 21	103 ± 8
$t\bar{t}+1b$	210 ± 60	210 ± 50	250 ± 80	180 ± 60	78 ± 28	25 ± 9	17 ± 5
$t\bar{t}+1B$	64 ± 19	73 ± 24	100 ± 40	87 ± 30	46 ± 19	22 ± 11	11 ± 4
$t\bar{t}+\geq 1c$	210 ± 50	210 ± 50	250 ± 50	190 ± 50	88 ± 24	27 ± 13	22 ± 8
$t\bar{t}+$light	42 ± 16	45 ± 12	68 ± 22	64 ± 19	31 ± 11	12 ± 11	3.2 ± 3
$t\bar{t}Z$	36 ± 6	38 ± 6	53 ± 8	43 ± 8	24 ± 5	7.2 ± 1.1	5.8 ± 1.2
tW	20 ± 8	35 ± 12	60 ± 33	55 ± 32	33 ± 25	17 ± 15	5 ± 4
W+jets	10 ± 6	12 ± 8	30 ± 15	29 ± 14	23 ± 12	12 ± 6	3.7 ± 1.9
$t\bar{t}W$	4.2 ± 0.5	5.9 ± 0.8	9.8 ± 1.6	8.9 ± 1.9	5.6 ± 0.7	3.2 ± 0.5	1.06 ± 0.26
Z+jets	2.5 ± 1.1	5.1 ± 2	6.5 ± 2.6	7.4 ± 2.7	3.1 ± 1.1	1.7 ± 0.6	0.5 ± 0.2
Diboson	1.3 ± 0.8	2.5 ± 1.40	4.4 ± 2.3	4.7 ± 2.7	3.1 ± 1.6	1.4 ± 0.7	0.7 ± 0.4
$t\bar{t}t\bar{t}$	5.1 ± 2.2	6.7 ± 3	11 ± 5	9 ± 4	4.8 ± 2.1	2.5 ± 1.1	1.1 ± 0.5
$tHjb$	0.77 ± 0.22	1.06 ± 0.21	1.61 ± 0.32	1.58 ± 0.28	1.11 ± 0.30	0.26 ± 0.12	0.72 ± 0.14
tWH	1.68 ± 0.23	2.16 ± 0.27	3.8 ± 0.4	4.1 ± 0.5	2.22 ± 0.25	1.03 ± 0.12	1.01 ± 0.11
Other	11.3 ± 1.2	11 ± 1.5	14.4 ± 2	11.9 ± 1.5	7.3 ± 1.1	2.43 ± 0.35	2.2 ± 0.6
Fakes	29 ± 12	29 ± 15	27 ± 12	31 ± 19	22 ± 13	3.8 ± 2.5	8 ± 5
Total	1670 ± 160	1710 ± 170	2060 ± 210	1520 ± 150	710 ± 80	250 ± 40	221 ± 19
Data	1672	1657	2016	1441	676	241	216

Table 2 Expected yields in the single-lepton control regions before the fit to data. The data-driven corrections to the $t\bar{t}+$ jets background are applied and all uncertainties are included, except the ones associated with the $t\bar{t}+$ jets background normalisation factors, which are not defined pre-fit. The "Other" category includes the s- and t-channel single-top, tZq and tWZ processes. The $t\bar{t}H$ signal is normalised to the SM $t\bar{t}H$ cross-section. For presentation purposes, uncertainties are symmetrised

	$t\bar{t}+$ light CR	$t\bar{t}+\geq 1c$ CR	$t\bar{t}+1b$ CR	$t\bar{t}+1B$ CR	$t\bar{t}+\geq 2b$ CR 1	$t\bar{t}+\geq 2b$ CR 2	$t\bar{t}+\geq 2b$ CR 3	Boosted CR
$t\bar{t}H$ truth p_{T}^{H} 0–60 GeV	56 ± 6	59 ± 7	89 ± 11	46 ± 6	80 ± 10	12.5 ± 1.7	2.09 ± 0.26	0.54 ± 0.14
$t\bar{t}H$ truth p_{T}^{H} 60–120 GeV	86 ± 5	98 ± 8	133 ± 12	92 ± 13	112 ± 11	33 ± 5	4.5 ± 0.9	1.15 ± 0.23
$t\bar{t}H$ truth p_{T}^{H} 120–200 GeV	59 ± 4	76 ± 7	76 ± 8	88 ± 11	41 ± 4	68 ± 8	5.4 ± 1.1	1.36 ± 0.28
$t\bar{t}H$ truth p_{T}^{H} 200–300 GeV	23 ± 2.5	31.9 ± 3.5	21.2 ± 3.1	41 ± 5	7.3 ± 1.1	34 ± 4	6.7 ± 1.1	1.42 ± 0.32
$t\bar{t}H$ truth p_{T}^{H} 300–450 GeV	7.7 ± 1.0	10 ± 1.5	4.7 ± 0.8	14.3 ± 2	1.12 ± 0.27	4.4 ± 0.8	9.8 ± 1.5	4.8 ± 0.7
$t\bar{t}H$ truth $p_{\mathrm{T}}^{H} \geq 450$ GeV	1.67 ± 0.27	2.4 ± 0.5	0.78 ± 0.19	4.1 ± 0.7	0.18 ± 0.05	0.35 ± 0.12	3 ± 0.7	1.75 ± 0.32
$t\bar{t}H$ $\lvert y\rvert > 2.5$	0.98 ± 0.08	0.72 ± 0.17	1.38 ± 0.22	0.57 ± 0.15	0.37 ± 0.05	0.188 ± 0.029	<0.1	<0.1
$t\bar{t}+\geq 2b$	2320 ± 280	3800 ± 400	5400 ± 600	3500 ± 400	7200 ± 600	4900 ± 500	1140 ± 170	141 ± 10
$t\bar{t}+1b$	3900 ± 400	4600 ± 700	10600 ± 1700	5100 ± 600	2100 ± 500	1120 ± 320	230 ± 100	54 ± 19
$t\bar{t}+1B$	890 ± 80	1390 ± 270	1780 ± 270	5100 ± 400	530 ± 190	380 ± 140	100 ± 50	32 ± 7
$t\bar{t}+\geq 1c$	17000 ± 3300	17900 ± 2600	7800 ± 1000	5400 ± 1300	2500 ± 500	1220 ± 270	240 ± 70	133 ± 35
$t\bar{t}+$ light	31800 ± 3500	5900 ± 1100	4000 ± 600	2000 ± 500	700 ± 180	320 ± 110	49 ± 26	34 ± 8
$t\bar{t}Z$	152 ± 20	171 ± 25	151 ± 21	146 ± 22	122 ± 18	117 ± 15	36 ± 5	5.7 ± 0.9
tW	1040 ± 200	750 ± 220	820 ± 240	560 ± 190	350 ± 140	360 ± 150	130 ± 90	10 ± 6
W+jets	370 ± 180	370 ± 180	230 ± 120	170 ± 80	370 ± 190	250 ± 130	90 ± 40	5.6 ± 2.9
$t\bar{t}W$	100 ± 12	114 ± 17	43 ± 7	44 ± 5	25.6 ± 3.5	26 ± 5	10.5 ± 1.6	1.97 ± 0.33
Z+jets	110 ± 40	110 ± 40	110 ± 40	64 ± 23	100 ± 40	55 ± 20	16 ± 6	0.9 ± 0.4
Diboson	37 ± 19	39 ± 20	23 ± 12	21 ± 11	24 ± 13	23 ± 12	10 ± 5	1.1 ± 0.7
$t\bar{t}t\bar{t}$	2.9 ± 1.2	24 ± 10	7.1 ± 3	19 ± 8	21 ± 9	33 ± 14	17 ± 7	1.4 ± 0.6
$tHjb$	8.2 ± 1.4	5.4 ± 0.9	8.1 ± 1.6	3.5 ± 0.6	5.4 ± 1.1	3.6 ± 0.7	0.53 ± 0.15	0.65 ± 0.20
tWH	7.1 ± 0.7	6.7 ± 0.7	9.6 ± 1	5.7 ± 0.6	5.4 ± 0.6	5.8 ± 0.7	1.78 ± 0.2	0.44 ± 0.07
Other	370 ± 40	370 ± 40	303 ± 35	228 ± 22	179 ± 22	111 ± 12	27.4 ± 2.8	3.9 ± 0.9
Fakes	810 ± 300	800 ± 400	880 ± 350	340 ± 140	660 ± 300	280 ± 130	57 ± 32	6.3 ± 3.3
Total	59000 ± 6000	37000 ± 4000	32500 ± 2900	22900 ± 2200	15200 ± 1700	9400 ± 1000	2190 ± 270	440 ± 50
Data	61954	36528	32887	23245	15595	9397	2097	426

Table 3 Expected yields in the dilepton signal regions before the fit to data. The data-driven corrections to the $t\bar{t}$+jets background are applied and all uncertainties are included, except the ones associated with the $t\bar{t}$+jets background normalisation factors, which are not defined pre-fit. The "Other" category includes the tZq, tWZ and diboson processes. The $t\bar{t}H$ signal is normalised to the SM $t\bar{t}H$ cross-section. For presentation purposes, uncertainties are symmetrised

	STXS 1 SR	STXS 2 SR	STXS 3 SR	STXS 4 SR	STXS 5 SR	STXS 6 SR
$t\bar{t}H$ truth p_{T}^{H} 0–60 GeV	10.6 ± 1.5	2.03 ± 0.31	1.14 ± 0.17	0.63 ± 0.11	0.19 ± 0.07	0.046 ± 0.023
$t\bar{t}H$ truth p_{T}^{H} 60–120 GeV	6.5 ± 0.7	13.0 ± 1.8	4.1 ± 0.7	1.9 ± 0.4	0.7 ± 0.11	0.13 ± 0.07
$t\bar{t}H$ truth p_{T}^{H} 120–200 GeV	3.06 ± 0.34	4.7 ± 0.5	16.3 ± 2.0	5.0 ± 0.7	1.36 ± 0.19	0.24 ± 0.07
$t\bar{t}H$ truth p_{T}^{H} 200–300 GeV	0.5 ± 0.07	0.72 ± 0.08	2.5 ± 0.29	13.0 ± 1.7	4.4 ± 0.6	0.41 ± 0.06
$t\bar{t}H$ truth p_{T}^{H} 300–450 GeV	<0.1	<0.1	0.197 ± 0.033	0.82 ± 0.18	8.0 ± 1.1	1.98 ± 0.32
$t\bar{t}H$ truth $p_{\mathrm{T}}^{H} \geq 450$ GeV	<0.1	<0.1	<0.1	<0.1	0.26 ± 0.08	2.8 ± 0.5
$t\bar{t}H$ $\lvert y\rvert > 2.5$	<0.1	<0.1	<0.1	<0.1	<0.1	<0.1
$t\bar{t} + \geq 2b$	81 ± 8	76 ± 7	81 ± 13	59 ± 4	36.2 ± 3.0	11.7 ± 2.1
$t\bar{t} + 1b$	14 ± 5	15 ± 6	20 ± 9	17 ± 5	11 ± 6	2.9 ± 1.9
$t\bar{t} + 1B$	4.4 ± 2.6	4.8 ± 3.2	5.7 ± 2.3	6.2 ± 1.9	6.6 ± 2.9	3.5 ± 2.3
$t\bar{t} + \geq 1c$	11.3 ± 2.4	11.7 ± 2.6	15.4 ± 3.4	12.5 ± 2.6	7.1 ± 2.6	3.0 ± 1.7
$t\bar{t}$ + light	1.1 ± 0.7	0.9 ± 0.5	1.4 ± 0.8	1.0 ± 0.5	1.0 ± 0.4	0.37 ± 0.30
$t\bar{t}Z$	4.6 ± 0.7	4.6 ± 1.1	7.2 ± 1.1	6.2 ± 1.3	5.3 ± 1.1	2 ± 0.6
tW	1.7 ± 0.8	3 ± 1.8	6 ± 4	8 ± 5	7 ± 5	3.1 ± 2.9
$t\bar{t}W$	0.65 ± 0.11	1.18 ± 0.15	2.1 ± 0.23	2.64 ± 0.3	2.7 ± 0.4	1.2 ± 0.5
Z+jets	1.8 ± 0.9	1.9 ± 0.9	3.4 ± 1.3	3.8 ± 1.4	3.3 ± 1.2	1.8 ± 0.7
$t\bar{t}t\bar{t}$	0.9 ± 0.4	1.1 ± 0.5	1.8 ± 0.7	1.7 ± 0.7	1.3 ± 0.6	0.65 ± 0.28
tWH	0.23 ± 0.04	0.31 ± 0.04	0.57 ± 0.07	0.7 ± 0.08	0.66 ± 0.07	0.24 ± 0.03
Other	<0.1	<0.1	0.28 ± 0.14	0.42 ± 0.19	0.23 ± 0.08	0.29 ± 0.13
Fakes	1.7 ± 0.9	2.2 ± 1.1	3.2 ± 1.6	2.9 ± 1.5	2.6 ± 1.3	1.1 ± 0.6
Total	144 ± 13	144 ± 13	173 ± 20	143 ± 12	100 ± 11	38 ± 6
Data	150	149	161	149	76	35

olution, and lepton trigger efficiencies are varied within their uncertainties [76,77] to estimate the corresponding systematic uncertainty.

The JES uncertainty [81] accounts for contributions from jet-flavour composition, η-intercalibration, punch-through, single-particle response, calorimeter response to different jet flavours, and pile-up, resulting in 31 uncorrelated JES uncertainty components. The jet energy resolution was measured separately for data and MC using two in situ techniques [81]. The systematic uncertainty is defined as the quadratic difference between the jet energy resolutions for data and simulation and split into 13 uncorrelated uncertainty components. The uncertainty associated with the JVT discriminant is obtained by varying the efficiency correction factors [80].

The uncertainties associated with the b-tagging algorithm calibration are derived separately for b-jets, c-jets and light-flavour jets, as a function of the jet p_{T}, and decomposed into several uncorrelated components for each category, corresponding to the number of p_{T} bins multiplied by the number of DL1r pseudo-continuous scores [94–96]. This yields a total of 45 components for b-jets and 20 each for c- and light jets. For jets with a p_{T} above the p_{T} threshold where the b-tagging algorithm is calibrated, high-p_{T} extrapolation uncertainties derived using MC simulation are included.

The uncertainty in $E_{\mathrm{T}}^{\mathrm{miss}}$ results from the propagation of the uncertainties in the energy scales and resolutions of photons, leptons and jets, and from the modelling of its soft term [85].

For the $t\bar{t}H$ signal, two cross-section uncertainties are applied accounting for the effect of varying the PDF and α_S and for missing higher order terms in the fixed order perturbative QCD calculations. They amount to $\pm 3.6\%$ and $\pm 9.2\%$, respectively [18]. The systematic uncertainty in the $t\bar{t}H$ cross-section includes theory uncertainties due to migrations of events between the truth Higgs boson p_{T} bins [97]. An uncertainty of 2.2% is assigned to the $H \to b\bar{b}$ branching fraction [18]. Two uncertainties due to missing higher order terms in the MC simulation are estimated by varying independently the renormalisation and factorisation scales in the ME of the nominal MC sample by a factor of two up and down. The uncertainties in the amount of initial- and final-state QCD radiation (ISR and FSR) predicted by the PS are estimated by varying the scale in α_S^{ISR} according to the values given by *var3c* in the PYTHIA8 A14 tune and by varying

Table 4 Expected yields in the dilepton control regions before the fit to data. The data-driven corrections to the $t\bar{t}$+jets background are applied and all uncertainties are included, except the ones associated with the $t\bar{t}$+jets background normalisation factors, which are not defined pre-fit. The "Other" category includes the tZq, tWZ and diboson processes. The $t\bar{t}H$ signal is normalised to the SM $t\bar{t}H$ cross-section. For presentation purposes, uncertainties are symmetrised

	$t\bar{t}$ + light CR	$t\bar{t} + \geq 1c$ CR	$t\bar{t} + 1b$ CR	$t\bar{t} + 1B$ CR	$t\bar{t} + \geq 2b$ CR
$t\bar{t}H$ truth p_{T}^{H} 0–60 GeV	11.9 ± 1.4	19.7 ± 2.3	19.8 ± 2.3	9.9 ± 1.4	26.0 ± 3.0
$t\bar{t}H$ truth p_{T}^{H} 60–120 GeV	17.0 ± 1.3	34.5 ± 2.9	29.5 ± 3.0	20.4 ± 2.5	42.0 ± 4.0
$t\bar{t}H$ truth p_{T}^{H} 120–200 GeV	10.0 ± 0.9	27.1 ± 2.7	17.0 ± 2.1	19.2 ± 2.4	34.0 ± 3.5
$t\bar{t}H$ truth p_{T}^{H} 200–300 GeV	3.1 ± 0.35	11.1 ± 1.3	4.6 ± 0.7	9.2 ± 1.2	14.9 ± 1.9
$t\bar{t}H$ truth p_{T}^{H} 300–450 GeV	0.94 ± 0.15	3.5 ± 0.5	0.94 ± 0.19	3.3 ± 0.5	5.4 ± 0.8
$t\bar{t}H$ truth $p_{\mathrm{T}}^{H} \geq 450$ GeV	0.33 ± 0.07	0.65 ± 0.12	0.116 ± 0.033	0.97 ± 0.15	1.33 ± 0.26
$t\bar{t}H$ $\lvert y\rvert > 2.5$	0.31 ± 0.05	0.25 ± 0.04	0.4 ± 0.05	0.127 ± 0.028	0.166 ± 0.018
$t\bar{t} + \geq 2b$	495 ± 35	860 ± 60	1080 ± 200	650 ± 100	2700 ± 200
$t\bar{t} + 1b$	1410 ± 130	1790 ± 230	3600 ± 700	1540± 180	1200 ± 400
$t\bar{t} + 1B$	310 ± 40	460 ± 40	540± 210	1560 ± 230	310 ± 110
$t\bar{t} + \geq 1c$	5600 ± 500	7700 ± 600	2210 ± 280	1590 ± 330	1070 ± 170
$t\bar{t}$ + light	9200 ± 1500	2800 ± 400	590 ± 130	410 ± 90	190 ± 70
$t\bar{t}Z$	43 ± 6	81 ± 12	35 ± 6	36 ± 5	92 ± 12
tW	300 ± 60	210 ± 50	220 ± 70	150 ± 50	300 ± 140
$t\bar{t}W$	37 ± 5	72 ± 7	12.1 ± 1.3	14.3 ± 3.3	29.8 ± 3.5
Z+jets	340 ± 130	260 ± 100	250 ± 90	93 ± 34	320 ± 120
$t\bar{t}t\bar{t}$	1.6 ± 0.7	10± 4	1± 0.4	4.8 ± 2	28 ± 12
tWH	0.98 ± 0.11	2.24 ± 0.22	2.69 ± 0.29	1.42 ± 0.14	4.0 ± 0.4
Other	5.6 ± 2.4	8.1 ± 3.1	4.4 ± 2.0	2.1 ± 0.7	12 ± 5
Fakes	110 ± 50	120 ± 60	40 ± 20	40 ± 20	80 ± 40
Total	18000 ± 2000	14400 ± 1100	8700 ± 900	6200 ± 500	6400 ± 700
Data	18557	14361	8624	5830	6448

the scale in α_S^{FSR} by a factor two up and down. To assess the uncertainties associated with the PS, hadronisation and underlying event, the nominal $t\bar{t}H$ sample is compared with the alternative POWHEG+HERWIG7 sample, while the uncertainty due to the NLO matching procedure is estimated with POWHEG+PYTHIA8 with a varied $p_{\mathrm{T}}^{\mathrm{hard}}$ parameter value.

All the modelling uncertainties in the $t\bar{t}$+jets background have independent nuisance parameters for the $t\bar{t}+1b$, $t\bar{t}+1B$, $t\bar{t}+\geq 2b$, $t\bar{t}+\geq 1c$ and $t\bar{t}$+light processes. These systematic variations are normalised to conserve the total nominal event count after the preselection for each process. Uncertainties due to missing higher order terms in the perturbative QCD calculations, in the amount of ISR and FSR as well as the uncertainties associated with the PS and hadronisation, and with the NLO matching procedure are estimated in the same way as for the $t\bar{t}H$ signal.

For $t\bar{t} + \geq 1b$, the choice of recoil scheme in the ISR PS has a sizeable effect in the normalisations and shapes of the distributions used in the analysis within the detector acceptance [22]. The uncertainty associated with the choice of the global recoil scheme is assessed by comparing the nominal sample with an alternative sample produced with the dipole recoil scheme. For $t\bar{t}$ + light and $t\bar{t} + \geq 1c$, the uncertainty in the choice of the h_{damp} parameter is estimated by using the alternative POWHEGBOX+PYTHIA8 sample with $h_{\mathrm{damp}} = 3\ m_{\mathrm{top}}$.

Uncertainties related to the H_{T} reweighting procedure described in Sect. 5.1 are assigned independently in the single-lepton and dilepton channels. The $t\bar{t}$ + light and $t\bar{t} + \geq 1c$ normalisation factors are varied within their uncertainties to estimate the corresponding systematic uncertainty. An additional uncertainty is estimated by comparing the distributions with and without the weights derived in the H_{T} reweighting procedure, in bins of jet multiplicity.

A ±5% normalisation uncertainty is considered for the cross-sections of the t- and s- single-top production modes [98,99]. The normalisation uncertainty of the tW background is 3.7% [100]. Modelling uncertainties in the tW production due to the choice of the PS and hadronisation model, the NLO matching and the h_{damp} parameter choice are evaluated in the same way as for the $t\bar{t}$ + light and $t\bar{t} + \geq 1c$ backgrounds. The uncertainty associated with the interference between tW and $t\bar{t}$ production at NLO is assessed by comparing the nominal POWHEGBOX+PYTHIA8 sample pro-

duced using the diagram removal scheme to an alternative sample produced with the same generator but using the diagram subtraction scheme.

The total uncertainty in the theoretical $t\bar{t}W$ cross-section computed at NNLO in the QCD and at NLO in the electroweak interactions is 7.4% [71]. The modelling uncertainty in the $t\bar{t}W$ background is evaluated by comparing the nominal SHERPA simulation with the sample produced using MADGRAPH5_AMC@NLO. For the $t\bar{t}Z$ production, the uncertainty in the predicted cross-section at NLO in QCD is 12% [18]. The modelling uncertainty in the $t\bar{t}Z$ background is evaluated by comparing the nominal MADGRAPH5_AMC@NLO+PYTHIA8 sample with the sample where PYTHIA8 is replaced by HERWIG7 to simulate the PS and hadronisation.

A normalisation uncertainty of $^{+70\%}_{-15\%}$ is assigned for the $t\bar{t}t\bar{t}$ background. The down variation corresponds to the theory uncertainty covering effects from varying the factorisation and renormalisation scales, the PDFs and α_S [101] while the up variation covers the measured $t\bar{t}t\bar{t}$ cross-section [102]. For tZq, the total normalisation uncertainty is 7.9% [37]. A normalisation uncertainty of 15.4% (9.2%) calculated using MADGRAPH5_AMC@NLO at NLO is applied to the $tHjb$ (tWH) background normalisation [103]. For tWZ, an uncertainty of ±50% is used [37].

The treatment of V+jets uncertainties follows the previous analysis [104]. An uncertainty of 40% is assumed for the W+jets cross-section, with an additional 30% normalisation uncertainty used for W boson production in association with heavy-flavour jets, taken as uncorrelated between events with two and events with more than two truth-level heavy-flavour jets. These uncertainties are based on variations of the factorisation and renormalisation scales and of the matching parameters in the SHERPA samples. An uncertainty of 35% is applied to the Z+jets normalisation to account for both the variations of the scales and matching parameters in the SHERPA samples and the uncertainty in the correction factor for the Z boson production accompanied by two b-jets extracted from data. A 50% normalisation uncertainty is used for the diboson background, which includes uncertainties in the inclusive cross-section and additional jet production [105–107].

A 50% normalisation uncertainty is assigned to the fake-lepton background estimate in the single-lepton and dilepton channels separately. An additional uncertainty obtained by using an alternative parameterisation of the fake rate (Sect. 5.2) is considered in the single-lepton channel.

8 Results

An excess of events over the expected background is found with an observed (expected) significance of 4.6 (5.4) standard deviations, in a combined profile-likelihood fit to data in all signal and control regions. The measured $t\bar{t}H$ signal strength for $m_H = 125.09$ GeV [108] is

$$\mu_{t\bar{t}H} = 0.81^{+0.22}_{-0.19} = 0.81 \pm 0.11(\text{stat.})\,^{+0.20}_{-0.16}(\text{syst.}). \quad (2)$$

The total statistical uncertainty is defined as the uncertainty in $\mu_{t\bar{t}H}$ when all nuisance parameters associated with the systematic uncertainties are fixed to their best-fit values. The total systematic uncertainty is then defined as the difference in quadrature between the total and statistical uncertainties. The systematic uncertainty in the signal strength $\mu_{t\bar{t}H}$ includes the theoretical uncertainties in the SM $t\bar{t}H$ cross-section described in Sect. 7. The measured $t\bar{t}H$ signal strength in the single-lepton channel is

$$\mu_{t\bar{t}H} = 0.72 \pm 0.12(\text{stat.})\,^{+0.21}_{-0.17}(\text{syst.}) \quad (3)$$

and in the dilepton channel is

$$\mu_{t\bar{t}H} = 1.03 \pm 0.26(\text{stat.})\,^{+0.28}_{-0.22}(\text{syst.}). \quad (4)$$

The combined $\mu_{t\bar{t}H}$ is converted into an inclusive cross-section using the SM theoretical cross-section of 507^{+35}_{-50} fb for $m_H = 125.09$ GeV and excluding its uncertainty [18]. The resulting cross-section is

$$\sigma_{t\bar{t}H} = 411\,^{+101}_{-92}\ \text{fb} = 411 \pm 54(\text{stat.})\,^{+85}_{-75}(\text{syst.})\ \text{fb}, \quad (5)$$

with a relative uncertainty of $^{+25\%}_{-22\%}$, consistent with the SM prediction. The sensitivity is driven by the single-lepton channel, where the systematic component of the uncertainty dominates. The sensitivity of the dilepton channel is limited by the size of the dataset.

The measured values of the $t\bar{t}$ + jets background normalisation factors, which are free parameters of the fit, are listed in Table 5. They are compatible between the single-lepton and the dilepton channels within two standard deviations. For $t\bar{t}+1b$, the measured value of the normalisation factor is slightly larger in the dilepton channel than in the single-lepton channel.

Compared with the previous analysis using the same dataset, the current analysis selects 64% (29%) new events in the single-lepton (dilepton) SR that did not enter the selection of the previous analysis. This is consistent with the increase of the overall acceptance by a factor of three. The statistical correlation between the two analyses is estimated using a booststrap method to be 19%, assuming that the systematic uncertainties are independent. This assumption is justified by the fact that the systematic model of the most important $t\bar{t}+\geq 1b$ background is different between the two analyses and the experimental uncertainties are updated. Based on

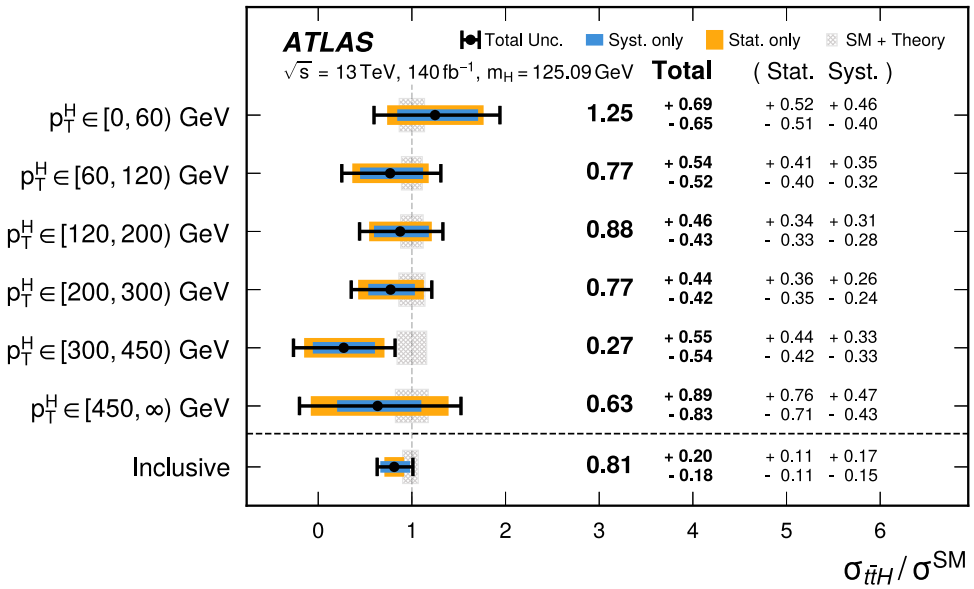

Fig. 3 The $t\bar{t}H$ cross-sections measured in bins of truth Higgs boson p_{T} for a Higgs boson rapidity $|y| \leq 2.5$, and measured inclusively in the full phase space, normalised to their SM predictions, as obtained from a combined profile-likelihood fit to data in all signal and control regions. The uncertainties are shown separately for the measurement and the prediction

Table 5 Best-fit values of the $t\bar{t}+$ jets normalisation factors obtained from the fit to data with a single inclusive $t\bar{t}H$ signal strength parameter. Independent normalisation factors for $t\bar{t}+1b$, $t\bar{t}+\geq 1c$ and $t\bar{t}+$ light components are used in the dilepton and single-lepton channels. Before the fit, the $t\bar{t}+$ light and $t\bar{t}+\geq 1c$ components are normalised to the $t\bar{t}$ cross-section computed at NNLO in QCD including the resummation of NNLL soft-gluon terms [72] while the $t\bar{t}+\geq 1b$ normalisation is taken from the $t\bar{t}b\bar{b}$ MC simulation

Normalisation factor	$t\bar{t}+$ light	$t\bar{t}+\geq 1c$	$t\bar{t}+1b$	$t\bar{t}+1B$	$t\bar{t}+\geq 2b$
Single-lepton	$0.78^{+0.08}_{-0.08}$	$1.51^{+0.19}_{-0.18}$	$1.06^{+0.10}_{-0.10}$	$1.15^{+0.15}_{-0.14}$	$0.94^{+0.08}_{-0.08}$
Dilepton	$0.88^{+0.11}_{-0.10}$	$1.36^{+0.10}_{-0.10}$	$1.24^{+0.09}_{-0.09}$		

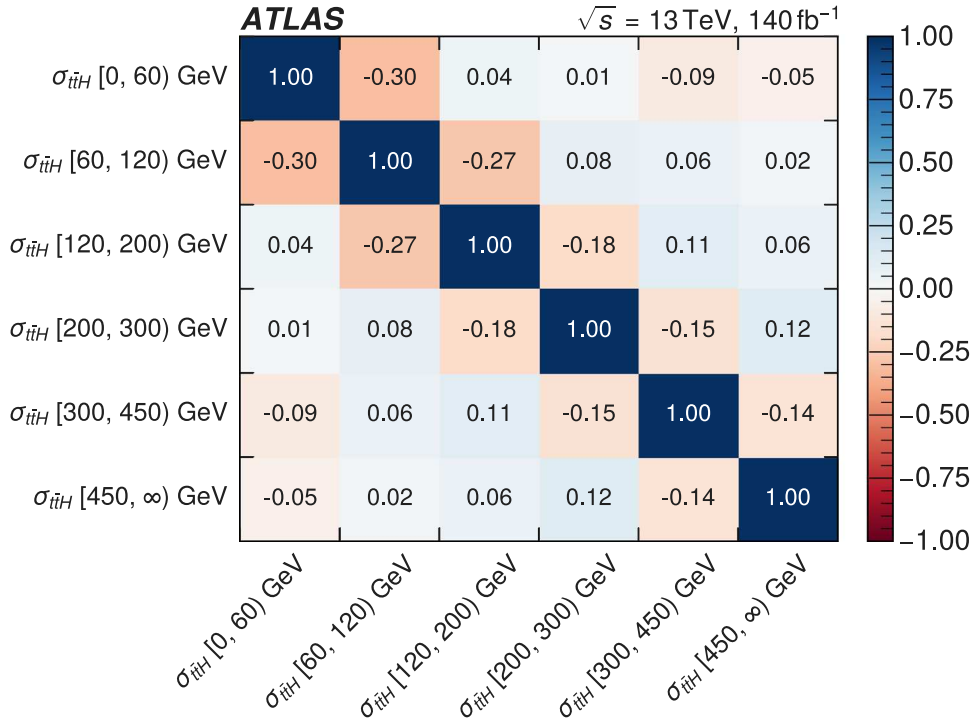

Fig. 4 Post-fit correlations between the measured values of the $t\bar{t}H$ cross-section, $\sigma_{t\bar{t}H}$, in bins of truth p_{T}^{H}

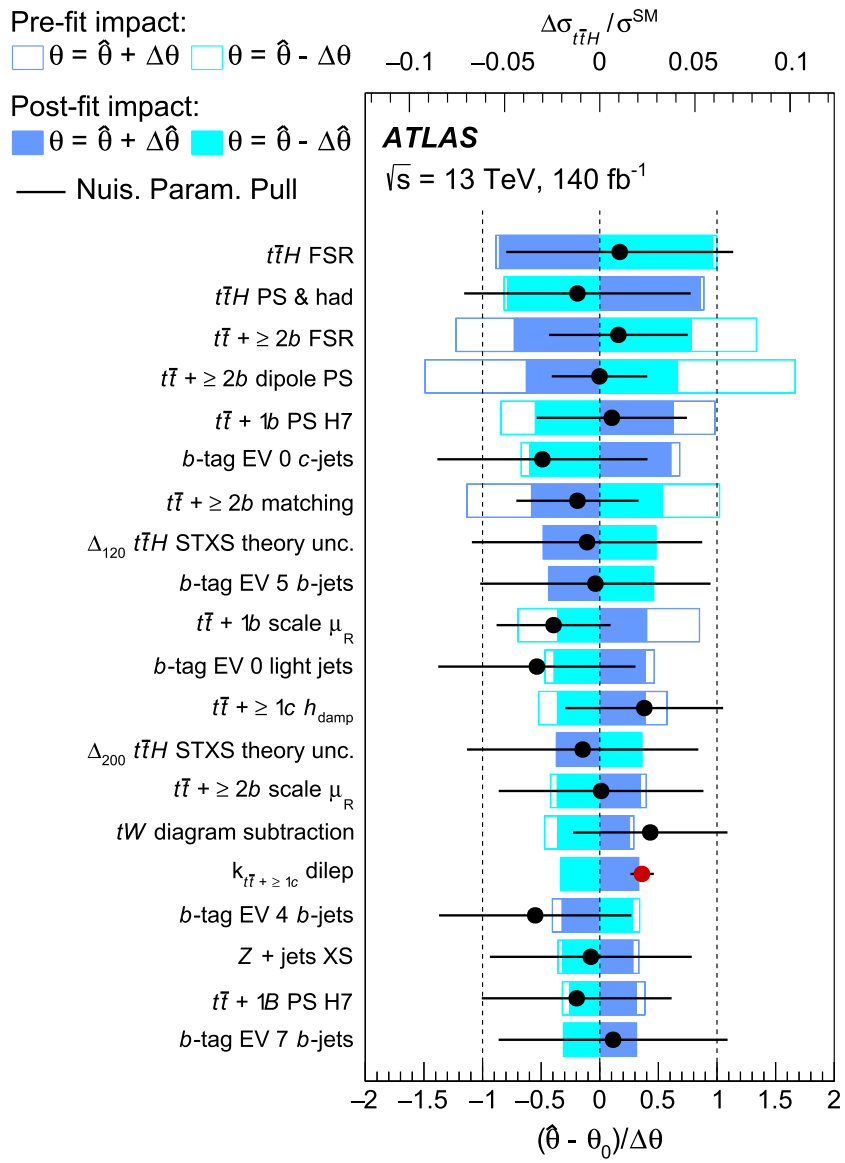

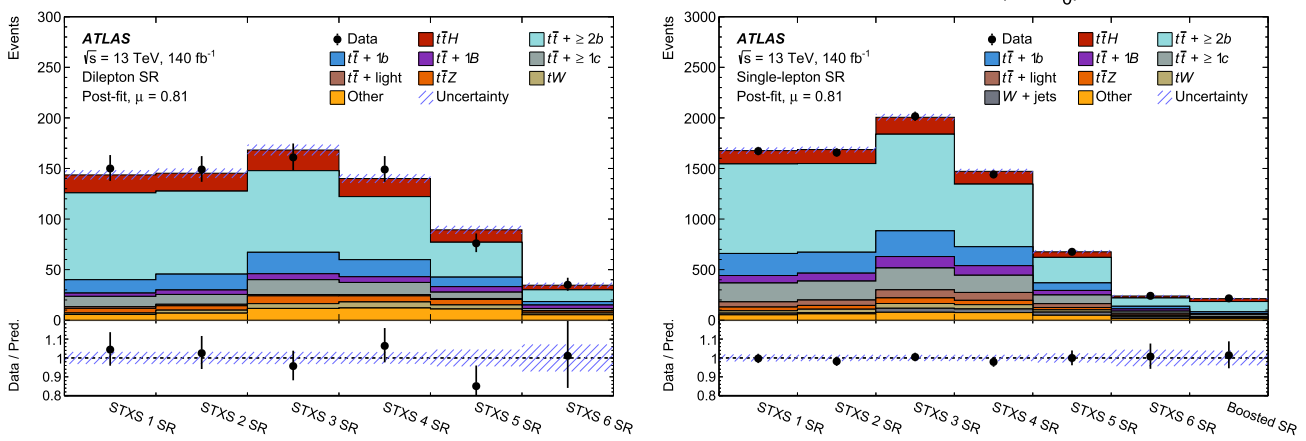

(a) (b)

Fig. 5 Ranking of the 20 modelling and experimental systematic uncertainties with the largest post-fit impact on the inclusive cross-section. The empty (filled) blue rectangles correspond to the pre-(post-)fit impact on $\sigma_{t\bar{t}H}/\sigma^{\mathrm{SM}}$ and refer to the upper scale of the plot. The impact of each nuisance parameter, $\Delta\sigma_{t\bar{t}H}/\sigma^{\mathrm{SM}}$, is computed by comparing the nominal best-fit value of $\sigma_{t\bar{t}H}/\sigma^{\mathrm{SM}}$ with the result of the fit when fixing the considered nuisance parameter to its best-fit value, $\hat{\theta}$, shifted by its pre-fit (post-fit) uncertainties $\pm\Delta\theta$ ($\pm\Delta\hat{\theta}$). The black markers show the pulls of the nuisance parameters relative to their nominal values, $\theta_0 = 0$. The red marker shows the pull of the $t\bar{t} + \geq 1c$ normalisation factor in the dilepton channel relative to its nominal value, $\theta_0 = 1$. No pre-fit uncertainty is defined for the normalisation factor as it is a free parameter of the fit. The pulls and their relative post-fit errors, $\Delta\hat{\theta}/\Delta\theta$, refer to the lower scale of the plot

Fig. 6 Post-fit summary of the yields in the (**a**) dilepton and (**b**) single-lepton signal regions, with all regions aggregated into a single bin each. The uncertainty band includes all uncertainties and their correlations

Table 6 A list of the absolute and relative uncertainties in the measured $\sigma_{t\bar{t}H}$ grouped in categories. The contributions from different sources of uncertainty are evaluated after the fit. The quoted values are obtained by repeating the fit, while fixing the set of nuisance parameters of the sources corresponding to each category to their best-fit values, and subtracting in quadrature the resulting uncertainty from the total uncertainty of the nominal fit presented in the last row. The total uncertainty is different from the sum in quadrature of the different components due to correlations between nuisance parameters in the fit. The $t\bar{t}H$ and $t\bar{t}+\geq 1b$ radiation uncertainty categories include the renormalisation and factorisation scales, ISR and FSR uncertainties. The "$t\bar{t}H$ theory" category includes STXS-related theoretical uncertainties and uncertainty in the $H \to b\bar{b}$ branching fraction. The "Minor background modelling" category includes uncertainties in the fake-lepton background and in minor backgrounds as defined in the text. The total statistical uncertainty includes uncertainties in the normalisation factors

Uncertainty source	$\Delta\sigma_{t\bar{t}H}$ (fb)		$\Delta\sigma_{t\bar{t}H}/\sigma_{t\bar{t}H}$ (%)	
Process modelling				
$t\bar{t}H$ modelling				
$t\bar{t}H$ radiation	+35	−21	+9	−5
$t\bar{t}H$ parton shower	+32	−19	+8	−5
$t\bar{t}H$ matching	<0.1	−0.3	<0.1	−0.1
$t\bar{t}H$ theory	+25	−17	+6	−4
$t\bar{t}+\geq 1b$ modelling				
$t\bar{t}+\geq 1b$ radiation	±31		±8	
$t\bar{t}+\geq 1b$ parton shower	±29		±7	
$t\bar{t}+\geq 1b$ matching	±19		±5	
$t\bar{t}+\geq 1c$ modelling	±18		±4	
$t\bar{t}+$ light modelling	±5		±1	
tW modelling	±16		±4	
Minor background modelling	±19		±5	
Flavour tagging	±36		±9	
Jet modelling	±22		±5	
Monte-Carlo statistics	±17		±4	
Other instrumental	±10		±2	
Total systematic uncertainty	+85	−75	+21	−18
Normalisation factors	±21		±5	
Total statistical uncertainty	±54		±13	
Total uncertainty	+101	− 92	+25	− 22

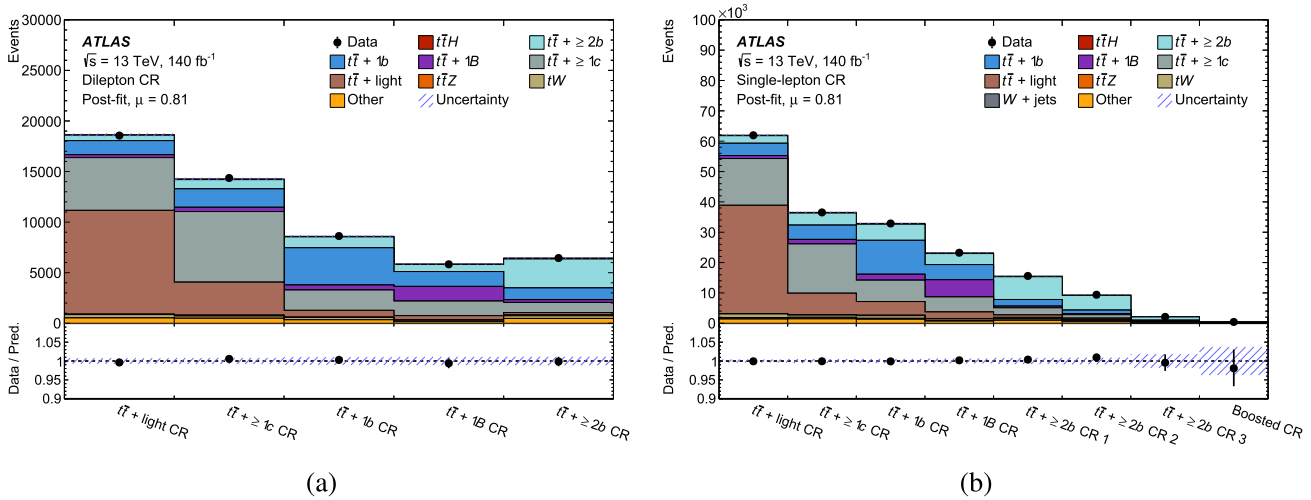

(a) (b)

Fig. 7 Post-fit summary of the yields in the (**a**) dilepton and (**b**) single-lepton control regions, with all regions aggregated into a single bin each. The uncertainty band includes all uncertainties and their correlations

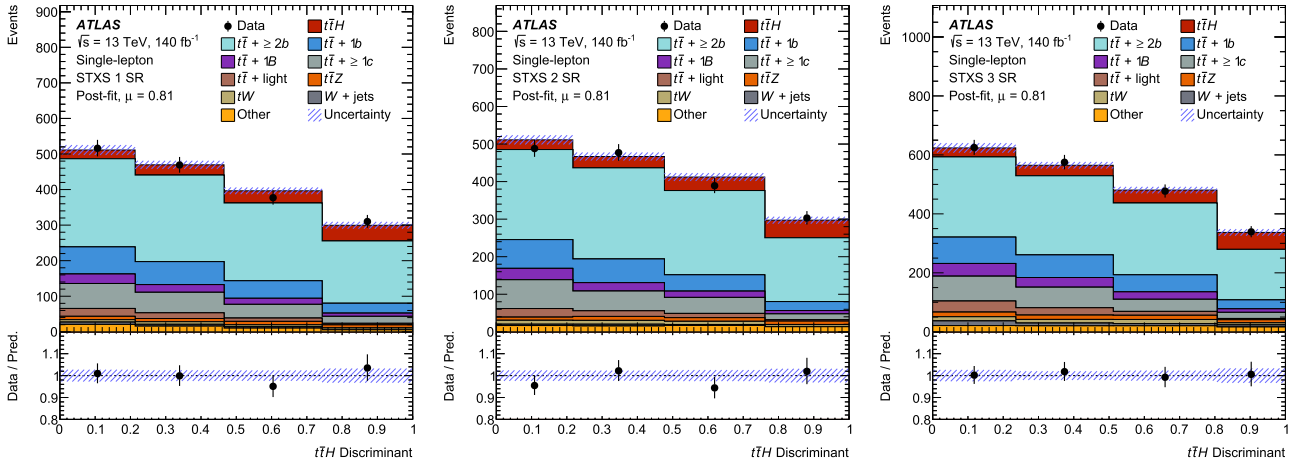

(a)

(b)

(c)

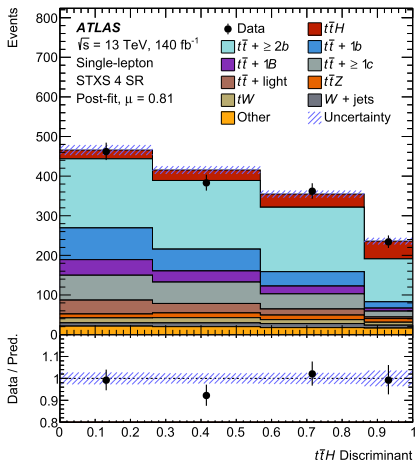

(d)

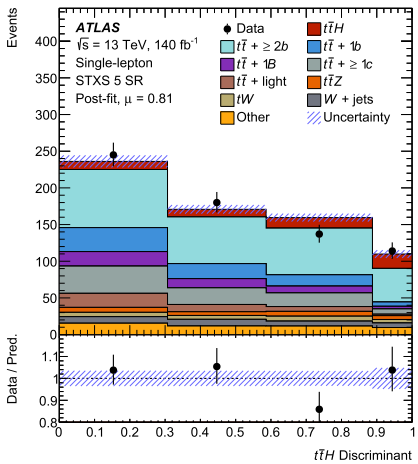

(e)

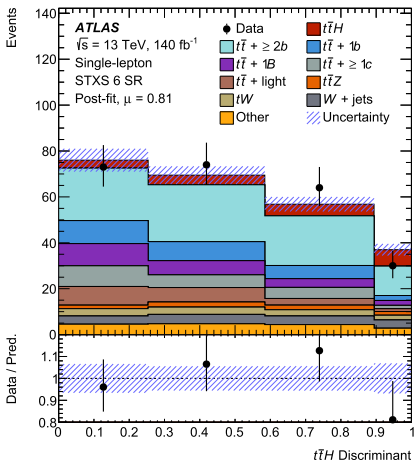

(f)

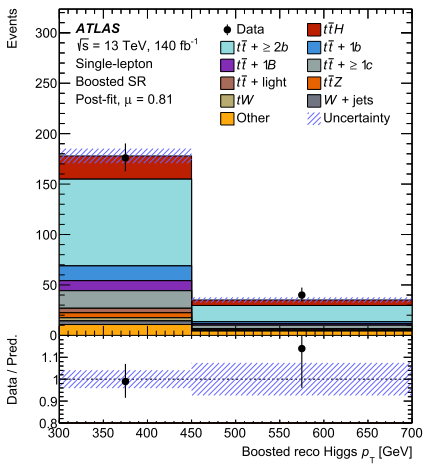

(g)

Fig. 8 Post-fit data/prediction comparisons of the signal region distributions entering the fit in the single-lepton channel. The discriminants are rescaled to lie between zero and one using a logistic function. The signal and background normalisation parameters and the nuisance parameters are set to their best-fit values. The uncertainty band includes all uncertainties and their correlations. For the reconstructed Higgs boson p_{T} in the boosted signal region, the first (last) bin includes the underflow (overflow) contributions

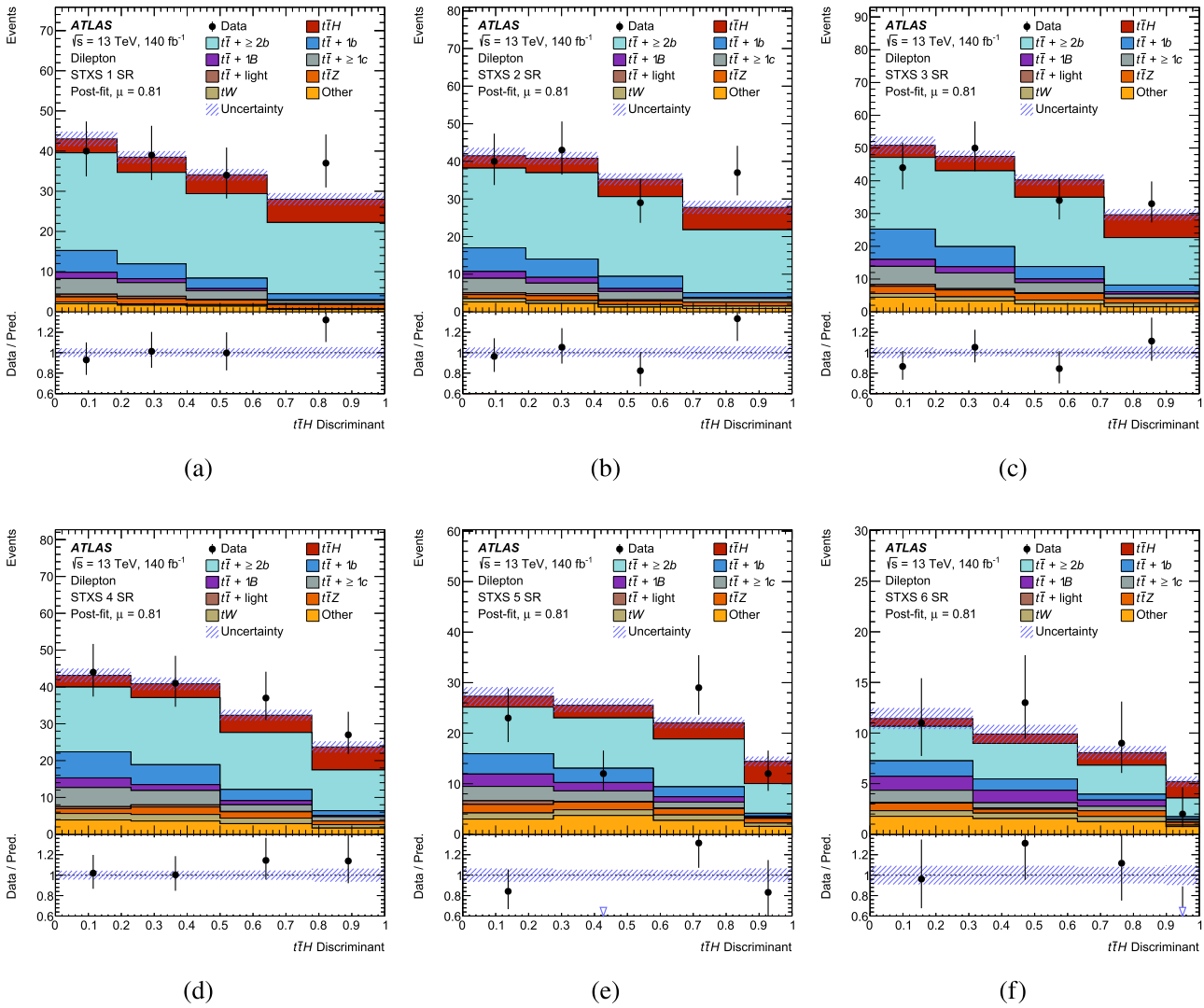

Fig. 9 Post-fit data/prediction comparisons of the signal region distributions entering the fit in the dilepton channel. The discriminants are rescaled to lie between zero and one using a logistic function. The signal and background normalisation parameters and the nuisance parameters are set to their best-fit values. The uncertainty band includes all uncertainties and their correlations

this, the probability that the current result is compatible with the result of Ref. [20] is estimated as 21%.

Figure 3 shows the measured values of $\sigma_{t\bar{t}H}/\sigma^{\mathrm{SM}}$ in bins of the Higgs boson p_{T}, obtained from a combined profile-likelihood fit to data with a free $t\bar{t}H$ signal strength parameter for each bin. The result of this measurement is compatible with the SM prediction with a p-value of 89%, taking into account theoretical uncertainties in the SM $t\bar{t}H$ cross-section. The measured value of the inclusive signal strength is also shown. The measurement of $\sigma_{t\bar{t}H}/\sigma^{\mathrm{SM}}$ in the [300, 450) GeV and [450, ∞) GeV p_{T}^{H} bins is limited by statistical uncertainties. In the remaining bins, there is a similar contribution from statistical and systematic uncertainties. Defining boosted regions improves sensitivity in the [450, ∞) GeV p_{T}^{H} bin by about 15%, compared with the scenario where only the resolved event selection is applied to these events. The correlations between the parameters of interest are shown in Fig. 4. They do not exceed 30% and are larger in the lower Higgs boson transverse momentum region.

The fitted values of $t\bar{t}$ + jets background normalisation factors are consistent with those obtained in the fit with a single $\mu_{t\bar{t}H}$ parameter shown in Table 5.

The absolute and relative systematic uncertainties in the measurement of $\sigma_{t\bar{t}H}$, grouped in categories, are shown in Table 6, and the effect of individual nuisance parameters ranked according to their impact on the inclusive $\sigma_{t\bar{t}H}/\sigma^{\mathrm{SM}}$ is shown in Fig. 5. The largest impact originates from the signal

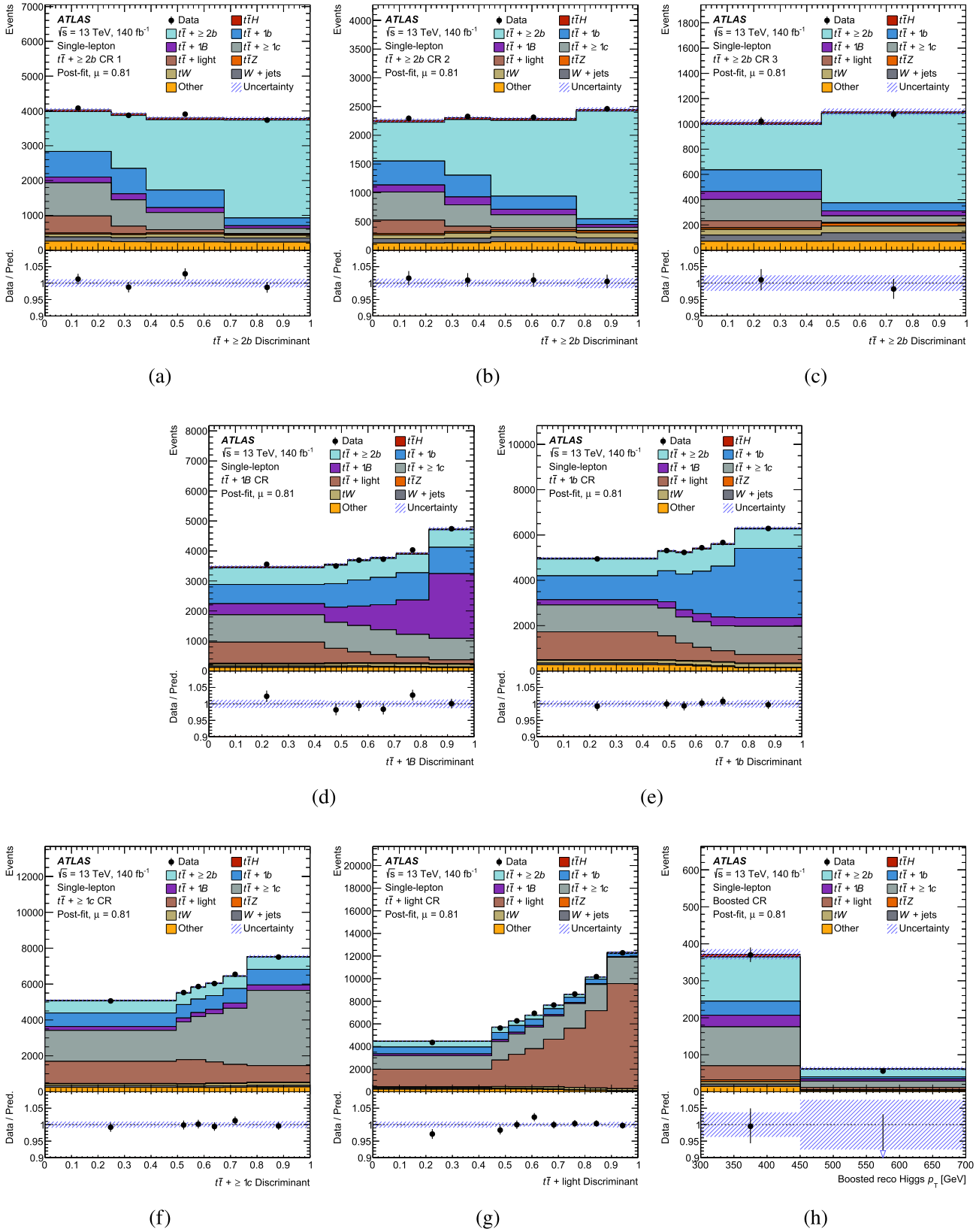

Fig. 10 Post-fit data/prediction comparisons of the control region distributions entering the fit in the single-lepton channel. The discriminants are rescaled to lie between zero and one using a logistic function. The signal and background normalisation parameters and the nuisance parameters are set to their best-fit values. The uncertainty band includes all uncertainties and their correlations. For the reconstructed Higgs boson p_{T} in the boosted control region, the first (last) bin includes the underflow (overflow) contributions

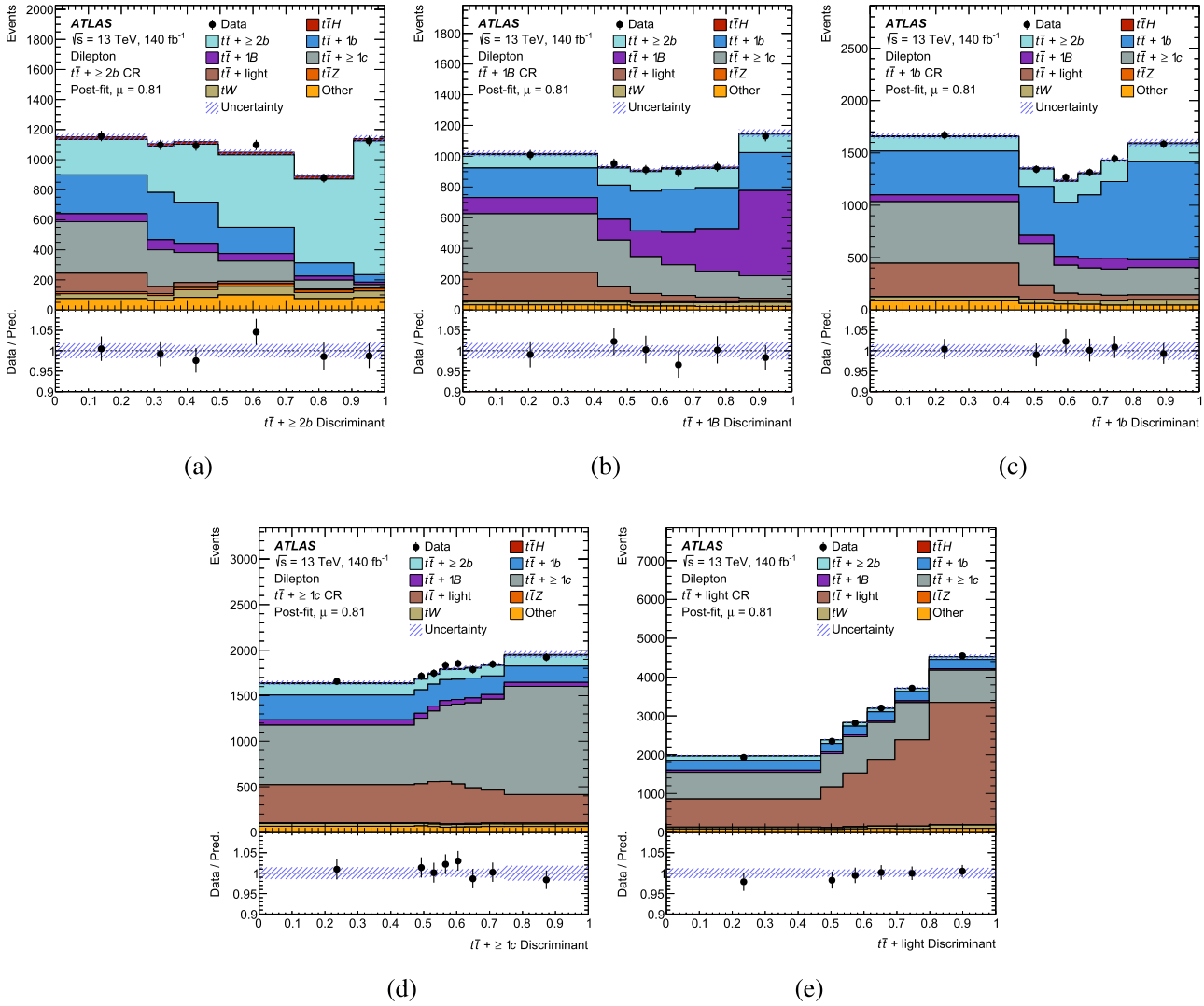

Fig. 11 Post-fit data/prediction comparisons of the control region distributions entering the fit in the dilepton channel. The discriminants are rescaled to lie between zero and one using a logistic function. The signal and background normalisation parameters and the nuisance parameters are set to their best-fit values. The uncertainty band includes all uncertainties and their correlations

modelling, followed by the $t\bar{t}+\geq 2b$ background modelling. In both cases, the dominant effects arise from the modelling of the FSR and the choice of the PS model. Among the experimental uncertainties, the largest effects come from the b-jet tagging and the jet energy scale.

Among the eight highest ranked nuisance parameters in Fig. 5, the largest constraints are observed for the $t\bar{t}+\geq 2b$ uncertainties arising from the dipole shower model and the choice of matching algorithm. These constraints predominantly originate from the single-lepton channel, and more specifically the SRs and the $t\bar{t}+\geq 2b$ CR where the $t\bar{t}+\geq 2b$ background contribution is large. The constraints are more pronounced when the $t\bar{t}+\geq 2b$ CR is split into three in the single-lepton channel to better control the $t\bar{t}+\geq 2b$ background modelling in bins of the reconstructed Higgs boson p_{T}.

The observed yields in all signal and control regions are compared to the post-fit predictions in Figs. 6 and 7. In each region, all bins are aggregated into a single bin. Figures 89 and 10 11 show a more detailed comparison in the single-lepton (dilepton) signal and control regions. The signal and background predictions in all post-fit distributions are obtained by setting the free parameters and the nuisance parameters to their best-fit values. In all post-fit plots, the uncertainty band includes all uncertainties and their correlations. The discriminant output in the plots is rescaled to be between zero and one using a logistic function.

The global goodness of fit [109,110] is 87% for the $\sigma_{t\bar{t}H}/\sigma^{\mathrm{SM}}$ measurement in p_{T}^{H} bins, highlighting that good post-fit modelling is achieved.

Figure 12 shows the event yield in data compared with the post-fit signal (S) and total background (B) predictions. It is ordered by the signal-to-background ratio of the bins from all the fitted regions. The predictions are shown for the best-fit signal strength and for the SM prediction. The observed data shows an excess over the background compatible with the best-fit signal strength $\mu_{t\bar{t}H}=0.81$ in the high $\log_{10}(S/B)$ region.

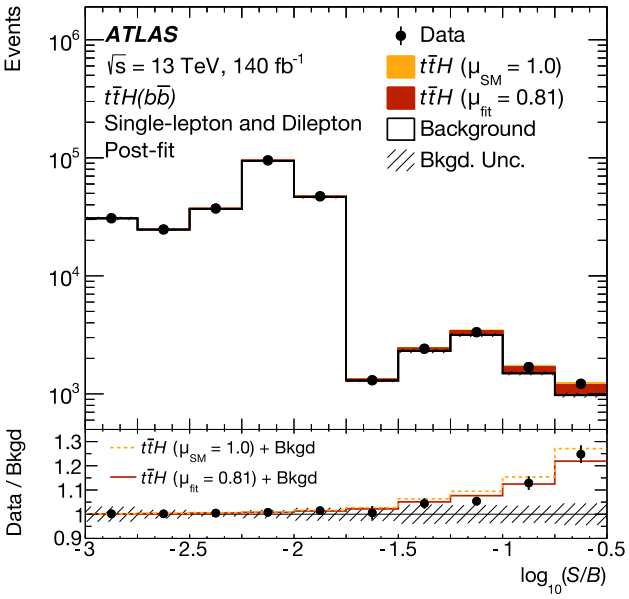

Fig. 12 Observed and expected event yields as a function of $\log_{10}(S/B)$, where S and B are the post-fit signal and total background yields, respectively. The bins in all fitted regions are ordered and grouped in bins of $\log_{10}(S/B)$. The signal is shown for the best-fit signal strength, $\mu=0.81$, or the SM prediction, $\mu=1.0$. The lower panel shows the ratio of the data to the post-fit background prediction, compared with the signal-plus-background prediction with the best-fit signal strength and the SM prediction. The shaded band represents the total uncertainty in the background prediction. The first (last) bin includes the underflow (overflow) contributions

9 Conclusion

The associated production of a Higgs boson with a pair of top quarks was measured in the $H\to b\bar{b}$ decay channel, using the full Run 2 proton–proton collision dataset collected at $\sqrt{s}=13$ TeV by the ATLAS detector at the LHC, corresponding to 140 fb^{-1}. The measurement uses final states containing one or two leptons. The measured inclusive cross-section assuming a Higgs boson mass of 125.09 GeV is $411\pm 54(\mathrm{stat.})\,^{+85}_{-75}(\mathrm{syst.})$ fb with a relative uncertainty of 24%, consistent with the SM prediction. The measurement is dominated by the systematic uncertainties arising from the $t\bar{t}H$ signal modelling followed by the $t\bar{t}+$ jets background modelling. The observed (expected) significance of the $t\bar{t}H$ signal relative to the SM background-only hypothesis is 4.6 (5.4) standard deviations. The cross-section measurement is also performed in six bins of p_{T}^{H} in the STXS framework with the highest bin probing Higgs bosons with p_{T}^{H} above 450 GeV. The uncertainty in the measurement for p_{T}^{H} above 300 GeV is dominated by the limited number of data events.

With respect to the previous iteration of the analysis, this measurement profits from looser selection requirements and improved b-jet identification that increase the $t\bar{t}H$ signal acceptance. Control regions enriched in each of the $t\bar{t}+$ jets components are defined based on a more powerful multi-class neural network. Together with data-driven modelling corrections for the $t\bar{t}+\geq 1c$ and $t\bar{t}+$ light components, and a dedicated MC simulation and systematic model for the $t\bar{t}+\geq 1b$ component, they provide improved signal sensitivity and better control over the background, such that the modelling uncertainty in $t\bar{t}+\geq 1b$ is no longer the dominant contribution to the total systematic uncertainty.

This analysis is the most precise $t\bar{t}H$ cross-section measurement in a single decay channel, inclusively and in each p_{T}^{H} bin.

Acknowledgements We thank CERN for the very successful operation of the LHC and its injectors, as well as the support staff at CERN and at our institutions worldwide without whom ATLAS could not be operated efficiently. The crucial computing support from all WLCG partners is acknowledged gratefully, in particular from CERN, the ATLAS Tier-1 facilities at TRIUMF/SFU (Canada), NDGF (Denmark, Norway, Sweden), CC-IN2P3 (France), KIT/GridKA (Germany), INFN-CNAF (Italy), NL-T1 (Netherlands), PIC (Spain), RAL (UK) and BNL (USA), the Tier-2 facilities worldwide and large non-WLCG resource providers. Major contributors of computing resources are listed in Ref. [111]. We gratefully acknowledge the support of ANPCyT, Argentina; YerPhI, Armenia; ARC, Australia; BMWFW and FWF, Austria; ANAS, Azerbaijan; CNPq and FAPESP, Brazil; NSERC, NRC and CFI, Canada; CERN; ANID, Chile; CAS, MOST and NSFC, China; Minciencias, Colombia; MEYS CR, Czech Republic; DNRF and DNSRC, Denmark; IN2P3-CNRS and CEA-DRF/IRFU, France; SRNSFG, Georgia; BMBF, HGF and MPG, Germany; GSRI, Greece; RGC and Hong Kong SAR, China; ISF and Benoziyo Center, Israel; INFN, Italy; MEXT and JSPS, Japan; CNRST, Morocco; NWO, Netherlands; RCN, Norway; MNiSW, Poland; FCT, Portugal; MNE/IFA, Romania; MSTDI, Serbia; MSSR, Slovakia; ARIS and MVZI, Slovenia; DSI/NRF, South Africa; MICIU/AEI, Spain; SRC and Wallenberg Foundation, Sweden; SERI, SNSF and Cantons of Bern and Geneva, Switzerland; NSTC, Taipei; TENMAK, Türkiye; STFC/UKRI, United Kingdom; DOE and NSF, United States of America. Individual groups and members have received support from BCKDF, CANARIE, CRC and DRAC, Canada; CERN-CZ, FORTE and PRIMUS, Czech Republic; COST, ERC, ERDF, Horizon 2020, ICSC-NextGenerationEU and Marie Skłodowska-Curie Actions, European Union; Investissements d'Avenir Labex, Investissements d'Avenir Idex and ANR, France; DFG and AvH Foundation, Germany; Herakleitos, Thales and Aristeia programmes co-financed by EU-ESF and the Greek NSRF, Greece; BSF-NSF and MINERVA, Israel; NCN and NAWA, Poland; La Caixa Banking Foundation, CERCA Programme Generalitat de Catalunya and PROMETEO and GenT Programmes Generalitat Valenciana, Spain; Göran Gustafssons Stiftelse, Sweden; The Royal Society and Leverhulme Trust, United Kingdom. In addition, individual members wish to acknowledge support from Armenia: Yerevan Physics Institute (FAPERJ); CERN: European Organization for Nuclear Research (CERN PJAS); Chile: Agencia Nacional de Investigación y Desarrollo (FONDECYT 1230812, FONDECYT 1230987, FONDECYT 1240864); China: Chinese Ministry of Science and Technology (MOST-2023YFA1605700), National Natural Science Foundation of China (NSFC - 12175119, NSFC 12275265, NSFC-12075060); Czech Republic: Czech Science Foundation (GACR - 24-11373S), Ministry of Education Youth and Sports (FORTE CZ.02.01.01/00/22_008/0004632), PRIMUS Research Programme (PRIMUS/21/SCI/017); EU: H2020 European Research Council (ERC - 101002463); European Union: European Research Council (ERC - 948254, ERC 101089007), Horizon 2020 Framework Programme (MUCCA - CHIST-ERA-19-XAI-00), European Union, Future Artificial Intelligence Research (FAIR-NextGenerationEU PE00000013), Italian Center for High Performance Computing, Big Data and Quantum Computing (ICSC, NextGenerationEU); France: Agence Nationale de la Recherche (ANR-20-CE31-0013, ANR-21-CE31-0013, ANR-21-CE31-0022, ANR-22-EDIR-0002), Investissements d'Avenir Labex (ANR-11-LABX-0012); Germany: Baden-Württemberg Stiftung (BW Stiftung-Postdoc Eliteprogramme), Deutsche Forschungsgemeinschaft (DFG - 469666862, DFG - CR 312/5-2); Italy: Istituto Nazionale di Fisica Nucleare (ICSC, NextGenerationEU), Ministero dell'Università e della Ricerca (PRIN - 20223N7F8K - PNRR M4.C2.1.1); Japan: Japan Society for the Promotion of Science (JSPS KAKENHI JP22H01227, JSPS KAKENHI JP22H04944, JSPS KAKENHI JP22KK0227, JSPS KAKENHI JP23KK0245); Netherlands: Netherlands Organisation for Scientific Research (NWO Veni 2020 - VI.Veni.202.179); Norway: Research Council of Norway (RCN-314472); Poland: Ministry of Science and Higher Education (IDUB AGH, POB8, D4 no 9722), Polish National Agency for Academic Exchange (PPN/PPO/2020/1/00002/U/00001), Polish National Science Centre (NCN 2021/42/E/ST2/00350, NCN OPUS nr 2022/47/B/ST2/03059, NCN UMO-2019/34/E/ST2/00393, NCN & H2020 MSCA 945339, UMO-2020/37/B/ST2/01043, UMO-2021/40/C/ST2/00187, UMO-2022/47/O/ST2/00148, UMO-2023/49/B/ST2/04085, UMO-2023/51/B/ST2/00920); Slovenia: Slovenian Research Agency (ARIS grant J1-3010); Spain: Generalitat Valenciana (Artemisa, FEDER, IDIFEDER/2018/048), Ministry of Science and Innovation (MCIN & NextGenEU PCI2022-135018-2, MICIN & FEDER PID2021-125273NB, RYC2019-028510-I, RYC2020-030254-I, RYC2021-031273-I, RYC2022-038164-I), PROMETEO and GenT Programmes Generalitat Valenciana (CIDEGENT/2019/027); Sweden: Carl Trygger Foundation (Carl Trygger Foundation CTS 22:2312), Swedish Research Council (Swedish Research Council 2023-04654, VR 2018-00482, VR 2022-03845, VR 2022-04683, VR 2023-03403, VR grant 2021-03651), Knut and Alice Wallenberg Foundation (KAW 2018.0157, KAW 2018.0458, KAW 2019.0447, KAW 2022.0358); Switzerland: Swiss National Science Foundation (SNSF - PCEFP2_194658); United Kingdom: Leverhulme Trust (Leverhulme Trust RPG-2020-004), Royal Society (NIF-R1-231091); United States of America: U.S. Department of Energy (ECA DE-AC02-76SF00515), Neubauer Family Foundation.

Data Availability Statement My manuscript has no associated data. [Authors' comment: All ATLAS scientific output is published in journals, and preliminary results are made available in Conference Notes. All are openly available, without restriction on use by external parties beyond copyright law and the standard conditions agreed by CERN. Data associated with journal publications are also made available: tables and data from plots (e.g. cross section values, likelihood profiles, selection efficiencies, cross section limits, ...) are stored in appropriate repositories such as HEPDATA (http://hepdata.cedar.ac.uk/). ATLAS also strives to make additional material related to the paper available that allows a reinterpretation of the data in the context of new theoretical models. For example, an extended encapsulation of the analysis is often provided for measurements in the framework of RIVET (http://rivet.hepforge.org/). This information is taken from the ATLAS Data Access Policy, which is a public document that can be downloaded from http://opendata.cern.ch/record/413 [opendata.cern.ch].]

Code Availability Statement My manuscript has no associated code/software. [Authors' comment: ATLAS collaboration software is open source, and all code necessary to recreate an analysis is publicly available. The Athena (http://gitlab.cern.ch/atlas/athena) software repository provides all code needed for calibration and uncertainty application, with configuration files that are also publicly available via Docker containers and cvmfs. The specific code and configurations written in support of this analysis are not public; however, these are internally preserved.]

Funded by SCOAP[3].

References

1. F. Englert, R. Brout, Broken symmetry and the mass of gauge vector mesons. Phys. Rev. Lett. **13**, 321 (1964). https://doi.org/10.1103/PhysRevLett.13.321
2. P.W. Higgs, Broken symmetries and the masses of gauge bosons. Phys. Rev. Lett. **13**, 508 (1964). https://doi.org/10.1103/PhysRevLett.13.508
3. G.S. Guralnik, C.R. Hagen, T.W.B. Kibble, Global conservation laws and massless particles. Phys. Rev. Lett. **13**, 585 (1964). https://doi.org/10.1103/PhysRevLett.13.585
4. ATLAS Collaboration, Observation of a new particle in the search for the Standard Model Higgs boson with the ATLAS detector at the LHC. Phys. Lett. B **716**, 1 (2012). https://doi.org/10.1016/j.physletb.2012.08.020. arXiv:1207.7214 [hep-ex]
5. C.M.S. Collaboration, Observation of a new boson at a mass of 125 GeV with the CMS experiment at the LHC. Phys. Lett. B **716**, 30 (2012). https://doi.org/10.1016/j.physletb.2012.08.021. arXiv:1207.7235 [hep-ex]
6. S.L. Glashow, Partial-symmetries of weak interactions. Nucl. Phys. **22**, 579 (1961). https://doi.org/10.1016/0029-5582(61)90469-2
7. S. Weinberg, A model of leptons. Phys. Rev. Lett. **19**, 1264 (1967). https://doi.org/10.1103/PhysRevLett.19.1264
8. A. Salam, Weak and electromagnetic interactions. Conf. Proc. **C680519**, 367 (1968)
9. C. Englert et al., Precision measurements of Higgs couplings: implications for new physics scales. J. Phys. G **41**, 113001 (2014). https://doi.org/10.1088/0954-3899/41/11/113001. arXiv:1403.7191 [hep-ph]
10. ATLAS Collaboration, A detailed map of Higgs boson interactions by the ATLAS experiment ten years after the discovery. Nature **607**, 52 (2022). https://doi.org/10.1038/s41586-022-04893-w. arXiv:2207.00092 [hep-ex]. [Erratum: Nature **612**, E24 (2022)]. https://doi.org/10.1038/s41586-022-05581-5
11. CMS Collaboration, A portrait of the Higgs boson by the CMS experiment ten years after the discovery. Nature **607**, 60 (2022). https://doi.org/10.1038/s41586-022-04892-x. arXiv:2207.00043 [hep-ex]. [Erratum: Nature **623**, E4 (2023)]. https://doi.org/10.1038/s41586-023-06164-8
12. J.N. Ng, P. Zakarauskas, QCD-parton calculation of conjoined production of Higgs bosons and heavy flavors in $p\bar{p}$ collision. Phys. Rev. D **29**, 876 (1984). https://doi.org/10.1103/PhysRevD.29.876
13. Z. Kunszt, Associated production of heavy Higgs boson with top quarks. Nucl. Phys. B **247**, 339 (1984). https://doi.org/10.1016/0550-3213(84)90553-4
14. S. Dawson, L.H. Orr, L. Reina, D. Wackeroth, Next-to-leading order QCD corrections to $pp \to t\bar{t}h$ at the CERN Large Hadron Collider. Phys. Rev. D **67**, 071503 (2003). https://doi.org/10.1103/PhysRevD.67.071503. arXiv:hep-ph/0211438
15. W. Beenakker et al., Higgs radiation off top quarks at the tevatron and the LHC. Phys. Rev. Lett. **87**, 201805 (2001). https://doi.org/10.1103/PhysRevLett.87.201805. arXiv:hep-ph/0107081
16. ATLAS Collaboration, Observation of Higgs boson production in association with a top quark pair at the LHC with the ATLAS detector. Phys. Lett. B **784**, 173 (2018). https://doi.org/10.1016/j.physletb.2018.07.035. arXiv:1806.00425 [hep-ex]
17. CMS Collaboration, Observation of $t\bar{t}H$ production. Phys. Rev. Lett. **120**, 231801 (2018). https://doi.org/10.1103/PhysRevLett.120.231801. arXiv:1804.02610 [hep-ex]
18. D. de Florian et al., Handbook of LHC Higgs Cross Sections: 4. Deciphering the Nature of the Higgs Sector (2017). https://doi.org/10.23731/CYRM-2017-002. arXiv:1610.07922 [hep-ph]
19. L. Evans, P. Bryant, LHC machine. JINST **3**, S08001 (2008). https://doi.org/10.1088/1748-0221/3/08/S08001
20. ATLAS Collaboration, Measurement of Higgs boson decay into b-quarks in associated production with a top-quark pair in pp collisions at $\sqrt{s} = 13$ TeV with the ATLAS detector. JHEP. **06**, 097 (2022). https://doi.org/10.1007/JHEP06(2022)097. arXiv:2111.06712 [hep-ex]
21. CMS Collaboration, Measurement of the $\mathrm{t\bar{t}}H$ and tH production rates in the $H \to \mathrm{b\bar{b}}$ decay channel using proton-proton collision data at $\sqrt{s} = 13$ TeV (2024). arXiv:2407.10896 [hep-ex]
22. ATLAS Collaboration, Studies of Monte Carlo predictions for the $t\bar{t}b\bar{b}$ process. ATL-PHYS-PUB-2022-006 (2022). https://cds.cern.ch/record/2802806
23. ATLAS Collaboration, Study of $ttbb$ and ttW background modelling for ttH analyses, ATL-PHYS-PUB-2022-026 (2022). https://cds.cern.ch/record/2810864
24. ATLAS Collaboration, The ATLAS experiment at the CERN Large Hadron Collider. JINST. **3**, S08003 (2008). https://doi.org/10.1088/1748-0221/3/08/S08003
25. G. Avoni et al., The new LUCID-2 detector for luminosity measurement and monitoring in ATLAS. JINST **13**, P07017 (2018). https://doi.org/10.1088/1748-0221/13/07/P07017
26. ATLAS Collaboration, Performance of the ATLAS trigger system in 2015. Eur. Phys. J. C **77**, 317 (2017). https://doi.org/10.1140/epjc/s10052-017-4852-3. arXiv:1611.09661 [hep-ex]
27. ATLAS Collaboration, Software and computing for Run 3 of the ATLAS experiment at the LHC (2024). arXiv:2404.06335 [hep-ex]
28. ATLAS Collaboration, ATLAS data quality operations and performance for 2015–2018 data-taking. JINST **15**, P04003 (2020). https://doi.org/10.1088/1748-0221/15/04/P04003. arXiv:1911.04632 [physics.ins-det]
29. T. Sjöstrand, S. Mrenna, P. Skands, A brief introduction to PYTHIA 8.1. Comput. Phys. Commun. **178**, 852 (2008). https://doi.org/10.1016/j.cpc.2008.01.036. arXiv:0710.3820 [hep-ph]
30. ATLAS Collaboration, The Pythia 8 A3 tune description of ATLAS minimum bias and inelastic measurements incorporating the Donnachie–Landshoff diffractive model, ATL-PHYS-PUB-2016-017 (2016). https://cds.cern.ch/record/2206965
31. ATLAS Collaboration, The ATLAS simulation infrastructure. Eur. Phys. J. C **70**, 823 (2010). https://doi.org/10.1140/epjc/s10052-010-1429-9. arXiv:1005.4568 [physics.ins-det]
32. S. Agostinelli et al., GEANT4—a simulation toolkit. Nucl. Instrum. Methods A **506**, 250 (2003). https://doi.org/10.1016/S0168-9002(03)01368-8
33. P. Nason, A new method for combining NLO QCD with shower Monte Carlo algorithms. JHEP **11**, 040 (2004). https://doi.org/10.1088/1126-6708/2004/11/040. arXiv:hep-ph/0409146
34. S. Frixione, G. Ridolfi, P. Nason, A positive-weight next-to-leading-order Monte Carlo for heavy flavour hadroproduction. JHEP **09**, 126 (2007). https://doi.org/10.1088/1126-6708/2007/09/126. arXiv:0707.3088 [hep-ph]
35. S. Frixione, P. Nason, C. Oleari, Matching NLO QCD computations with parton shower simulations: the POWHEG method. JHEP **11**, 070 (2007). https://doi.org/10.1088/1126-6708/2007/11/070. arXiv:0709.2092 [hep-ph]
36. S. Alioli, P. Nason, C. Oleari, E. Re, A general framework for implementing NLO calculations in shower Monte Carlo programs: the POWHEG BOX. JHEP **06**, 043 (2010). https://doi.org/10.1007/JHEP06(2010)043. arXiv:1002.2581 [hep-ph]
37. J. Alwall et al., The automated computation of tree-level and next-to-leading order differential cross sections, and their matching to parton shower simulations. JHEP **07**, 079 (2014). https://doi.org/10.1007/JHEP07(2014)079. arXiv:1405.0301 [hep-ph]

38. T. Sjöstrand et al., An introduction to PYTHIA 8.2. Comput. Phys. Commun. **191**, 159 (2015). https://doi.org/10.1016/j.cpc.2015.01.024. arXiv:1410.3012 [hep-ph]
39. ATLAS Collaboration, ATLAS Pythia 8 tunes to 7 TeV data, ATL-PHYS-PUB-2014-021 (2014). https://cds.cern.ch/record/1966419
40. NNPDF Collaboration, R.D. Ball et al., Parton distributions for the LHC run II. JHEP **04**, 040 (2015). https://doi.org/10.1007/JHEP04(2015)040. arXiv:1410.8849 [hep-ph]
41. M. Bähr et al., Herwig++ physics and manual. Eur. Phys. J. C **58**, 639 (2008). https://doi.org/10.1140/epjc/s10052-008-0798-9. arXiv:0803.0883 [hep-ph]
42. J. Bellm et al., Herwig 7.0/Herwig++ 3.0 release note. Eur. Phys. J. C **76**, 196 (2016). https://doi.org/10.1140/epjc/s10052-016-4018-8. arXiv:1512.01178 [hep-ph]
43. L.A. Harland-Lang, A.D. Martin, P. Motylinski, R.S. Thorne, Parton distributions in the LHC era: MMHT 2014 PDFs. Eur. Phys. J. C **75**, 204 (2015). https://doi.org/10.1140/epjc/s10052-015-3397-6. arXiv:1412.3989 [hep-ph]
44. D.J. Lange, The EvtGen particle decay simulation package. Nucl. Instrum. Methods A **462**, 152 (2001). https://doi.org/10.1016/S0168-9002(01)00089-4
45. H.B. Hartanto, B. Jäger, L. Reina, D. Wackeroth, Higgs boson production in association with top quarks in the POWHEG BOX. Phys. Rev. D **91**, 094003 (2015). https://doi.org/10.1103/PhysRevD.91.094003. arXiv:1501.04498 [hep-ph]
46. S. Catani et al., Higgs boson production in association with a top-antitop quark pair in next-to-next-to-leading order QCD. Phys. Rev. Lett. **130**, 111902 (2023). https://doi.org/10.1103/physrevlett.130.111902. arXiv:2210.07846 [hep-ph]
47. ATLAS Collaboration, Studies on the improvement of the matching uncertainty definition in top-quark processes simulated with POWHEG+PYTHIA8, ATL-PHYS-PUB-2023-029 (2013). https://cds.cern.ch/record/2872787
48. S. Höche, S. Mrenna, S. Payne, C.T. Preuss, P. Skands, A study of QCD radiation in VBF Higgs production with Vincia and Pythia. SciPost Phys. **12**, 010 (2022). https://doi.org/10.21468/SciPostPhys.12.1.010. arXiv:2106.10987 [hep-ph]
49. ATLAS Collaboration, Search for the Standard Model Higgs boson produced in association with top quarks and decaying into $b\bar{b}$ in pp collisions at $\sqrt{s} = 8$ TeV with the ATLAS detector. Eur. Phys. J. C **75**, 349 (2015). https://doi.org/10.1140/epjc/s10052-015-3543-1. arXiv:1503.05066 [hep-ex]
50. M. Cacciari, G.P. Salam, G. Soyez, The anti-k_t jet clustering algorithm. JHEP **04**, 063 (2008). https://doi.org/10.1088/1126-6708/2008/04/063. arXiv:0802.1189 [hep-ph]
51. ATLAS Collaboration, Studies on top-quark Monte Carlo modelling for Top2016, ATL-PHYS-PUB-2016-020 (2016). https://cds.cern.ch/record/2216168
52. T. Ježo, J.M. Lindert, N. Moretti, S. Pozzorini, New NLOPS predictions for $t\bar{t} + b$-jet production at the LHC. Eur. Phys. J. C **78**, 502 (2018). https://doi.org/10.1140/epjc/s10052-018-5956-0. arXiv:1802.00426 [hep-ph]
53. F. Buccioni et al., OpenLoops 2. Eur. Phys. J. C **79**, 866 (2019). https://doi.org/10.1140/epjc/s10052-019-7306-2. arXiv:1907.13071 [hep-ph]
54. F. Cascioli, P. Maierhöfer, S. Pozzorini, Scattering amplitudes with open loops. Phys. Rev. Lett. **108**, 111601 (2012). https://doi.org/10.1103/PhysRevLett.108.111601. arXiv:1111.5206 [hep-ph]
55. A. Denner, S. Dittmaier, L. Hofer, COLLIER: a fortran-based complex one-loop library in extended regularizations. Comput. Phys. Commun. **212**, 220 (2017). https://doi.org/10.1016/j.cpc.2016.10.013. arXiv:1604.06792 [hep-ph]
56. T. Ježo, Powheg-Box-Res $ttbb$ source code (2019). https://gitlab.cern.ch/tjezo/powheg-box-res_ttbb/
57. E. Bothmann et al., Event generation with Sherpa 2.2. SciPost Phys. **7**, 034 (2019). https://doi.org/10.21468/SciPostPhys.7.3.034. arXiv:1905.09127 [hep-ph]
58. T. Gleisberg, S. Höche, Comix, a new matrix element generator. JHEP **12**, 039 (2008). https://doi.org/10.1088/1126-6708/2008/12/039. arXiv:0808.3674 [hep-ph]
59. S. Schumann, F. Krauss, A parton shower algorithm based on Catani–Seymour dipole factorisation. JHEP **03**, 038 (2008). https://doi.org/10.1088/1126-6708/2008/03/038. arXiv:0709.1027 [hep-ph]
60. S. Höche, F. Krauss, M. Schönherr, F. Siegert, A critical appraisal of NLO+PS matching methods. JHEP **09**, 049 (2012). https://doi.org/10.1007/JHEP09(2012)049. arXiv:1111.1220 [hep-ph]
61. S. Höche, F. Krauss, M. Schönherr, F. Siegert, QCD matrix elements + parton showers. The NLO case. JHEP **04**, 027 (2013). https://doi.org/10.1007/JHEP04(2013)027. arXiv:1207.5030 [hep-ph]
62. S. Catani, F. Krauss, B.R. Webber, R. Kuhn, QCD matrix elements + parton showers. JHEP **11**, 063 (2001). https://doi.org/10.1088/1126-6708/2001/11/063. arXiv:hep-ph/0109231
63. S. Höche, F. Krauss, S. Schumann, F. Siegert, QCD matrix elements and truncated showers. JHEP **05**, 053 (2009). https://doi.org/10.1088/1126-6708/2009/05/053. arXiv:0903.1219 [hep-ph]
64. E. Re, Single-top Wt-channel production matched with parton showers using the POWHEG method. Eur. Phys. J. C **71**, 1547 (2011). https://doi.org/10.1140/epjc/s10052-011-1547-z. arXiv:1009.2450 [hep-ph]
65. S. Alioli, P. Nason, C. Oleari, E. Re, NLO single-top production matched with shower in POWHEG: s- and t-channel contributions, JHEP **09**, 111 (2009). https://doi.org/10.1088/1126-6708/2009/09/111. arXiv:0907.4076 [hep-ph], Erratum: **02**, 011 (2010). https://doi.org/10.1007/JHEP02(2010)011JHEP
66. S. Frixione, E. Laenen, P. Motylinski, C. White, B.R. Webber, Single-top hadroproduction in association with a W boson. JHEP **07**, 029 (2008). https://doi.org/10.1088/1126-6708/2008/07/029. arXiv:0805.3067 [hep-ph]
67. ATLAS Collaboration, Studies of $t\bar{t}/tW$ interference effects in $b\bar{b}\ell^+\ell^-\nu\bar{\nu}'$ final states with POWHEG and MADGRAPH5_AMC@NLO setups, ATL-PHYS-PUB-2021-042 (2021). https://cds.cern.ch/record/2792254
68. T. Gleisberg et al., Event generation with SHERPA 1.1. JHEP **02**, 007 (2009). https://doi.org/10.1088/1126-6708/2009/02/007. arXiv:0811.4622 [hep-ph]
69. NNPDF Collaboration, R.D. Ball et al., Parton distributions from high-precision collider data. Eur. Phys. J. C 77, 663 (2017). https://doi.org/10.1140/epjc/s10052-017-5199-5. arXiv:1706.00428 [hep-ph]
70. R. Frederix, S. Frixione, Merging meets matching in MC@NLO. JHEP **12**, 061 (2012). https://doi.org/10.1007/JHEP12(2012)061. arXiv:1209.6215 [hep-ph]
71. L. Buonocore et al., Precise predictions for the associated production of a W boson with a top-antitop quark pair at the LHC. Phys. Rev. Lett. 131 (2023). https://doi.org/10.1103/physrevlett.131.231901. arXiv:2306.16311 [hep-ph]
72. M. Czakon, A. Mitov, Top++: a program for the calculation of the top-pair cross-section at hadron colliders. Comput. Phys. Commun. **185**, 2930 (2014). https://doi.org/10.1016/j.cpc.2014.06.021. arXiv:1112.5675 [hep-ph]
73. ATLAS Collaboration, Performance of the ATLAS muon triggers in Run 2. JINST **15**, P09015 (2020). https://doi.org/10.1088/1748-0221/15/09/p09015. arXiv:2004.13447 [physics.ins-det]
74. ATLAS Collaboration, Performance of electron and photon triggers in ATLAS during LHC Run 2. Eur. Phys. J. C **80**, 47 (2020). https://doi.org/10.1140/epjc/s10052-019-7500-2. arXiv:1909.00761 [hep-ex]

75. ATLAS Collaboration, Vertex Reconstruction Performance of the ATLAS Detector at $\sqrt{s} = 13$ TeV, ATL-PHYS-PUB-2015-026 (2015). https://cds.cern.ch/record/2037717
76. ATLAS Collaboration, Electron and photon performance measurements with the ATLAS detector using the 2015–2017 LHC proton–proton collision data. JINST **14**, P12006 (2019). https://doi.org/10.1088/1748-0221/14/12/P12006. arXiv:1908.00005 [hep-ex]
77. ATLAS Collaboration, Muon reconstruction and identification efficiency in ATLAS using the full Run 2 pp collision data set at $\sqrt{s} = 13$ TeV. Eur. Phys. J. C **81**, 578 (2021). https://doi.org/10.1140/epjc/s10052-021-09233-2. arXiv:2012.00578 [hep-ex]
78. ATLAS Collaboration, Jet reconstruction and performance using particle flow with the ATLAS detector. Eur. Phys. J. C **77**, 466 (2017). https://doi.org/10.1140/epjc/s10052-017-5031-2. arXiv:1703.10485 [hep-ex]
79. M. Cacciari, G.P. Salam, G. Soyez, FastJet user manual. Eur. Phys. J. C **72**, 1896 (2012). https://doi.org/10.1140/epjc/s10052-012-1896-2. arXiv:1111.6097 [hep-ph]
80. ATLAS Collaboration, Performance of pile-up mitigation techniques for jets in pp collisions at $\sqrt{s} = 8$ TeV using the ATLAS detector. Eur. Phys. J. C **76**, 581 (2016). https://doi.org/10.1140/epjc/s10052-016-4395-z. arXiv:1510.03823 [hep-ex]
81. ATLAS Collaboration, Jet energy scale and resolution measured in proton–proton collisions at $\sqrt{s} = 13$ TeV with the ATLAS detector. Eur. Phys. J. C **81**, 689 (2021). https://doi.org/10.1140/epjc/s10052-021-09402-3. arXiv:2007.02645 [hep-ex]
82. ATLAS Collaboration, ATLAS flavour-tagging algorithms for the LHC Run 2 pp collision dataset. Eur. Phys. J. C **83**, 681 (2023). https://doi.org/10.1140/epjc/s10052-023-11699-1. arXiv:2211.16345 [physics.data-an]
83. ATLAS Collaboration, Evidence for the $H \to b\bar{b}$ decay with the ATLAS detector. JHEP **12**, 024 (2017). https://doi.org/10.1007/JHEP12(2017)024. arXiv:1708.03299 [hep-ex]
84. ATLAS Collaboration, Identification of hadronic tau lepton decays using neural networks in the ATLAS experiment, ATL-PHYS-PUB-2019-033 (2019). https://cds.cern.ch/record/2688062
85. ATLAS Collaboration, The performance of missing transverse momentum reconstruction and its significance with the ATLAS detector using 140 fb^{-1} of $\sqrt{s} = 13$ TeV pp collisions (2024). arXiv:2402.05858 [hep-ex]
86. B. Nachman, P. Nef, A. Schwartzman, M. Swiatlowski, C. Wanotayaroj, Jets from jets: re-clustering as a tool for large radius jet reconstruction and grooming at the LHC. JHEP **02**, 075 (2015). https://doi.org/10.1007/JHEP02(2015)075. arXiv:1407.2922 [hep-ph]
87. ATLAS Collaboration, Measurements of top-quark pair differential and double-differential cross-sections in the ℓ+jets channel with pp collisions at $\sqrt{s} = 13$ TeV using the ATLAS detector. Eur. Phys. J. C **79**, 1028 (2019). https://doi.org/10.1140/epjc/s10052-019-7525-6. arXiv:1908.07305 [hep-ex]. [Erratum: Eur. Phys. J. C **80**, 1092 (2020)]. https://doi.org/10.1140/epjc/s10052-020-08541-3
88. ATLAS Collaboration, Tools for estimating fake/non-prompt lepton backgrounds with the ATLAS detector at the LHC. JINST **18**, T11004 (2023). https://doi.org/10.1088/1748-0221/18/11/T11004. arXiv:2211.16178 [hep-ex]
89. A. Vaswani et al., Attention Is All You Need (2023). arXiv:1706.03762 [cs.CL]
90. K. Cranmer, G. Lewis, L. Moneta, A. Shibata, W. Verkerke, HistFactory: a tool for creating statistical models for use with RooFit and RooStats, CERN-OPEN-2012-016 (2012). https://cds.cern.ch/record/1456844
91. W. Verkerke, D. Kirkby, The RooFit toolkit for data modeling (2003). arXiv:physics/0306116 [physics.data-an]
92. G. Cowan, K. Cranmer, E. Gross, O. Vitells, Asymptotic formulae for likelihood-based tests of new physics. Eur. Phys. J. C **71**, 1554 (2011). https://doi.org/10.1140/epjc/s10052-013-2501-z. arXiv:1007.1727 [physics.data-an]. [Erratum: Eur. Phys. J. C **73**, 2501 (2013)]. https://doi.org/10.1140/epjc/s10052-011-1554-0
93. ATLAS Collaboration, Luminosity determination in pp collisions at $\sqrt{s} = 13$ TeV using the ATLAS detector at the LHC. Eur. Phys. J. C **83**, 982 (2023). https://doi.org/10.1140/epjc/s10052-023-11747-w. arXiv:2212.09379 [hep-ex]
94. ATLAS Collaboration, ATLAS b-jet identification performance and efficiency measurement with $t\bar{t}$ events in pp collisions at $\sqrt{s} = 13$ TeV. Eur. Phys. J. C **79**, 970 (2019). https://doi.org/10.1140/epjc/s10052-019-7450-8. arXiv:1907.05120 [hep-ex]
95. ATLAS Collaboration, Measurement of the c-jet mistagging efficiency in $t\bar{t}$ events using pp collision data at $\sqrt{s} = 13$ TeV collected with the ATLAS detector. Eur. Phys. J. C **82**, 95 (2022). https://doi.org/10.1140/epjc/s10052-021-09843-w. arXiv:2109.10627 [hep-ex]
96. ATLAS Collaboration, Calibration of the light-flavour jet mistagging efficiency of the b-tagging algorithms with Z+jets events using 139 fb^{-1} of ATLAS proton–proton collision data at $\sqrt{s} = 13$ TeV. Eur. Phys. J. C **83**, 728 (2023). https://doi.org/10.1140/epjc/s10052-023-11736-z. arXiv:2301.06319 [hep-ex]
97. ATLAS Collaboration, Evaluation of QCD uncertainties for Higgs boson production through gluon fusion and in association with two top quarks for simplified template cross-section measurements, ATL-PHYS-PUB-2023-031 (2023). https://cds.cern.ch/record/2878797
98. N. Kidonakis, Next-to-next-to-leading-order collinear and soft gluon corrections for t-channel single top quark production. Phys. Rev. D **83**, 091503 (2011). https://doi.org/10.1103/PhysRevD.83.091503. arXiv:1103.2792 [hep-ph]
99. N. Kidonakis, Next-to-next-to-leading logarithm resummation for s-channel single top quark production. Phys. Rev. D **81**, 054028 (2010). https://doi.org/10.1103/PhysRevD.81.054028. arXiv:1001.5034 [hep-ph]
100. N. Kidonakis, N. Yamanaka, Higher-order corrections for tW production at high-energy hadron colliders. JHEP **05**, 278 (2021). https://doi.org/10.1007/JHEP05(2021)278. arXiv:2102.11300 [hep-ph]
101. M. van Beekveld, A. Kulesza, L.M. Valero, Threshold resummation for the production of four top quarks at the LHC (2022). arXiv:2212.03259 [hep-ph]
102. ATLAS Collaboration, Observation of four-top-quark production in the multilepton final state with the ATLAS detector. Eur. Phys. J. C **83**, 496 (2023). https://doi.org/10.1140/epjc/s10052-023-11573-0. arXiv:2303.15061 [hep-ex]

103. ATLAS Collaboration, Probing the CP nature of the top-Higgs Yukawa coupling in $t\bar{t}H$ and tH events with $H \to b\bar{b}$ decays using the ATLAS detector at the LHC. Phys. Lett. B **849**, 138469 (2023). https://doi.org/10.1016/j.physletb.2024.138469. arXiv:2303.05974 [hep-ex]
104. ATLAS Collaboration, Probing the CP nature of the top-Higgs Yukawa coupling in $t\bar{t}H$ and tH events with $H \to b\bar{b}$ decays using the ATLAS detector at the LHC. Phys. Lett. B **849**, 138469 (2024). https://doi.org/10.1016/j.physletb.2024.138469. arXiv:2303.05974 [hep-ex]
105. M. Grazzini, S. Kallweit, D. Rathlev, M. Wiesemann, $W^{\pm}Z$ production at hadron colliders in NNLO QCD. Phys. Lett. B **761**, 179 (2016). https://doi.org/10.1016/j.physletb.2016.08.017. arXiv:1604.08576 [hep-ph]
106. ATLAS Collaboration, Multi-boson simulation for 13 TeV ATLAS analyses, ATL-PHYS-PUB-2016-002 (2016). https://cds.cern.ch/record/2119986
107. ATLAS Collaboration, Measurement of $W^{\pm}Z$ production cross sections and gauge boson polarisation in pp collisions at $\sqrt{s} =$ 13 TeV with the ATLAS detector. Eur. Phys. J. C **79**, 535 (2019). https://doi.org/10.1140/epjc/s10052-019-7027-6. arXiv:1902.05759 [hep-ex]
108. ATLAS and CMS Collaborations, Combined measurement of the Higgs boson mass in pp collisions at $\sqrt{s} = 7$ and 8 TeV with the ATLAS and CMS experiments. Phys. Rev. Lett. **114**, 191803 (2015). https://doi.org/10.1103/PhysRevLett.114.191803. arXiv:1503.07589 [hep-ex]
109. S. Baker, R.D. Cousins, Clarification of the use of CHI-square and likelihood functions in fits to histograms. Nucl. Instrum. Methods **221**, 437 (1984). https://doi.org/10.1016/0167-5087(84)90016-4
110. R.D. Cousins, Lectures on Statistics in Theory: Prelude to Statistics in Practice (2024). arXiv:1807.05996 [physics.data-an]
111. ATLAS Collaboration, ATLAS Computing Acknowledgements, ATL-SOFT-PUB-2023-001 (2023). https://cds.cern.ch/record/2869272

ATLAS Collaboration*

G. Aad[104], E. Aakvaag[17], B. Abbott[123], S. Abdelhameed[119a], K. Abeling[56], N. J. Abicht[50], S. H. Abidi[30], M. Aboelela[45], A. Aboulhorma[36e], H. Abramowicz[155], H. Abreu[154], Y. Abulaiti[120], B. S. Acharya[70a,70b,k], A. Ackermann[64a], C. Adam Bourdarios[4], L. Adamczyk[87a], S. V. Addepalli[27], M. J. Addison[103], J. Adelman[118], A. Adiguzel[22c], T. Adye[137], A. A. Affolder[139], Y. Afik[40], M. N. Agaras[13], J. Agarwala[74a,74b], A. Aggarwal[102], C. Agheorghiesei[28c], F. Ahmadov[39,y], W. S. Ahmed[106], S. Ahuja[97], X. Ai[63e], G. Aielli[77a,77b], A. Aikot[166], M. Ait Tamlihat[36e], B. Aitbenchikh[36a], M. Akbiyik[102], T. P. A. Åkesson[100], A. V. Akimov[38], D. Akiyama[171], N. N. Akolkar[25], S. Aktas[22a], K. Al Khoury[42], G. L. Alberghi[24b], J. Albert[168], P. Albicocco[54], G. L. Albouy[61], S. Alderweireldt[53], Z. L. Alegria[124], M. Aleksa[37], I. N. Aleksandrov[39], C. Alexa[28b], T. Alexopoulos[10], F. Alfonsi[24b], M. Algren[57], M. Alhroob[170], B. Ali[135], H. M. J. Ali[93,s], S. Ali[32], S. W. Alibocus[94], M. Aliev[34c], G. Alimonti[72a], W. Alkakhi[56], C. Allaire[67], B. M. M. Allbrooke[150], J. S. Allen[103], J. F. Allen[53], C. A. Allendes Flores[140f], P. P. Allport[21], A. Aloisio[73a,73b], F. Alonso[92], C. Alpigiani[142], Z. M. K. Alsolami[93], M. Alvarez Estevez[101], A. Alvarez Fernandez[102], M. Alves Cardoso[57], M. G. Alviggi[73a,73b], M. Aly[103], Y. Amaral Coutinho[84b], A. Ambler[106], C. Amelung[37], M. Amerl[103], C. G. Ames[111], D. Amidei[108], B. Amini[55], K. J. Amirie[158], S. P. Amor Dos Santos[133a], K. R. Amos[166], D. Amperiadou[156], S. An[85], V. Ananiev[128], C. Anastopoulos[143], T. Andeen[11], J. K. Anders[37], A. C. Anderson[60], S. Y. Andrean[48a,48b], A. Andreazza[72a,72b], S. Angelidakis[9], A. Angerami[42], A. V. Anisenkov[38], A. Annovi[75a], C. Antel[57], E. Antipov[149], M. Antonelli[54], F. Anulli[76a], M. Aoki[85], T. Aoki[157], M. A. Aparo[150], L. Aperio Bella[49], C. Appelt[19], A. Apyan[27], S. J. Arbiol Val[88], C. Arcangeletti[54], A. T. H. Arce[52], J.-F. Arguin[110], S. Argyropoulos[156], J.-H. Arling[49], O. Arnaez[4], H. Arnold[149], G. Artoni[76a,76b], H. Asada[113], K. Asai[121], S. Asai[157], N. A. Asbah[37], R. A. Ashby Pickering[170], K. Assamagan[30], R. Astalos[29a], K. S. V. Astrand[100], S. Atashi[162], R. J. Atkin[34a], M. Atkinson[165], H. Atmani[36f], P. A. Atmasiddha[131], K. Augsten[135], S. Auricchio[73a,73b], A. D. Auriol[21], V. A. Austrup[103], G. Avolio[37], K. Axiotis[57], G. Azuelos[110,ad], D. Babal[29b], H. Bachacou[138], K. Bachas[156,o], A. Bachiu[35], E. Bachmann[51], F. Backman[48a,48b], A. Badea[40], T. M. Baer[108], P. Bagnaia[76a,76b], M. Bahmani[19], D. Bahner[55], K. Bai[126], J. T. Baines[137], L. Baines[96], O. K. Baker[175], E. Bakos[16], D. Bakshi Gupta[8], L. E. Balabram Filho[84b], V. Balakrishnan[123], R. Balasubramanian[4], E. M. Baldin[38], P. Balek[87a], E. Ballabene[24a,24b], F. Balli[138], L. M. Baltes[64a], W. K. Balunas[33], J. Balz[102], I. Bamwidhi[119b], E. Banas[88], M. Bandieramonte[132], A. Bandyopadhyay[25], S. Bansal[25], L. Barak[155], M. Barakat[49], E. L. Barberio[107], D. Barberis[58a,58b], M. Barbero[104], M. Z. Barel[117], T. Barillari[112], M.-S. Barisits[37], T. Barklow[147], P. Baron[125], D. A. Baron Moreno[103], A. Baroncelli[63a], A. J. Barr[129], J. D. Barr[98], F. Barreiro[101], J. Barreiro Guimarães da Costa[14], U. Barron[155], M. G. Barros Teixeira[133a], S. Barsov[38], F. Bartels[64a], R. Bartoldus[147], A. E. Barton[93], P. Bartos[29a], A. Basan[102], M. Baselga[50], A. Bassalat[67,b], M. J. Basso[159a], S. Bataju[45], R. Bate[167], R. L. Bates[60], S. Batlamous[101], B. Batool[145], M. Battaglia[139], D. Battulga[19], M. Bauce[76a,76b], M. Bauer[80], P. Bauer[25], L. T. Bazzano Hurrell[31], J. B. Beacham[52],

T. Beau[130], J. Y. Beaucamp[92], P. H. Beauchemin[161], P. Bechtle[25], H. P. Beck[20,n], K. Becker[170], A. J. Beddall[83], V. A. Bednyakov[39], C. P. Bee[149], L. J. Beemster[16], T. A. Beermann[37], M. Begalli[84d], M. Begel[30], A. Behera[149], J. K. Behr[49], J. F. Beirer[37], F. Beisiegel[25], M. Belfkir[119b], G. Bella[155], L. Bellagamba[24b], A. Bellerive[35], P. Bellos[21], K. Beloborodov[38], D. Benchekroun[36a], F. Bendebba[36a], Y. Benhammou[155], K. C. Benkendorfer[62], L. Beresford[49], M. Beretta[54], E. Bergeaas Kuutmann[164], N. Berger[4], B. Bergmann[135], J. Beringer[18a], G. Bernardi[5], C. Bernius[147], F. U. Bernlochner[25], F. Bernon[37], A. Berrocal Guardia[13], T. Berry[97], P. Berta[136], A. Berthold[51], S. Bethke[112], A. Betti[76a,76b], A. J. Bevan[96], N. K. Bhalla[55], S. Bhatta[149], D. S. Bhattacharya[169], P. Bhattarai[147], K. D. Bhide[55], V. S. Bhopatkar[124], R. M. Bianchi[132], G. Bianco[24a,24b], O. Biebel[111], R. Bielski[126], M. Biglietti[78a], C. S. Billingsley[45], Y. Bimgdi[36f], M. Bindi[56], A. Bingul[22b], C. Bini[76a,76b], G. A. Bird[33], M. Birman[172], M. Biros[136], S. Biryukov[150], T. Bisanz[50], E. Bisceglie[44a,44b], J. P. Biswal[137], D. Biswas[145], I. Bloch[49], A. Blue[60], U. Blumenschein[96], J. Blumenthal[102], V. S. Bobrovnikov[38], M. Boehler[55], B. Boehm[169], D. Bogavac[37], A. G. Bogdanchikov[38], L. S. Boggia[130], C. Bohm[48a], V. Boisvert[97], P. Bokan[37], T. Bold[87a], M. Bomben[5], M. Bona[96], M. Boonekamp[138], C. D. Booth[97], A. G. Borbély[60], I. S. Bordulev[38], G. Borissov[93], D. Bortoletto[129], D. Boscherini[24b], M. Bosman[13], J. D. Bossio Sola[37], K. Bouaouda[36a], N. Bouchhar[166], L. Boudet[4], J. Boudreau[132], E. V. Bouhova-Thacker[93], D. Boumediene[41], R. Bouquet[58a,58b], A. Boveia[122], J. Boyd[37], D. Boye[30], I. R. Boyko[39], L. Bozianu[57], J. Bracinik[21], N. Brahimi[4], G. Brandt[174], O. Brandt[33], F. Braren[49], B. Brau[105], J. E. Brau[126], R. Brener[172], L. Brenner[117], R. Brenner[164], S. Bressler[172], G. Brianti[79a,79b], D. Britton[60], D. Britzger[112], I. Brock[25], R. Brock[109], G. Brooijmans[42], E. M. Brooks[159b], E. Brost[30], L. M. Brown[168], L. E. Bruce[62], T. L. Bruckler[129], P. A. Bruckman de Renstrom[88], B. Brüers[49], A. Bruni[24b], G. Bruni[24b], M. Bruschi[24b], N. Bruscino[76a,76b], T. Buanes[17], Q. Buat[142], D. Buchin[112], A. G. Buckley[60], O. Bulekov[38], B. A. Bullard[147], S. Burdin[94], C. D. Burgard[50], A. M. Burger[37], B. Burghgrave[8], O. Burlayenko[55], J. Burleson[165], J. T. P. Burr[33], J. C. Burzynski[146], E. L. Busch[42], V. Büscher[102], P. J. Bussey[60], J. M. Butler[26], C. M. Buttar[60], J. M. Butterworth[98], W. Buttinger[137], C. J. Buxo Vazquez[109], A. R. Buzykaev[38], S. Cabrera Urbán[166], L. Cadamuro[67], D. Caforio[59], H. Cai[132], Y. Cai[14,114c], Y. Cai[114a], V. M. M. Cairo[37], O. Cakir[3a], N. Calace[37], P. Calafiura[18a], G. Calderini[130], P. Calfayan[69], G. Callea[60], L. P. Caloba[84b], D. Calvet[41], S. Calvet[41], M. Calvetti[75a,75b], R. Camacho Toro[130], S. Camarda[37], D. Camarero Munoz[27], P. Camarri[77a,77b], M. T. Camerlingo[73a,73b], D. Cameron[37], C. Camincher[168], M. Campanelli[98], A. Camplani[43], V. Canale[73a,73b], A. C. Canbay[3a], E. Canonero[97], J. Cantero[166], Y. Cao[165], F. Capocasa[27], M. Capua[44a,44b], A. Carbone[72a,72b], R. Cardarelli[77a], J. C. J. Cardenas[8], G. Carducci[44a,44b], T. Carli[37], G. Carlino[73a], J. I. Carlotto[13], B. T. Carlson[132,p], E. M. Carlson[159a,168], J. Carmignani[94], L. Carminati[72a,72b], A. Carnelli[138], M. Carnesale[37], S. Caron[116], E. Carquin[140f], I. B. Carr[107], S. Carrá[72a], G. Carratta[24a,24b], A. M. Carroll[126], M. P. Casado[13,h], M. Caspar[49], F. L. Castillo[4], L. Castillo Garcia[13], V. Castillo Gimenez[166], N. F. Castro[133a,133e], A. Catinaccio[37], J. R. Catmore[128], T. Cavaliere[4], V. Cavaliere[30], N. Cavalli[24a,24b], L. J. Caviedes Betancourt[23b], Y. C. Cekmecelioglu[49], E. Celebi[83], S. Cella[37], M. S. Centonze[71a,71b], V. Cepaitis[57], K. Cerny[125], A. S. Cerqueira[84a], A. Cerri[150], L. Cerrito[77a,77b], F. Cerutti[18a], B. Cervato[145], A. Cervelli[24b], G. Cesarini[54], S. A. Cetin[83], D. Chakraborty[118], J. Chan[18a], W. Y. Chan[157], J. D. Chapman[33], E. Chapon[138], B. Chargeishvili[153b], D. G. Charlton[21], M. Chatterjee[20], C. Chauhan[136], Y. Che[114a], S. Chekanov[6], S. V. Chekulaev[159a], G. A. Chelkov[39,a], A. Chen[108], B. Chen[155], B. Chen[168], H. Chen[114a], H. Chen[30], J. Chen[63c], J. Chen[146], M. Chen[129], S. Chen[89], S. J. Chen[114a], X. Chen[63c], X. Chen[15,ac], Y. Chen[63a], C. L. Cheng[173], H. C. Cheng[65a], S. Cheong[147], A. Cheplakov[39], E. Cheremushkina[49], E. Cherepanova[117], R. Cherkaoui El Moursli[36e], E. Cheu[7], K. Cheung[66], L. Chevalier[138], V. Chiarella[54], G. Chiarelli[75a], N. Chiedde[104], G. Chiodini[71a], A. S. Chisholm[21], A. Chitan[28b], M. Chitishvili[166], M. V. Chizhov[39,q], K. Choi[11], Y. Chou[142], E. Y. S. Chow[116], K. L. Chu[172], M. C. Chu[65a], X. Chu[14,114c], Z. Chubinidze[54], J. Chudoba[134], J. J. Chwastowski[88], D. Cieri[112], K. M. Ciesla[87a], V. Cindro[95], A. Ciocio[18a], F. Cirotto[73a,73b], Z. H. Citron[172], M. Citterio[72a], D. A. Ciubotaru[28b], A. Clark[57], P. J. Clark[53], N. Clarke Hall[98], C. Clarry[158], J. M. Clavijo Columbie[49], S. E. Clawson[49], C. Clement[48a,48b], Y. Coadou[104], M. Cobal[70a,70c], A. Coccaro[58b], R. F. Coelho Barrue[133a], R. Coelho Lopes De Sa[105], S. Coelli[72a], L. S. Colangeli[158], B. Cole[42], J. Collot[61], P. Conde Muiño[133a,133g], M. P. Connell[34c], S. H. Connell[34c], E. I. Conroy[129], F. Conventi[73a,ae], H. G. Cooke[21], A. M. Cooper-Sarkar[129], F. A. Corchia[24a,24b], A. Cordeiro Oudot Choi[130], L. D. Corpe[41], M. Corradi[76a,76b], F. Corriveau[106,x], A. Cortes-Gonzalez[19], M. J. Costa[166], F. Costanza[4], D. Costanzo[143], B. M. Cote[122], J. Couthures[4], G. Cowan[97], K. Cranmer[173], L. Cremer[50], D. Cremonini[24a,24b], S. Crépé-Renaudin[61],

F. Crescioli[130], M. Cristinziani[145], M. Cristoforetti[79a,79b], V. Croft[117], J. E. Crosby[124], G. Crosetti[44a,44b], A. Cueto[101], H. Cui[98], Z. Cui[7], W. R. Cunningham[60], F. Curcio[166], J. R. Curran[53], P. Czodrowski[37], M. J. Da Cunha Sargedas De Sousa[58a,58b], J. V. Da Fonseca Pinto[84b], C. Da Via[103], W. Dabrowski[87a], T. Dado[37], S. Dahbi[152], T. Dai[108], D. Dal Santo[20], C. Dallapiccola[105], M. Dam[43], G. D'amen[30], V. D'Amico[111], J. Damp[102], J. R. Dandoy[35], D. Dannheim[37], M. Danninger[146], V. Dao[149], G. Darbo[58b], S. J. Das[30], F. Dattola[49], S. D'Auria[72a,72b], A. D'Avanzo[73a,73b], C. David[34a], T. Davidek[136], I. Dawson[96], H. A. Day-hall[135], K. De[8], R. De Asmundis[73a], N. De Biase[49], S. De Castro[24a,24b], N. De Groot[116], P. de Jong[117], H. De la Torre[118], A. De Maria[114a], A. De Salvo[76a], U. De Sanctis[77a,77b], F. De Santis[71a,71b], A. De Santo[150], J. B. De Vivie De Regie[61], J. Debevc[95], D. V. Dedovich[39], J. Degens[94], A. M. Deiana[45], F. Del Corso[24a,24b], J. Del Peso[101], L. Delagrange[130], F. Deliot[138], C. M. Delitzsch[50], M. Della Pietra[73a,73b], D. Della Volpe[57], A. Dell'Acqua[37], L. Dell'Asta[72a,72b], M. Delmastro[4], P. A. Delsart[61], S. Demers[175], M. Demichev[39], S. P. Denisov[38], L. D'Eramo[41], D. Derendarz[88], F. Derue[130], P. Dervan[94], K. Desch[25], C. Deutsch[25], F. A. Di Bello[58a,58b], A. Di Ciaccio[77a,77b], L. Di Ciaccio[4], A. Di Domenico[76a,76b], C. Di Donato[73a,73b], A. Di Girolamo[37], G. Di Gregorio[37], A. Di Luca[79a,79b], B. Di Micco[78a,78b], R. Di Nardo[78a,78b], K. F. Di Petrillo[40], M. Diamantopoulou[35], F. A. Dias[117], T. Dias Do Vale[146], M. A. Diaz[140a,140b], F. G. Diaz Capriles[25], A. R. Didenko[39], M. Didenko[166], E. B. Diehl[108], S. Díez Cornell[49], C. Diez Pardos[145], C. Dimitriadi[164], A. Dimitrievska[21], J. Dingfelder[25], T. Dingley[129], I.-M. Dinu[28b], S. J. Dittmeier[64b], F. Dittus[37], M. Divisek[136], B. Dixit[94], F. Djama[104], T. Djobava[153b], C. Doglioni[100,103], A. Dohnalova[29a], J. Dolejsi[136], Z. Dolezal[136], K. Domijan[87a], K. M. Dona[40], M. Donadelli[84d], B. Dong[109], J. Donini[41], A. D'Onofrio[73a,73b], M. D'Onofrio[94], J. Dopke[137], A. Doria[73a], N. Dos Santos Fernandes[133a], P. Dougan[103], M. T. Dova[92], A. T. Doyle[60], M. A. Draguet[129], M. P. Drescher[56], E. Dreyer[172], I. Drivas-koulouris[10], M. Drnevich[120], M. Drozdova[57], D. Du[63a], T. A. du Pree[117], F. Dubinin[38], M. Dubovsky[29a], E. Duchovni[172], G. Duckeck[111], O. A. Ducu[28b], D. Duda[53], A. Dudarev[37], E. R. Duden[27], M. D'uffizi[103], L. Duflot[67], M. Dührssen[37], I. Duminica[28g], A. E. Dumitriu[28b], M. Dunford[64a], S. Dungs[50], K. Dunne[48a,48b], A. Duperrin[104], H. Duran Yildiz[3a], M. Düren[59], A. Durglishvili[153b], B. L. Dwyer[118], G. I. Dyckes[18a], M. Dyndal[87a], B. S. Dziedzic[37], Z. O. Earnshaw[150], G. H. Eberwein[129], B. Eckerova[29a], S. Eggebrecht[56], E. Egidio Purcino De Souza[84e], L. F. Ehrke[57], G. Eigen[17], K. Einsweiler[18a], T. Ekelof[164], P. A. Ekman[100], S. El Farkh[36b], Y. El Ghazali[63a], H. El Jarrari[37], A. El Moussaouy[36a], V. Ellajosyula[164], M. Ellert[164], F. Ellinghaus[174], N. Ellis[37], J. Elmsheuser[30], M. Elsawy[119a], M. Elsing[37], D. Emeliyanov[137], Y. Enari[85], I. Ene[18a], S. Epari[13], P. A. Erland[88], D. Ernani Martins Neto[88], M. Errenst[174], M. Escalier[67], C. Escobar[166], E. Etzion[155], G. Evans[133a], H. Evans[69], L. S. Evans[97], A. Ezhilov[38], S. Ezzarqtouni[36a], F. Fabbri[24a,24b], L. Fabbri[24a,24b], G. Facini[98], V. Fadeyev[139], R. M. Fakhrutdinov[38], D. Fakoudis[102], S. Falciano[76a], L. F. Falda Ulhoa Coelho[37], F. Fallavollita[112], G. Falsetti[44a,44b], J. Faltova[136], C. Fan[165], K. Y. Fan[65b], Y. Fan[14], Y. Fang[14,114c], M. Fanti[72a,72b], M. Faraj[70a,70b], Z. Farazpay[99], A. Farbin[8], A. Farilla[78a], T. Farooque[109], S. M. Farrington[53], F. Fassi[36e], D. Fassouliotis[9], M. Faucci Giannelli[77a,77b], W. J. Fawcett[33], L. Fayard[67], P. Federic[136], P. Federicova[134], O. L. Fedin[38,a], M. Feickert[173], L. Feligioni[104], D. E. Fellers[126], C. Feng[63b], Z. Feng[117], M. J. Fenton[162], L. Ferencz[49], R. A. M. Ferguson[93], S. I. Fernandez Luengo[140f], P. Fernandez Martinez[68], M. J. V. Fernoux[104], J. Ferrando[93], A. Ferrari[164], P. Ferrari[116,117], R. Ferrari[74a], D. Ferrere[57], C. Ferretti[108], D. Fiacco[76a,76b], F. Fiedler[102], P. Fiedler[135], S. Filimonov[38], A. Filipčič[95], E. K. Filmer[159a], F. Filthaut[116], M. C. N. Fiolhais[133a,133c,c], L. Fiorini[166], W. C. Fisher[109], T. Fitschen[103], P. M. Fitzhugh[138], I. Fleck[145], P. Fleischmann[108], T. Flick[174], M. Flores[34d,aa], L. R. Flores Castillo[65a], L. Flores Sanz De Acedo[37], F. M. Follega[79a,79b], N. Fomin[33], J. H. Foo[158], A. Formica[138], A. C. Forti[103], E. Fortin[37], A. W. Fortman[18a], M. G. Foti[18a], L. Fountas[9,i], D. Fournier[67], H. Fox[93], P. Francavilla[75a,75b], S. Francescato[62], S. Franchellucci[57], M. Franchini[24a,24b], S. Franchino[64a], D. Francis[37], L. Franco[116], V. Franco Lima[37], L. Franconi[49], M. Franklin[62], G. Frattari[27], Y. Y. Frid[155], J. Friend[60], N. Fritzsche[37], A. Froch[55], D. Froidevaux[37], J. A. Frost[129], Y. Fu[63a], S. Fuenzalida Garrido[140f], M. Fujimoto[104], K. Y. Fung[65a], E. Furtado De Simas Filho[84e], M. Furukawa[157], J. Fuster[166], A. Gaa[56], A. Gabrielli[24a,24b], A. Gabrielli[158], P. Gadow[37], G. Gagliardi[58a,58b], L. G. Gagnon[18a], S. Gaid[163], S. Galantzan[155], J. Gallagher[1], E. J. Gallas[129], B. J. Gallop[137], K. K. Gan[122], S. Ganguly[157], Y. Gao[53], F. M. Garay Walls[140a,140b], B. Garcia[30], C. García[166], A. Garcia Alonso[117], A. G. Garcia Caffaro[175], J. E. García Navarro[166], M. Garcia-Sciveres[18a], G. L. Gardner[131], R. W. Gardner[40], N. Garelli[161], D. Garg[81], R. B. Garg[147], J. M. Gargan[53], C. A. Garner[158], C. M. Garvey[34a], V. K. Gassmann[161], G. Gaudio[74a], V. Gautam[13], P. Gauzzi[76a,76b], J. Gavranovic[95], I. L. Gavrilenko[38], A. Gavrilyuk[38], C. Gay[167], G. Gaycken[126],

E. N. Gazis[10], A. A. Geanta[28b], C. M. Gee[139], A. Gekow[122], C. Gemme[58b], M. H. Genest[61], A. D. Gentry[115], S. George[97], W. F. George[21], T. Geralis[47], P. Gessinger-Befurt[37], M. E. Geyik[174], M. Ghani[170], K. Ghorbanian[96], A. Ghosal[145], A. Ghosh[162], A. Ghosh[7], B. Giacobbe[24b], S. Giagu[76a,76b], T. Giani[117], A. Giannini[63a], S. M. Gibson[97], M. Gignac[139], D. T. Gil[87b], A. K. Gilbert[87a], B. J. Gilbert[42], D. Gillberg[35], G. Gilles[117], L. Ginabat[130], D. M. Gingrich[2,ad], M. P. Giordani[70a,70c], P. F. Giraud[138], G. Giugliarelli[70a,70c], D. Giugni[72a], F. Giuli[77a,77b], I. Gkialas[9,i], L. K. Gladilin[38], C. Glasman[101], G. R. Gledhill[126], G. Glemža[49], M. Glisic[126], I. Gnesi[44b], Y. Go[30], M. Goblirsch-Kolb[37], B. Gocke[50], D. Godin[110], B. Gokturk[22a], S. Goldfarb[107], T. Golling[57], M. G. D. Gololo[34g], D. Golubkov[38], J. P. Gombas[109], A. Gomes[133a,133b], G. Gomes Da Silva[145], A. J. Gomez Delegido[166], R. Gonçalo[133a], L. Gonella[21], A. Gongadze[153c], F. Gonnella[21], J. L. Gonski[147], R. Y. González Andana[53], S. González de la Hoz[166], R. Gonzalez Lopez[94], C. Gonzalez Renteria[18a], M. V. Gonzalez Rodrigues[49], R. Gonzalez Suarez[164], S. Gonzalez-Sevilla[57], L. Goossens[37], B. Gorini[37], E. Gorini[71a,71b], A. Gorišek[95], T. C. Gosart[131], A. T. Goshaw[52], M. I. Gostkin[39], S. Goswami[124], C. A. Gottardo[37], S. A. Gotz[111], M. Gouighri[36b], V. Goumarre[49], A. G. Goussiou[142], N. Govender[34c], R. P. Grabarczyk[129], I. Grabowska-Bold[87a], K. Graham[35], E. Gramstad[128], S. Grancagnolo[71a,71b], C. M. Grant[1,138], P. M. Gravila[28f], F. G. Gravili[71a,71b], H. M. Gray[18a], M. Greco[71a,71b], M. J. Green[1], C. Grefe[25], A. S. Grefsrud[17], I. M. Gregor[49], K. T. Greif[162], P. Grenier[147], S. G. Grewe[112], A. A. Grillo[139], K. Grimm[32], S. Grinstein[13,t], J.-F. Grivaz[67], E. Gross[172], J. Grosse-Knetter[56], L. Guan[108], J. G. R. Guerrero Rojas[166], G. Guerrieri[37], R. Gugel[102], J. A. M. Guhit[108], A. Guida[19], E. Guilloton[170], S. Guindon[37], F. Guo[14,114c], J. Guo[63c], L. Guo[49], L. Guo[14], Y. Guo[108], A. Gupta[50], R. Gupta[132], S. Gurbuz[25], S. S. Gurdasani[55], G. Gustavino[76a,76b], P. Gutierrez[123], L. F. Gutierrez Zagazeta[131], M. Gutsche[51], C. Gutschow[98], C. Gwenlan[129], C. B. Gwilliam[94], E. S. Haaland[128], A. Haas[120], M. Habedank[60], C. Haber[18a], H. K. Hadavand[8], A. Hadef[51], S. Hadzic[112], A. I. Hagan[93], J. J. Hahn[145], E. H. Haines[98], M. Haleem[169], J. Haley[124], G. D. Hallewell[104], L. Halser[20], K. Hamano[168], M. Hamer[25], E. J. Hampshire[97], J. Han[63b], L. Han[114a], L. Han[63a], S. Han[18a], Y. F. Han[158], K. Hanagaki[85], M. Hance[139], D. A. Hangal[42], H. Hanif[146], M. D. Hank[131], J. B. Hansen[43], P. H. Hansen[43], D. Harada[57], T. Harenberg[174], S. Harkusha[176], M. L. Harris[105], Y. T. Harris[25], J. Harrison[13], N. M. Harrison[122], P. F. Harrison[170], N. M. Hartman[112], N. M. Hartmann[111], R. Z. Hasan[97,137], Y. Hasegawa[144], F. Haslbeck[129], S. Hassan[17], R. Hauser[109], C. M. Hawkes[21], R. J. Hawkings[37], Y. Hayashi[157], D. Hayden[109], C. Hayes[108], R. L. Hayes[117], C. P. Hays[129], J. M. Hays[96], H. S. Hayward[94], F. He[63a], M. He[14,114c], Y. He[49], Y. He[98], N. B. Heatley[96], V. Hedberg[100], A. L. Heggelund[128], N. D. Hehir[96,*], C. Heidegger[55], K. K. Heidegger[55], J. Heilman[35], S. Heim[49], T. Heim[18a], J. G. Heinlein[131], J. J. Heinrich[126], L. Heinrich[112,ab], J. Hejbal[134], A. Held[173], S. Hellesund[17], C. M. Helling[167], S. Hellman[48a,48b], R. C. W. Henderson[93], L. Henkelmann[33], A. M. Henriques Correia[37], H. Herde[100], Y. Hernández Jiménez[149], L. M. Herrmann[25], T. Herrmann[51], G. Herten[55], R. Hertenberger[111], L. Hervas[37], M. E. Hesping[102], N. P. Hessey[159a], J. Hessler[112], M. Hidaoui[36b], N. Hidic[136], E. Hill[158], S. J. Hillier[21], J. R. Hinds[109], F. Hinterkeuser[25], M. Hirose[127], S. Hirose[160], D. Hirschbuehl[174], T. G. Hitchings[103], B. Hiti[95], J. Hobbs[149], R. Hobincu[28e], N. Hod[172], M. C. Hodgkinson[143], B. H. Hodkinson[129], A. Hoecker[37], D. D. Hofer[108], J. Hofer[166], T. Holm[25], M. Holzbock[37], L. B. A. H. Hommels[33], B. P. Honan[103], J. J. Hong[69], J. Hong[63c], T. M. Hong[132], B. H. Hooberman[165], W. H. Hopkins[6], M. C. Hoppesch[165], Y. Horii[113], M. E. Horstmann[112], S. Hou[152], A. S. Howard[95], J. Howarth[60], J. Hoya[6], M. Hrabovsky[125], A. Hrynevich[49], T. Hryn'ova[4], P. J. Hsu[66], S.-C. Hsu[142], T. Hsu[67], M. Hu[18a], Q. Hu[63a], S. Huang[33], X. Huang[14,114c], Y. Huang[143], Y. Huang[102], Y. Huang[14], Z. Huang[103], Z. Hubacek[135], M. Huebner[25], F. Huegging[25], T. B. Huffman[129], M. Hufnagel Maranha De Faria[84a], C. A. Hugli[49], M. Huhtinen[37], S. K. Huiberts[17], R. Hulsken[106], N. Huseynov[12,f], J. Huston[109], J. Huth[62], R. Hyneman[147], G. Iacobucci[57], G. Iakovidis[30], L. Iconomidou-Fayard[67], J. P. Iddon[37], P. Iengo[73a,73b], R. Iguchi[157], Y. Iiyama[157], T. Iizawa[129], Y. Ikegami[85], N. Ilic[158], H. Imam[84c], G. Inacio Goncalves[84d], T. Ingebretsen Carlson[48a,48b], J. M. Inglis[96], G. Introzzi[74a,74b], M. Iodice[78a], V. Ippolito[76a,76b], R. K. Irwin[94], M. Ishino[157], W. Islam[173], C. Issever[19], S. Istin[22a,ah], H. Ito[171], R. Iuppa[79a,79b], A. Ivina[172], J. M. Izen[46], V. Izzo[73a], P. Jacka[134], P. Jackson[1], C. S. Jagfeld[111], G. Jain[159a], P. Jain[49], K. Jakobs[55], T. Jakoubek[172], J. Jamieson[60], W. Jang[157], M. Javurkova[105], P. Jawahar[103], L. Jeanty[126], J. Jejelava[153a,z], P. Jenni[55,e], C. E. Jessiman[35], C. Jia[63b], H. Jia[167], J. Jia[149], X. Jia[14,114c], Z. Jia[114a], C. Jiang[53], S. Jiggins[49], J. Jimenez Pena[13], S. Jin[114a], A. Jinaru[28b], O. Jinnouchi[141], P. Johansson[143], K. A. Johns[7], J. W. Johnson[139], F. A. Jolly[49], D. M. Jones[150], E. Jones[49], K. S. Jones[8], P. Jones[33], R. W. L. Jones[93], T. J. Jones[94], H. L. Joos[37,56], R. Joshi[122],

J. Jovicevic[16], X. Ju[18a], J. J. Junggeburth[105], T. Junkermann[64a], A. Juste Rozas[13,t], M. K. Juzek[88], S. Kabana[140e], A. Kaczmarska[88], M. Kado[112], H. Kagan[122], M. Kagan[147], A. Kahn[131], C. Kahra[102], T. Kaji[157], E. Kajomovitz[154], N. Kakati[172], I. Kalaitzidou[55], C. W. Kalderon[30], N. J. Kang[139], D. Kar[34g], K. Karava[129], M. J. Kareem[159b], E. Karentzos[55], O. Karkout[117], S. N. Karpov[39], Z. M. Karpova[39], V. Kartvelishvili[93], A. N. Karyukhin[38], E. Kasimi[156], J. Katzy[49], S. Kaur[35], K. Kawade[144], M. P. Kawale[123], C. Kawamoto[89], T. Kawamoto[63a], E. F. Kay[37], F. I. Kaya[161], S. Kazakos[109], V. F. Kazanin[38], Y. Ke[149], J. M. Keaveney[34a], R. Keeler[168], G. V. Kehris[62], J. S. Keller[35], J. J. Kempster[150], O. Kepka[134], B. P. Kerridge[137], S. Kersten[174], B. P. Kerševan[95], L. Keszeghova[29a], S. Ketabchi Haghighat[158], R. A. Khan[132], A. Khanov[124], A. G. Kharlamov[38], T. Kharlamova[38], E. E. Khoda[142], M. Kholodenko[133a], T. J. Khoo[19], G. Khoriauli[169], J. Khubua[153b,*], Y. A. R. Khwaira[130], B. Kibirige[34g], D. Kim[6], D. W. Kim[48a,48b], Y. K. Kim[40], N. Kimura[98], M. K. Kingston[56], A. Kirchhoff[56], C. Kirfel[25], F. Kirfel[25], J. Kirk[137], A. E. Kiryunin[112], S. Kita[160], C. Kitsaki[10], O. Kivernyk[25], M. Klassen[161], C. Klein[35], L. Klein[169], M. H. Klein[45], S. B. Klein[57], U. Klein[94], A. Klimentov[30], T. Klioutchnikova[37], P. Kluit[117], S. Kluth[112], E. Kneringer[80], T. M. Knight[158], A. Knue[50], D. Kobylianskii[172], S. F. Koch[129], M. Kocian[147], P. Kodyš[136], D. M. Koeck[126], P. T. Koenig[25], T. Koffas[35], O. Kolay[51], I. Koletsou[4], T. Komarek[88], K. Köneke[55], A. X. Y. Kong[1], T. Kono[121], N. Konstantinidis[98], P. Kontaxakis[57], B. Konya[100], R. Kopeliansky[42], S. Koperny[87a], K. Korcyl[88], K. Kordas[156,d], A. Korn[98], S. Korn[56], I. Korolkov[13], N. Korotkova[38], B. Kortman[117], O. Kortner[112], S. Kortner[112], W. H. Kostecka[118], V. V. Kostyukhin[145], A. Kotsokechagia[37], A. Kotwal[52], A. Koulouris[37], A. Kourkoumeli-Charalampidi[74a,74b], C. Kourkoumelis[9], E. Kourlitis[112,ab], O. Kovanda[126], R. Kowalewski[168], W. Kozanecki[126], A. S. Kozhin[38], V. A. Kramarenko[38], G. Kramberger[95], P. Kramer[102], M. W. Krasny[130], A. Krasznahorkay[37], A. C. Kraus[118], J. W. Kraus[174], J. A. Kremer[49], T. Kresse[51], L. Kretschmann[174], J. Kretzschmar[94], K. Kreul[19], P. Krieger[158], M. Krivos[136], K. Krizka[21], K. Kroeninger[50], H. Kroha[112], J. Kroll[134], J. Kroll[131], K. S. Krowpman[109], U. Kruchonak[39], H. Krüger[25], N. Krumnack[82], M. C. Kruse[52], O. Kuchinskaia[38], S. Kuday[3a], S. Kuehn[37], R. Kuesters[55], T. Kuhl[49], V. Kukhtin[39], Y. Kulchitsky[38,a], S. Kuleshov[140b,140d], M. Kumar[34g], N. Kumari[49], P. Kumari[159b], A. Kupco[134], T. Kupfer[50], A. Kupich[38], O. Kuprash[55], H. Kurashige[86], L. L. Kurchaninov[159a], O. Kurdysh[67], Y. A. Kurochkin[38], A. Kurova[38], M. Kuze[141], A. K. Kvam[105], J. Kvita[125], T. Kwan[106], N. G. Kyriacou[108], L. A. O. Laatu[104], C. Lacasta[166], F. Lacava[76a,76b], H. Lacker[19], D. Lacour[130], N. N. Lad[98], E. Ladygin[39], A. Lafarge[41], B. Laforge[130], T. Lagouri[175], F. Z. Lahbabi[36a], S. Lai[56], J. E. Lambert[168], S. Lammers[69], W. Lampl[7], C. Lampoudis[156,d], G. Lamprinoudis[102], A. N. Lancaster[118], E. Lançon[30], U. Landgraf[55], M. P. J. Landon[96], V. S. Lang[55], O. K. B. Langrekken[128], A. J. Lankford[162], F. Lanni[37], K. Lantzsch[25], A. Lanza[74a], M. Lanzac Berrocal[166], J. F. Laporte[138], T. Lari[72a], F. Lasagni Manghi[24b], M. Lassnig[37], V. Latonova[134], A. Laurier[154], S. D. Lawlor[143], Z. Lawrence[103], R. Lazaridou[170], M. Lazzaroni[72a,72b], B. Le[103], H. D. M. Le[109], E. M. Le Boulicaut[175], L. T. Le Pottier[18a], B. Leban[24a,24b], A. Lebedev[82], M. LeBlanc[103], F. Ledroit-Guillon[61], S. C. Lee[152], S. Lee[48a,48b], T. F. Lee[94], L. L. Leeuw[34c], H. P. Lefebvre[97], M. Lefebvre[168], C. Leggett[18a], G. Lehmann Miotto[37], M. Leigh[57], W. A. Leight[105], W. Leinonen[116], A. Leisos[156,r], M. A. L. Leite[84c], C. E. Leitgeb[19], R. Leitner[136], K. J. C. Leney[45], T. Lenz[25], S. Leone[75a], C. Leonidopoulos[53], A. Leopold[148], R. Les[109], C. G. Lester[33], M. Levchenko[38], J. Levêque[4], L. J. Levinson[172], G. Levrini[24a,24b], M. P. Lewicki[88], C. Lewis[142], D. J. Lewis[4], L. Lewitt[143], A. Li[30], B. Li[63b], C. Li[63a], C.-Q. Li[112], H. Li[63a], H. Li[63b], H. Li[114a], H. Li[15], H. Li[63b], J. Li[63c], K. Li[14], L. Li[63c], M. Li[14,114c], S. Li[14,114c], S. Li[63c,63d], T. Li[5], X. Li[106], Z. Li[157], Z. Li[14,114c], Z. Li[63a], S. Liang[14,114c], Z. Liang[14], M. Liberatore[138], B. Liberti[77a], K. Lie[65c], J. Lieber Marin[84e], H. Lien[69], H. Lin[108], K. Lin[109], R. E. Lindley[7], J. H. Lindon[2], J. Ling[62], E. Lipeles[131], A. Lipniacka[17], A. Lister[167], J. D. Little[69], B. Liu[14], B. X. Liu[114b], D. Liu[63c,63d], E. H. L. Liu[21], J. B. Liu[63a], J. K. K. Liu[33], K. Liu[63d], K. Liu[63c,63d], M. Liu[63a], M. Y. Liu[63a], P. Liu[14], Q. Liu[63c,63d,142], X. Liu[63a], X. Liu[63b], Y. Liu[114b,114c], Y. L. Liu[63b], Y. W. Liu[63a], S. L. Lloyd[96], E. M. Lobodzinska[49], P. Loch[7], E. Lodhi[158], T. Lohse[19], K. Lohwasser[143], E. Loiacono[49], J. D. Lomas[21], J. D. Long[42], I. Longarini[162], R. Longo[165], I. Lopez Paz[68], A. Lopez Solis[49], N. A. Lopez-canelas[7], N. Lorenzo Martinez[4], A. M. Lory[111], M. Losada[119a], G. Löschcke Centeno[150], O. Loseva[38], X. Lou[48a,48b], X. Lou[14,114c], A. Lounis[67], P. A. Love[93], G. Lu[14,114c], M. Lu[67], S. Lu[131], Y. J. Lu[66], H. J. Lubatti[142], C. Luci[76a,76b], F. L. Lucio Alves[114a], F. Luehring[69], O. Lukianchuk[67], B. S. Lunday[131], O. Lundberg[148], B. Lund-Jensen[148,*], N. A. Luongo[6], M. S. Lutz[37], A. B. Lux[26], D. Lynn[30], R. Lysak[134], E. Lytken[100], V. Lyubushkin[39], T. Lyubushkina[39], M. M. Lyukova[149], M. Firdaus M. Soberi[53], H. Ma[30], K. Ma[63a], L. L. Ma[63b],

W. Ma[63a], Y. Ma[124], J. C. MacDonald[102], P. C. Machado De Abreu Farias[84e], R. Madar[41], T. Madula[98], J. Maeda[86], T. Maeno[30], H. Maguire[143], V. Maiboroda[138], A. Maio[133a,133b,133d], K. Maj[87a], O. Majersky[49], S. Majewski[126], N. Makovec[67], V. Maksimovic[16], B. Malaescu[130], Pa. Malecki[88], V. P. Maleev[38], F. Malek[61,m], M. Mali[95], D. Malito[97], U. Mallik[81,*], S. Maltezos[10], S. Malyukov[39], J. Mamuzic[13], G. Mancini[54], M. N. Mancini[27], G. Manco[74a,74b], J. P. Mandalia[96], S. S. Mandarry[150], I. Mandić[95], L. Manhaes de Andrade Filho[84a], I. M. Maniatis[172], J. Manjarres Ramos[91], D. C. Mankad[172], A. Mann[111], S. Manzoni[37], L. Mao[63c], X. Mapekula[34c], A. Marantis[156,r], G. Marchiori[5], M. Marcisovsky[134], C. Marcon[72a], E. Maricic[16], M. Marinescu[21], S. Marium[49], M. Marjanovic[123], A. Markhoos[55], M. Markovitch[67], E. J. Marshall[93], Z. Marshall[18a], S. Marti-Garcia[166], J. Martin[98], T. A. Martin[137], V. J. Martin[53], B. Martin dit Latour[17], L. Martinelli[76a,76b], M. Martinez[13,t], P. Martinez Agullo[166], V. I. Martinez Outschoorn[105], P. Martinez Suarez[13], S. Martin-Haugh[137], G. Martinovicova[136], V. S. Martoiu[28b], A. C. Martyniuk[98], A. Marzin[37], D. Mascione[79a,79b], L. Masetti[102], J. Masik[103], A. L. Maslennikov[38], S. L. Mason[42], P. Massarotti[73a,73b], P. Mastrandrea[75a,75b], A. Mastroberardino[44a,44b], T. Masubuchi[127], T. T. Mathew[126], T. Mathisen[164], J. Matousek[136], D. M. Mattern[50], J. Maurer[28b], T. Maurin[60], A. J. Maury[67], B. Maček[95], D. A. Maximov[38], A. E. May[103], R. Mazini[152], I. Maznas[118], M. Mazza[109], S. M. Mazza[139], E. Mazzeo[72a,72b], C. Mc Ginn[30], J. P. Mc Gowan[168], S. P. Mc Kee[108], C. A. Mc Lean[6], C. C. McCracken[167], E. F. McDonald[107], A. E. McDougall[117], J. A. Mcfayden[150], R. P. McGovern[131], R. P. Mckenzie[34g], T. C. Mclachlan[49], D. J. Mclaughlin[98], S. J. McMahon[137], C. M. Mcpartland[94], R. A. McPherson[168,x], S. Mehlhase[111], A. Mehta[94], D. Melini[166], B. R. Mellado Garcia[34g], A. H. Melo[56], F. Meloni[49], A. M. Mendes Jacques Da Costa[103], H. Y. Meng[158], L. Meng[93], S. Menke[112], M. Mentink[37], E. Meoni[44a,44b], G. Mercado[118], S. Merianos[156], C. Merlassino[70a,70c], L. Merola[73a,73b], C. Meroni[72a,72b], J. Metcalfe[6], A. S. Mete[6], E. Meuser[102], C. Meyer[69], J.-P. Meyer[138], R. P. Middleton[137], L. Mijović[53], G. Mikenberg[172], M. Mikestikova[134], M. Mikuž[95], H. Mildner[102], A. Milic[37], D. W. Miller[40], E. H. Miller[147], L. S. Miller[35], A. Milov[172], D. A. Milstead[48a,48b], T. Min[114a], A. A. Minaenko[38], I. A. Minashvili[153b], L. Mince[60], A. I. Mincer[120], B. Mindur[87a], M. Mineev[39], Y. Mino[89], L. M. Mir[13], M. Miralles Lopez[60], M. Mironova[18a], M. C. Missio[116], A. Mitra[170], V. A. Mitsou[166], Y. Mitsumori[113], O. Miu[158], P. S. Miyagawa[96], T. Mkrtchyan[64a], M. Mlinarevic[98], T. Mlinarevic[98], M. Mlynarikova[37], S. Mobius[20], P. Mogg[111], M. H. Mohamed Farook[115], A. F. Mohammed[14,114c], S. Mohapatra[42], G. Mokgatitswane[34g], L. Moleri[172], B. Mondal[145], S. Mondal[135], K. Mönig[49], E. Monnier[104], L. Monsonis Romero[166], J. Montejo Berlingen[13], A. Montella[48a,48b], M. Montella[122], F. Montereali[78a,78b], F. Monticelli[92], S. Monzani[70a,70c], A. Morancho Tarda[43], N. Morange[67], A. L. Moreira De Carvalho[49], M. Moreno Llácer[166], C. Moreno Martinez[57], J. M. Moreno Perez[23b], P. Morettini[58b], S. Morgenstern[37], M. Morii[62], M. Morinaga[157], M. Moritsu[90], F. Morodei[76a,76b], P. Moschovakos[37], B. Moser[129], M. Mosidze[153b], T. Moskalets[45], P. Moskvitina[116], J. Moss[32,j], P. Moszkowicz[87a], A. Moussa[36d], E. J. W. Moyse[105], O. Mtintsilana[34g], S. Muanza[104], J. Mueller[132], D. Muenstermann[93], R. Müller[37], G. A. Mullier[164], A. J. Mullin[33], J. J. Mullin[131], A. E. Mulski[62], D. P. Mungo[158], D. Munoz Perez[166], F. J. Munoz Sanchez[103], M. Murin[103], W. J. Murray[137,170], M. Muškinja[95], C. Mwewa[30], A. G. Myagkov[38,a], A. J. Myers[8], G. Myers[108], M. Myska[135], B. P. Nachman[18a], O. Nackenhorst[50], K. Nagai[129], K. Nagano[85], R. Nagasaka[157], J. L. Nagle[30,af], E. Nagy[104], A. M. Nairz[37], Y. Nakahama[85], K. Nakamura[85], K. Nakkalil[5], H. Nanjo[127], E. A. Narayanan[45], I. Naryshkin[38], L. Nasella[72a,72b], M. Naseri[35], S. Nasri[119b], C. Nass[25], G. Navarro[23a], J. Navarro-Gonzalez[166], R. Nayak[155], A. Nayaz[19], P. Y. Nechaeva[38], S. Nechaeva[24a,24b], F. Nechansky[134], L. Nedic[129], T. J. Neep[21], A. Negri[74a,74b], M. Negrini[24b], C. Nellist[117], C. Nelson[106], K. Nelson[108], S. Nemecek[134], M. Nessi[37,g], M. S. Neubauer[165], F. Neuhaus[102], J. Neundorf[49], J. Newell[94], P. R. Newman[21], C. W. Ng[132], Y. W. Y. Ng[49], B. Ngair[119a], H. D. N. Nguyen[110], R. B. Nickerson[129], R. Nicolaidou[138], J. Nielsen[139], M. Niemeyer[56], J. Niermann[56], N. Nikiforou[37], V. Nikolaenko[38,a], I. Nikolic-Audit[130], K. Nikolopoulos[21], P. Nilsson[30], I. Ninca[49], G. Ninio[155], A. Nisati[76a], N. Nishu[2], R. Nisius[112], N. Nitika[70a,70c], J.-E. Nitschke[51], E. K. Nkadimeng[34g], T. Nobe[157], T. Nommensen[151], M. B. Norfolk[143], B. J. Norman[35], M. Noury[36a], J. Novak[95], T. Novak[95], L. Novotny[135], R. Novotny[115], L. Nozka[125], K. Ntekas[162], N. M. J. Nunes De Moura Junior[84b], J. Ocariz[130], A. Ochi[86], I. Ochoa[133a], S. Oerdek[49,u], J. T. Offermann[40], A. Ogrodnik[136], A. Oh[103], C. C. Ohm[148], H. Oide[85], R. Oishi[157], M. L. Ojeda[37], Y. Okumura[157], L. F. Oleiro Seabra[133a], I. Oleksiyuk[57], S. A. Olivares Pino[140d], G. Oliveira Correa[13], D. Oliveira Damazio[30], J. L. Oliver[162], Ö. O. Öncel[55], A. P. O'Neill[20], A. Onofre[133a,133e], P. U. E. Onyisi[11], M. J. Oreglia[40], G. E. Orellana[92], D. Orestano[78a,78b],

N. Orlando[13], R. S. Orr[158], L. M. Osojnak[131], R. Ospanov[63a], Y. Osumi[113], G. Otero y Garzon[31], H. Otono[90], P. S. Ott[64a], G. J. Ottino[18a], M. Ouchrif[36d], F. Ould-Saada[128], T. Ovsiannikova[142], M. Owen[60], R. E. Owen[137], V. E. Ozcan[22a], F. Ozturk[88], N. Ozturk[8], S. Ozturk[83], H. A. Pacey[129], A. Pacheco Pages[13], C. Padilla Aranda[13], G. Padovano[76a,76b], S. Pagan Griso[18a], G. Palacino[69], A. Palazzo[71a,71b], J. Pampel[25], J. Pan[175], T. Pan[65a], D. K. Panchal[11], C. E. Pandini[117], J. G. Panduro Vazquez[137], H. D. Pandya[1], H. Pang[15], P. Pani[49], G. Panizzo[70a,70c], L. Panwar[130], L. Paolozzi[57], S. Parajuli[165], A. Paramonov[6], C. Paraskevopoulos[54], D. Paredes Hernandez[65b], A. Pareti[74a,74b], K. R. Park[42], T. H. Park[158], M. A. Parker[33], F. Parodi[58a,58b], E. W. Parrish[118], V. A. Parrish[53], J. A. Parsons[42], U. Parzefall[55], B. Pascual Dias[110], L. Pascual Dominguez[101], E. Pasqualucci[76a], S. Passaggio[58b], F. Pastore[97], P. Patel[88], U. M. Patel[52], J. R. Pater[103], T. Pauly[37], F. Pauwels[136], C. I. Pazos[161], M. Pedersen[128], R. Pedro[133a], S. V. Peleganchuk[38], O. Penc[37], E. A. Pender[53], S. Peng[15], G. D. Penn[175], K. E. Penski[111], M. Penzin[38], B. S. Peralva[84d], A. P. Pereira Peixoto[142], L. Pereira Sanchez[147], D. V. Perepelitsa[30,af], G. Perera[105], E. Perez Codina[159a], M. Perganti[10], H. Pernegger[37], S. Perrella[76a,76b], O. Perrin[41], K. Peters[49], R. F. Y. Peters[103], B. A. Petersen[37], T. C. Petersen[43], E. Petit[104], V. Petousis[135], C. Petridou[156,d], T. Petru[136], A. Petrukhin[145], M. Pettee[18a], A. Petukhov[38], K. Petukhova[37], R. Pezoa[140f], L. Pezzotti[37], G. Pezzullo[175], A. J. Pfleger[37], T. M. Pham[173], T. Pham[107], P. W. Phillips[137], G. Piacquadio[149], E. Pianori[18a], F. Piazza[126], R. Piegaia[31], D. Pietreanu[28b], A. D. Pilkington[103], M. Pinamonti[70a,70c], J. L. Pinfold[2], B. C. Pinheiro Pereira[133a], J. Pinol Bel[13], A. E. Pinto Pinoargote[138], L. Pintucci[70a,70c], K. M. Piper[150], A. Pirttikoski[57], D. A. Pizzi[35], L. Pizzimento[65b], A. Pizzini[117], M.-A. Pleier[30], V. Pleskot[136], E. Plotnikova[39], G. Poddar[96], R. Poettgen[100], L. Poggioli[130], I. Pokharel[56], S. Polacek[136], G. Polesello[74a], A. Poley[146,159a], A. Polini[24b], C. S. Pollard[170], Z. B. Pollock[122], E. Pompa Pacchi[76a,76b], N. I. Pond[98], D. Ponomarenko[69], L. Pontecorvo[37], S. Popa[28a], G. A. Popeneciu[28d], A. Poreba[37], D. M. Portillo Quintero[159a], S. Pospisil[135], M. A. Postill[143], P. Postolache[28c], K. Potamianos[170], P. A. Potepa[87a], I. N. Potrap[39], C. J. Potter[33], H. Potti[151], J. Poveda[166], M. E. Pozo Astigarraga[37], A. Prades Ibanez[77a,77b], J. Pretel[168], D. Price[103], M. Primavera[71a], L. Primomo[70a,70c], M. A. Principe Martin[101], R. Privara[125], T. Procter[60], M. L. Proffitt[142], N. Proklova[131], K. Prokofiev[65c], G. Proto[112], J. Proudfoot[6], M. Przybycien[87a], W. W. Przygoda[87b], A. Psallidas[47], J. E. Puddefoot[143], D. Pudzha[55], D. Pyatiizbyantseva[38], J. Qian[108], R. Qian[109], D. Qichen[103], Y. Qin[13], T. Qiu[53], A. Quadt[56], M. Queitsch-Maitland[103], G. Quetant[57], R. P. Quinn[167], G. Rabanal Bolanos[62], D. Rafanoharana[55], F. Raffaeli[77a,77b], F. Ragusa[72a,72b], J. L. Rainbolt[40], J. A. Raine[57], S. Rajagopalan[30], E. Ramakoti[38], L. Rambelli[58a,58b], I. A. Ramirez-Berend[35], K. Ran[49,114c], D. S. Rankin[131], N. P. Rapheeha[34g], H. Rasheed[28b], V. Raskina[130], D. F. Rassloff[64a], A. Rastogi[18a], S. Rave[102], S. Ravera[58a,58b], B. Ravina[56], I. Ravinovich[172], M. Raymond[37], A. L. Read[128], N. P. Readioff[143], D. M. Rebuzzi[74a,74b], G. Redlinger[30], A. S. Reed[112], K. Reeves[27], J. A. Reidelsturz[174], D. Reikher[126], A. Rej[50], C. Rembser[37], M. Renda[28b], F. Renner[49], A. G. Rennie[162], A. L. Rescia[49], S. Resconi[72a], M. Ressegotti[58a,58b], S. Rettie[37], J. G. Reyes Rivera[109], E. Reynolds[18a], O. L. Rezanova[38], P. Reznicek[136], H. Riani[36d], N. Ribaric[52], E. Ricci[79a,79b], R. Richter[112], S. Richter[48a,48b], E. Richter-Was[87b], M. Ridel[130], S. Ridouani[36d], P. Rieck[120], P. Riedler[37], E. M. Riefel[48a,48b], J. O. Rieger[117], M. Rijssenbeek[149], M. Rimoldi[37], L. Rinaldi[24a,24b], P. Rincke[56,164], T. T. Rinn[30], M. P. Rinnagel[111], G. Ripellino[164], I. Riu[13], J. C. Rivera Vergara[168], F. Rizatdinova[124], E. Rizvi[96], B. R. Roberts[18a], S. S. Roberts[139], S. H. Robertson[106,x], D. Robinson[33], M. Robles Manzano[102], A. Robson[60], A. Rocchi[77a,77b], C. Roda[75a,75b], S. Rodriguez Bosca[37], Y. Rodriguez Garcia[23a], A. Rodriguez Rodriguez[55], A. M. Rodríguez Vera[118], S. Roe[37], J. T. Roemer[37], A. R. Roepe-Gier[139], O. Røhne[128], R. A. Rojas[105], C. P. A. Roland[130], J. Roloff[30], A. Romaniouk[80], E. Romano[74a,74b], M. Romano[24b], A. C. Romero Hernandez[165], N. Rompotis[94], L. Roos[130], S. Rosati[76a], B. J. Rosser[40], E. Rossi[129], E. Rossi[73a,73b], L. P. Rossi[62], L. Rossini[55], R. Rosten[122], M. Rotaru[28b], B. Rottler[55], C. Rougier[91], D. Rousseau[67], D. Rousso[49], A. Roy[165], S. Roy-Garand[158], A. Rozanov[104], Z. M. A. Rozario[60], Y. Rozen[154], A. Rubio Jimenez[166], A. J. Ruby[94], V. H. Ruelas Rivera[19], T. A. Ruggeri[1], A. Ruggiero[129], A. Ruiz-Martinez[166], A. Rummler[37], Z. Rurikova[55], N. A. Rusakovich[39], H. L. Russell[168], G. Russo[76a,76b], J. P. Rutherfoord[7], S. Rutherford Colmenares[33], M. Rybar[136], E. B. Rye[128], A. Ryzhov[45], J. A. Sabater Iglesias[57], H. F.-W. Sadrozinski[139], F. Safai Tehrani[76a], B. Safarzadeh Samani[137], S. Saha[1], M. Sahinsoy[83], A. Saibel[166], M. Saimpert[138], M. Saito[157], T. Saito[157], A. Sala[72a,72b], D. Salamani[37], A. Salnikov[147], J. Salt[166], A. Salvador Salas[155], D. Salvatore[44a,44b], F. Salvatore[150], A. Salzburger[37], D. Sammel[55], E. Sampson[93], D. Sampsonidis[156,d], D. Sampsonidou[126], J. Sánchez[166], V. Sanchez Sebastian[166], H. Sandaker[128], C. O. Sander[49], J. A. Sandesara[105], M. Sandhoff[174], C. Sandoval[23b],

L. Sanfilippo[64a], D. P. C. Sankey[137], T. Sano[89], A. Sansoni[54], L. Santi[37,76b], C. Santoni[41], H. Santos[133a,133b], A. Santra[172], E. Sanzani[24a,24b], K. A. Saoucha[163], J. G. Saraiva[133a,133d], J. Sardain[7], O. Sasaki[85], K. Sato[160], C. Sauer[64b], E. Sauvan[4], P. Savard[158,ad], R. Sawada[157], C. Sawyer[137], L. Sawyer[99], C. Sbarra[24b], A. Sbrizzi[24a,24b], T. Scanlon[98], J. Schaarschmidt[142], U. Schäfer[102], A. C. Schaffer[45,67], D. Schaile[111], R. D. Schamberger[149], C. Scharf[19], M. M. Schefer[20], V. A. Schegelsky[38], D. Scheirich[136], M. Schernau[162], C. Scheulen[56], C. Schiavi[58a,58b], M. Schioppa[44a,44b], B. Schlag[147], S. Schlenker[37], J. Schmeing[174], M. A. Schmidt[174], K. Schmieden[102], C. Schmitt[102], N. Schmitt[102], S. Schmitt[49], L. Schoeffel[138], A. Schoening[64b], P. G. Scholer[35], E. Schopf[129], M. Schott[25], J. Schovancova[37], S. Schramm[57], T. Schroer[57], H.-C. Schultz-Coulon[64a], M. Schumacher[55], B. A. Schumm[139], Ph. Schune[138], A. J. Schuy[142], H. R. Schwartz[139], A. Schwartzman[147], T. A. Schwarz[108], Ph. Schwemling[138], R. Schwienhorst[109], F. G. Sciacca[20], A. Sciandra[30], G. Sciolla[27], F. Scuri[75a], C. D. Sebastiani[94], K. Sedlaczek[118], S. C. Seidel[115], A. Seiden[139], B. D. Seidlitz[42], C. Seitz[49], J. M. Seixas[84b], G. Sekhniaidze[73a], L. Selem[61], N. Semprini-Cesari[24a,24b], D. Sengupta[57], V. Senthilkumar[166], L. Serin[67], M. Sessa[77a,77b], H. Severini[123], F. Sforza[58a,58b], A. Sfyrla[57], Q. Sha[14], E. Shabalina[56], A. H. Shah[33], R. Shaheen[148], J. D. Shahinian[131], D. Shaked Renous[172], L. Y. Shan[14], M. Shapiro[18a], A. Sharma[37], A. S. Sharma[167], P. Sharma[81], P. B. Shatalov[38], K. Shaw[150], S. M. Shaw[103], Q. Shen[63c], D. J. Sheppard[146], P. Sherwood[98], L. Shi[98], X. Shi[14], S. Shimizu[85], C. O. Shimmin[175], J. D. Shinner[97], I. P. J. Shipsey[129,*], S. Shirabe[90], M. Shiyakova[39,v], M. J. Shochet[40], D. R. Shope[128], B. Shrestha[123], S. Shrestha[122,ag], I. Shreyber[38], M. J. Shroff[168], P. Sicho[134], A. M. Sickles[165], E. Sideras Haddad[34g], A. C. Sidley[117], A. Sidoti[24b], F. Siegert[51], Dj. Sijacki[16], F. Sili[92], J. M. Silva[53], I. Silva Ferreira[84b], M. V. Silva Oliveira[30], S. B. Silverstein[48a], S. Simion[67], R. Simoniello[37], E. L. Simpson[103], H. Simpson[150], L. R. Simpson[108], S. Simsek[83], S. Sindhu[56], P. Sinervo[158], S. Singh[30], S. Sinha[49], S. Sinha[103], M. Sioli[24a,24b], I. Siral[37], E. Sitnikova[49], J. Sjölin[48a,48b], A. Skaf[56], E. Skorda[21], P. Skubic[123], M. Slawinska[88], V. Smakhtin[172], B. H. Smart[137], S.Yu. Smirnov[38], Y. Smirnov[38], L. N. Smirnova[38,a], O. Smirnova[100], A. C. Smith[42], D. R. Smith[162], E. A. Smith[40], J. L. Smith[103], R. Smith[147], M. Smizanska[93], K. Smolek[135], A. A. Snesarev[38], H. L. Snoek[117], S. Snyder[30], R. Sobie[168,x], A. Soffer[155], C. A. Solans Sanchez[37], E.Yu. Soldatov[38], U. Soldevila[166], A. A. Solodkov[38], S. Solomon[27], A. Soloshenko[39], K. Solovieva[55], O. V. Solovyanov[41], P. Sommer[51], A. Sonay[13], W. Y. Song[159b], A. Sopczak[135], A. L. Sopio[53], F. Sopkova[29b], J. D. Sorenson[115], I. R. Sotarriva Alvarez[141], V. Sothilingam[64a], O. J. Soto Sandoval[140b,140c], S. Sottocornola[69], R. Soualah[163], Z. Soumaimi[36e], D. South[49], N. Soybelman[172], S. Spagnolo[71a,71b], M. Spalla[112], D. Sperlich[55], G. Spigo[37], B. Spisso[73a,73b], D. P. Spiteri[60], M. Spousta[136], E. J. Staats[35], R. Stamen[64a], A. Stampekis[21], E. Stanecka[88], W. Stanek-Maslouska[49], M. V. Stange[51], B. Stanislaus[18a], M. M. Stanitzki[49], B. Stapf[49], E. A. Starchenko[38], G. H. Stark[139], J. Stark[91], P. Staroba[134], P. Starovoitov[64a], S. Stärz[106], R. Staszewski[88], G. Stavropoulos[47], A. Stefl[37], P. Steinberg[30], B. Stelzer[146,159a], H. J. Stelzer[132], O. Stelzer-Chilton[159a], H. Stenzel[59], T. J. Stevenson[150], G. A. Stewart[37], J. R. Stewart[124], M. C. Stockton[37], G. Stoicea[28b], M. Stolarski[133a], S. Stonjek[112], A. Straessner[51], J. Strandberg[148], S. Strandberg[48a,48b], M. Stratmann[174], M. Strauss[123], T. Strebler[104], P. Strizenec[29b], R. Ströhmer[169], D. M. Strom[126], R. Stroynowski[45], A. Strubig[48a,48b], S. A. Stucci[30], B. Stugu[17], J. Stupak[123], N. A. Styles[49], D. Su[147], S. Su[63a], W. Su[63d], X. Su[63a], D. Suchy[29a], K. Sugizaki[157], V. V. Sulin[38], M. J. Sullivan[94], D. M. S. Sultan[129], L. Sultanaliyeva[38], S. Sultansoy[3b], T. Sumida[89], S. Sun[173], O. Sunneborn Gudnadottir[164], N. Sur[104], M. R. Sutton[150], H. Suzuki[160], M. Svatos[134], M. Swiatlowski[159a], T. Swirski[169], I. Sykora[29a], M. Sykora[136], T. Sykora[136], D. Ta[102], K. Tackmann[49,u], A. Taffard[162], R. Tafirout[159a], J. S. Tafoya Vargas[67], Y. Takubo[85], M. Talby[104], A. A. Talyshev[38], K. C. Tam[65b], N. M. Tamir[155], A. Tanaka[157], J. Tanaka[157], R. Tanaka[67], M. Tanasini[149], Z. Tao[167], S. Tapia Araya[140f], S. Tapprogge[102], A. Tarek Abouelfadl Mohamed[109], S. Tarem[154], K. Tariq[14], G. Tarna[28b], G. F. Tartarelli[72a], M. J. Tartarin[91], P. Tas[136], M. Tasevsky[134], E. Tassi[44a,44b], A. C. Tate[165], G. Tateno[157], Y. Tayalati[36e,w], G. N. Taylor[107], W. Taylor[159b], R. Teixeira De Lima[147], P. Teixeira-Dias[97], J. J. Teoh[158], K. Terashi[157], J. Terron[101], S. Terzo[13], M. Testa[54], R. J. Teuscher[158,x], A. Thaler[80], O. Theiner[57], T. Theveneaux-Pelzer[104], O. Thielmann[174], D. W. Thomas[97], J. P. Thomas[21], E. A. Thompson[18a], P. D. Thompson[21], E. Thomson[131], R. E. Thornberry[45], C. Tian[63a], Y. Tian[57], V. Tikhomirov[38,a], Yu.A. Tikhonov[38], S. Timoshenko[38], D. Timoshyn[136], E. X. L. Ting[1], P. Tipton[175], A. Tishelman-Charny[30], S. H. Tlou[34g], K. Todome[141], S. Todorova-Nova[136], S. Todt[51], L. Toffolin[70a,70c], M. Togawa[85], J. Tojo[90], S. Tokár[29a], K. Tokushuku[85], O. Toldaiev[69], M. Tomoto[85,113], L. Tompkins[147,l], K. W. Topolnicki[87b], E. Torrence[126], H. Torres[91], E. Torró Pastor[166], M. Toscani[31],

C. Tosciri[40], M. Tost[11], D. R. Tovey[143], I. S. Trandafir[28b], T. Trefzger[169], A. Tricoli[30], I. M. Trigger[159a], S. Trincaz-Duvoid[130], D. A. Trischuk[27], B. Trocmé[61], A. Tropina[39], L. Truong[34c], M. Trzebinski[88], A. Trzupek[88], F. Tsai[149], M. Tsai[108], A. Tsiamis[156], P. V. Tsiareshka[38], S. Tsigaridas[159a], A. Tsirigotis[156,r], V. Tsiskaridze[158], E. G. Tskhadadze[153a], M. Tsopoulou[156], Y. Tsujikawa[89], I. I. Tsukerman[38], V. Tsulaia[18a], S. Tsuno[85], K. Tsuri[121], D. Tsybychev[149], Y. Tu[65b], A. Tudorache[28b], V. Tudorache[28b], A. N. Tuna[62], S. Turchikhin[58a,58b], I. Turk Cakir[3a], R. Turra[72a], T. Turtuvshin[39], P. M. Tuts[42], S. Tzamarias[156,d], E. Tzovara[102], F. Ukegawa[160], P. A. Ulloa Poblete[140b,140c], E. N. Umaka[30], G. Unal[37], A. Undrus[30], G. Unel[162], J. Urban[29b], P. Urrejola[140a], G. Usai[8], R. Ushioda[141], M. Usman[110], F. Ustuner[53], Z. Uysal[83], V. Vacek[135], B. Vachon[106], T. Vafeiadis[37], A. Vaitkus[98], C. Valderanis[111], E. Valdes Santurio[48a,48b], M. Valente[159a], S. Valentinetti[24a,24b], A. Valero[166], E. Valiente Moreno[166], A. Vallier[91], J. A. Valls Ferrer[166], D. R. Van Arneman[117], T. R. Van Daalen[142], A. Van Der Graaf[50], P. Van Gemmeren[6], M. Van Rijnbach[37], S. Van Stroud[98], I. Van Vulpen[117], P. Vana[136], M. Vanadia[77a,77b], U. M. Vande Voorde[148], W. Vandelli[37], E. R. Vandewall[124], D. Vannicola[155], L. Vannoli[54], R. Vari[76a], E. W. Varnes[7], C. Varni[18b], T. Varol[152], D. Varouchas[67], L. Varriale[166], K. E. Varvell[151], M. E. Vasile[28b], L. Vaslin[85], G. A. Vasquez[168], A. Vasyukov[39], L. M. Vaughan[124], R. Vavricka[102], T. Vazquez Schroeder[37], J. Veatch[32], V. Vecchio[103], M. J. Veen[105], I. Veliscek[30], L. M. Veloce[158], F. Veloso[133a,133c], S. Veneziano[76a], A. Ventura[71a,71b], S. Ventura Gonzalez[138], A. Verbytskyi[112], M. Verducci[75a,75b], C. Vergis[96], M. Verissimo De Araujo[84b], W. Verkerke[117], J. C. Vermeulen[117], C. Vernieri[147], M. Vessella[105], M. C. Vetterli[146,ad], A. Vgenopoulos[102], N. Viaux Maira[140f], T. Vickey[143], O. E. Vickey Boeriu[143], G. H. A. Viehhauser[129], L. Vigani[64b], M. Vigl[112], M. Villa[24a,24b], M. Villaplana Perez[166], E. M. Villhauer[53], E. Vilucchi[54], M. G. Vincter[35], A. Visibile[117], C. Vittori[37], I. Vivarelli[24a,24b], E. Voevodina[112], F. Vogel[111], J. C. Voigt[51], P. Vokac[135], Yu. Volkotrub[87b], E. Von Toerne[25], B. Vormwald[37], V. Vorobel[136], K. Vorobev[38], M. Vos[166], K. Voss[145], M. Vozak[117], L. Vozdecky[123], N. Vranjes[16], M. Vranjes Milosavljevic[16], M. Vreeswijk[117], N. K. Vu[63c,63d], R. Vuillermet[37], O. Vujinovic[102], I. Vukotic[40], I. K. Vyas[35], S. Wada[160], C. Wagner[147], J. M. Wagner[18a], W. Wagner[174], S. Wahdan[174], H. Wahlberg[92], C. H. Waits[123], J. Walder[137], R. Walker[111], W. Walkowiak[145], A. Wall[131], E. J. Wallin[100], T. Wamorkar[6], A. Z. Wang[139], C. Wang[102], C. Wang[11], H. Wang[18a], J. Wang[65c], P. Wang[98], R. Wang[62], R. Wang[6], S. M. Wang[152], S. Wang[63b], S. Wang[14], T. Wang[63a], W. T. Wang[81], W. Wang[14], X. Wang[114a], X. Wang[165], X. Wang[63c], Y. Wang[63d], Y. Wang[114a], Y. Wang[63a], Z. Wang[108], Z. Wang[52,63c,63d], Z. Wang[108], A. Warburton[106], R. J. Ward[21], N. Warrack[60], S. Waterhouse[97], A. T. Watson[21], H. Watson[53], M. F. Watson[21], E. Watton[60,137], G. Watts[142], B. M. Waugh[98], J. M. Webb[55], C. Weber[30], H. A. Weber[19], M. S. Weber[20], S. M. Weber[64a], C. Wei[63a], Y. Wei[55], A. R. Weidberg[129], E. J. Weik[120], J. Weingarten[50], C. Weiser[55], C. J. Wells[49], T. Wenaus[30], B. Wendland[50], T. Wengler[37], N. S. Wenke[112], N. Wermes[25], M. Wessels[64a], A. M. Wharton[93], A. S. White[62], A. White[8], M. J. White[1], D. Whiteson[162], L. Wickremasinghe[127], W. Wiedenmann[173], M. Wielers[137], C. Wiglesworth[43], D. J. Wilbern[123], H. G. Wilkens[37], J. J. H. Wilkinson[33], D. M. Williams[42], H. H. Williams[131], S. Williams[33], S. Willocq[105], B. J. Wilson[103], P. J. Windischhofer[40], F. I. Winkel[31], F. Winklmeier[126], B. T. Winter[55], J. K. Winter[103], M. Wittgen[147], M. Wobisch[99], T. Wojtkowski[61], Z. Wolffs[117], J. Wollrath[162], M. W. Wolter[88], H. Wolters[133a,133c], M. C. Wong[139], E. L. Woodward[42], S. D. Worm[49], B. K. Wosiek[88], K. W. Woźniak[88], S. Wozniewski[56], K. Wraight[60], C. Wu[21], M. Wu[114b], M. Wu[116], S. L. Wu[173], X. Wu[57], Y. Wu[63a], Z. Wu[4], J. Wuerzinger[112,ab], T. R. Wyatt[103], B. M. Wynne[53], S. Xella[43], L. Xia[114a], M. Xia[15], M. Xie[63a], S. Xin[14,114c], A. Xiong[126], J. Xiong[18a], D. Xu[14], H. Xu[63a], L. Xu[63a], R. Xu[131], T. Xu[108], Y. Xu[15], Z. Xu[53], Z. Xu[114a], B. Yabsley[151], S. Yacoob[34a], Y. Yamaguchi[85], E. Yamashita[157], H. Yamauchi[160], T. Yamazaki[18a], Y. Yamazaki[86], S. Yan[60], Z. Yan[105], H. J. Yang[63c,63d], H. T. Yang[63a], S. Yang[63a], T. Yang[65c], X. Yang[37], X. Yang[14], Y. Yang[45], Y. Yang[63a], Z. Yang[63a], W.-M. Yao[18a], H. Ye[114a], H. Ye[56], J. Ye[14], S. Ye[30], X. Ye[63a], Y. Yeh[98], I. Yeletskikh[39], B. Yeo[18b], M. R. Yexley[98], T. P. Yildirim[129], P. Yin[42], K. Yorita[171], S. Younas[28b], C. J. S. Young[37], C. Young[147], C. Yu[14,114c], Y. Yu[63a], J. Yuan[14,114c], M. Yuan[108], R. Yuan[63c,63d], L. Yue[98], M. Zaazoua[63a], B. Zabinski[88], E. Zaid[53], Z. K. Zak[88], T. Zakareishvili[166], S. Zambito[57], J. A. Zamora Saa[140b,140d], J. Zang[157], D. Zanzi[55], O. Zaplatilek[135], C. Zeitnitz[174], H. Zeng[14], J. C. Zeng[165], D. T. Zenger Jr[27], O. Zenin[38], T. Ženiš[29a], S. Zenz[96], S. Zerradi[36a], D. Zerwas[67], M. Zhai[14,114c], D. F. Zhang[143], J. Zhang[63b], J. Zhang[6], K. Zhang[14,114c], L. Zhang[63a], L. Zhang[114a], P. Zhang[14,114c], R. Zhang[173], S. Zhang[108], S. Zhang[91], T. Zhang[157], X. Zhang[63c], X. Zhang[63b], Y. Zhang[142], Y. Zhang[98], Y. Zhang[114a], Z. Zhang[18a], Z. Zhang[63b], Z. Zhang[67], H. Zhao[142], T. Zhao[63b], Y. Zhao[139], Z. Zhao[63a], Z. Zhao[63a], A. Zhemchugov[39], J. Zheng[114a],

K. Zheng[165], X. Zheng[63a], Z. Zheng[147], D. Zhong[165], B. Zhou[108], H. Zhou[7], N. Zhou[63c], Y. Zhou[15], Y. Zhou[114a], Y. Zhou[7], C. G. Zhu[63b], J. Zhu[108], X. Zhu[63d], Y. Zhu[63c], Y. Zhu[63a], X. Zhuang[14], K. Zhukov[69], N. I. Zimine[39], J. Zinsser[64b], M. Ziolkowski[145], L. Živković[16], A. Zoccoli[24a,24b], K. Zoch[62], T. G. Zorbas[143], O. Zormpa[47], W. Zou[42], L. Zwalinski[37]

[1] Department of Physics, University of Adelaide, Adelaide, Australia
[2] Department of Physics, University of Alberta, Edmonton, AB, Canada
[3] [(a)]Department of Physics, Ankara University, Ankara, Türkiye; [(b)]Division of Physics, TOBB University of Economics and Technology, Ankara, Türkiye
[4] LAPP, CNRS/IN2P3, Université Savoie Mont Blanc, Annecy, France
[5] APC, CNRS/IN2P3, Université Paris Cité, Paris, France
[6] High Energy Physics Division, Argonne National Laboratory, Argonne, IL, USA
[7] Department of Physics, University of Arizona, Tucson, AZ, USA
[8] Department of Physics, University of Texas at Arlington, Arlington, TX, USA
[9] Physics Department, National and Kapodistrian University of Athens, Athens, Greece
[10] Physics Department, National Technical University of Athens, Zografou, Greece
[11] Department of Physics, University of Texas at Austin, Austin, TX, USA
[12] Institute of Physics, Azerbaijan Academy of Sciences, Baku, Azerbaijan
[13] Institut de Física d'Altes Energies (IFAE), Barcelona Institute of Science and Technology, Barcelona, Spain
[14] Institute of High Energy Physics, Chinese Academy of Sciences, Beijing, China
[15] Physics Department, Tsinghua University, Beijing, China
[16] Institute of Physics, University of Belgrade, Belgrade, Serbia
[17] Department for Physics and Technology, University of Bergen, Bergen, Norway
[18] [(a)]Physics Division, Lawrence Berkeley National Laboratory, Berkeley, CA, USA; [(b)]University of California, Berkeley, CA, USA
[19] Institut für Physik, Humboldt Universität zu Berlin, Berlin, Germany
[20] Albert Einstein Center for Fundamental Physics and Laboratory for High Energy Physics, University of Bern, Bern, Switzerland
[21] School of Physics and Astronomy, University of Birmingham, Birmingham, UK
[22] [(a)]Department of Physics, Bogazici University, Istanbul, Türkiye; [(b)]Department of Physics Engineering, Gaziantep University, Gaziantep, Türkiye; [(c)]Department of Physics, Istanbul University, Istanbul, Türkiye
[23] [(a)]Facultad de Ciencias y Centro de Investigaciónes, Universidad Antonio Nariño, Bogotá, Colombia; [(b)]Departamento de Física, Universidad Nacional de Colombia, Bogotá, Colombia
[24] [(a)]Dipartimento di Fisica e Astronomia A. Righi, Università di Bologna, Bologna, Italy; [(b)]INFN Sezione di Bologna, Bologna, Italy
[25] Physikalisches Institut, Universität Bonn, Bonn, Germany
[26] Department of Physics, Boston University, Boston, MA, USA
[27] Department of Physics, Brandeis University, Waltham, MA, USA
[28] [(a)]Transilvania University of Brasov, Brasov, Romania; [(b)]Horia Hulubei National Institute of Physics and Nuclear Engineering, Bucharest, Romania; [(c)]Department of Physics, Alexandru Ioan Cuza University of Iasi, Iasi, Romania; [(d)]National Institute for Research and Development of Isotopic and Molecular Technologies, Physics Department, Cluj-Napoca, Romania; [(e)]National University of Science and Technology Politechnica, Bucharest, Romania; [(f)]West University in Timisoara, Timisoara, Romania; [(g)]Faculty of Physics, University of Bucharest, Bucharest, Romania
[29] [(a)]Faculty of Mathematics, Physics and Informatics, Comenius University, Bratislava, Slovakia; [(b)]Department of Subnuclear Physics, Institute of Experimental Physics of the Slovak Academy of Sciences, Kosice, Slovak Republic
[30] Physics Department, Brookhaven National Laboratory, Upton, NY, USA
[31] Universidad de Buenos Aires, Facultad de Ciencias Exactas y Naturales, Departamento de Física, y CONICET, Instituto de Física de Buenos Aires (IFIBA), Buenos Aires, Argentina
[32] California State University, Los Angeles, CA, USA
[33] Cavendish Laboratory, University of Cambridge, Cambridge, UK
[34] [(a)]Department of Physics, University of Cape Town, Cape Town, South Africa; [(b)]iThemba Labs, Western Cape, South Africa; [(c)]Department of Mechanical Engineering Science, University of Johannesburg, Johannesburg,

South Africa; [d]National Institute of Physics, University of the Philippines Diliman (Philippines), Quezon City, Philippines; [e]University of South Africa, Department of Physics, Pretoria, South Africa; [f]University of Zululand, KwaDlangezwa, South Africa; [g]School of Physics, University of the Witwatersrand, Johannesburg, South Africa
[35] Department of Physics, Carleton University, Ottawa, ON, Canada
[36] [a]Faculté des Sciences Ain Chock, Université Hassan II de Casablanca, Casablanca, Morocco; [b]Faculté des Sciences, Université Ibn-Tofail, Kenitra, Morocco; [c]Faculté des Sciences Semlalia, LPHEA-Marrakech, Université Cadi Ayyad, Marrakech, Morocco; [d]LPMR, Faculté des Sciences, Université Mohamed Premier, Oujda, Morocco; [e]Faculté des sciences, Université Mohammed V, Rabat, Morocco; [f]Institute of Applied Physics, Mohammed VI Polytechnic University, Ben Guerir, Morocco
[37] CERN, Geneva, Switzerland
[38] Affiliated with an Institute Covered by a Cooperation Agreement with CERN, Geneva, Switzerland
[39] Affiliated with an International Laboratory Covered by a Cooperation Agreement with CERN, Geneva, Switzerland
[40] Enrico Fermi Institute, University of Chicago, Chicago, IL, USA
[41] LPC, CNRS/IN2P3, Université Clermont Auvergne, Clermont-Ferrand, France
[42] Nevis Laboratory, Columbia University, Irvington, NY, USA
[43] Niels Bohr Institute, University of Copenhagen, Copenhagen, Denmark
[44] [a]Dipartimento di Fisica, Università della Calabria, Rende, Italy; [b]INFN Gruppo Collegato di Cosenza, Laboratori Nazionali di Frascati, Cosenza, Italy
[45] Physics Department, Southern Methodist University, Dallas, TX, USA
[46] Physics Department, University of Texas at Dallas, Richardson, TX, USA
[47] National Centre for Scientific Research "Demokritos", Agia Paraskevi, Greece
[48] [a]Department of Physics, Stockholm University, Stockholm, Sweden; [b]Oskar Klein Centre, Stockholm, Sweden
[49] Deutsches Elektronen-Synchrotron DESY, Hamburg and Zeuthen, Germany
[50] Fakultät Physik , Technische Universität Dortmund, Dortmund, Germany
[51] Institut für Kern- und Teilchenphysik, Technische Universität Dresden, Dresden, Germany
[52] Department of Physics, Duke University, Durham, NC, USA
[53] SUPA-School of Physics and Astronomy, University of Edinburgh, Edinburgh, UK
[54] INFN e Laboratori Nazionali di Frascati, Frascati, Italy
[55] Physikalisches Institut, Albert-Ludwigs-Universität Freiburg, Freiburg, Germany
[56] II. Physikalisches Institut, Georg-August-Universität Göttingen, Göttingen, Germany
[57] Département de Physique Nucléaire et Corpusculaire, Université de Genève, Geneva, Switzerland
[58] [a]Dipartimento di Fisica, Università di Genova, Genoa, Italy; [b]INFN Sezione di Genova, Genoa, Italy
[59] II. Physikalisches Institut, Justus-Liebig-Universität Giessen, Giessen, Germany
[60] SUPA-School of Physics and Astronomy, University of Glasgow, Glasgow, UK
[61] LPSC, Université Grenoble Alpes, CNRS/IN2P3, Grenoble INP, Grenoble, France
[62] Laboratory for Particle Physics and Cosmology, Harvard University, Cambridge, MA, USA
[63] [a]Department of Modern Physics and State Key Laboratory of Particle Detection and Electronics, University of Science and Technology of China, Hefei, China; [b]Institute of Frontier and Interdisciplinary Science and Key Laboratory of Particle Physics and Particle Irradiation (MOE), Shandong University, Qingdao, China; [c]School of Physics and Astronomy, Key Laboratory for Particle Astrophysics and Cosmology (MOE), Shanghai Jiao Tong University, SKLPPC, Shanghai, China; [d]Tsung-Dao Lee Institute, Shanghai, China; [e]School of Physics, Zhengzhou University, Zhengzhou, China
[64] [a]Kirchhoff-Institut für Physik, Ruprecht-Karls-Universität Heidelberg, Heidelberg, Germany; [b]Physikalisches Institut, Ruprecht-Karls-Universität Heidelberg, Heidelberg, Germany
[65] [a]Department of Physics, Chinese University of Hong Kong, Shatin, N.T., Hong Kong, China; [b]Department of Physics, University of Hong Kong, Pok Fu Lam, Hong Kong, China; [c]Department of Physics and Institute for Advanced Study, Hong Kong University of Science and Technology, Clear Water Bay, Kowloon, Hong Kong, China
[66] Department of Physics, National Tsing Hua University, Hsinchu, Taiwan
[67] IJCLab, CNRS/IN2P3, Université Paris-Saclay, 91405 Orsay, France
[68] Centro Nacional de Microelectrónica (IMB-CNM-CSIC), Barcelona, Spain
[69] Department of Physics, Indiana University, Bloomington, IN, USA
[70] [a]INFN Gruppo Collegato di Udine, Sezione di Trieste, Udine, Italy; [b]ICTP, Trieste, Italy; [c]Dipartimento Politecnico di Ingegneria e Architettura, Università di Udine, Udine, Italy

[71] [(a)]INFN Sezione di Lecce, Lecce, Italy; [(b)]Dipartimento di Matematica e Fisica, Università del Salento, Lecce, Italy
[72] [(a)]INFN Sezione di Milano, Milan, Italy; [(b)]Dipartimento di Fisica, Università di Milano, Milan, Italy
[73] [(a)]INFN Sezione di Napoli, Naples, Italy; [(b)]Dipartimento di Fisica, Università di Napoli, Naples, Italy
[74] [(a)]INFN Sezione di Pavia, Pavia, Italy; [(b)]Dipartimento di Fisica, Università di Pavia, Pavia, Italy
[75] [(a)]INFN Sezione di Pisa, Pisa, Italy; [(b)]Dipartimento di Fisica E. Fermi, Università di Pisa, Pisa, Italy
[76] [(a)]INFN Sezione di Roma, Rome, Italy; [(b)]Dipartimento di Fisica, Sapienza Università di Roma, Rome, Italy
[77] [(a)]INFN Sezione di Roma Tor Vergata, Rome, Italy; [(b)]Dipartimento di Fisica, Università di Roma Tor Vergata, Rome, Italy
[78] [(a)]INFN Sezione di Roma Tre, Rome, Italy; [(b)]Dipartimento di Matematica e Fisica, Università Roma Tre, Rome, Italy
[79] [(a)]INFN-TIFPA, Povo, Italy; [(b)]Università degli Studi di Trento, Trento, Italy
[80] Universität Innsbruck, Department of Astro and Particle Physics, Innsbruck, Austria
[81] University of Iowa, Iowa City, IA, USA
[82] Department of Physics and Astronomy, Iowa State University, Ames, IA, USA
[83] Istinye University, Sariyer, Istanbul, Türkiye
[84] [(a)]Departamento de Engenharia Elétrica, Universidade Federal de Juiz de Fora (UFJF), Juiz de Fora, Brazil; [(b)]Universidade Federal do Rio De Janeiro COPPE/EE/IF, Rio de Janeiro, Brazil; [(c)]Instituto de Física, Universidade de São Paulo, São Paulo, Brazil; [(d)]Rio de Janeiro State University, Rio de Janeiro, Brazil; [(e)]Federal University of Bahia, Bahia, Brazil
[85] KEK, High Energy Accelerator Research Organization, Tsukuba, Japan
[86] Graduate School of Science, Kobe University, Kobe, Japan
[87] [(a)]AGH University of Krakow, Faculty of Physics and Applied Computer Science, Kraków, Poland; [(b)]Marian Smoluchowski Institute of Physics, Jagiellonian University, Kraków, Poland
[88] Institute of Nuclear Physics Polish Academy of Sciences, Kraków, Poland
[89] Faculty of Science, Kyoto University, Kyoto, Japan
[90] Research Center for Advanced Particle Physics and Department of Physics, Kyushu University, Fukuoka , Japan
[91] L2IT, CNRS/IN2P3, UPS, Université de Toulouse, Toulouse, France
[92] Instituto de Física La Plata, Universidad Nacional de La Plata and CONICET, La Plata, Argentina
[93] Physics Department, Lancaster University, Lancaster, UK
[94] Oliver Lodge Laboratory, University of Liverpool, Liverpool, UK
[95] Department of Experimental Particle Physics, Jožef Stefan Institute and Department of Physics, University of Ljubljana, Ljubljana, Slovenia
[96] School of Physics and Astronomy, Queen Mary University of London, London, UK
[97] Department of Physics, Royal Holloway University of London, Egham, UK
[98] Department of Physics and Astronomy, University College London, London, UK
[99] Louisiana Tech University, Ruston, LA, USA
[100] Fysiska institutionen, Lunds universitet, Lund, Sweden
[101] Departamento de Física Teorica C-15 and CIAFF, Universidad Autónoma de Madrid, Madrid, Spain
[102] Institut für Physik, Universität Mainz, Mainz, Germany
[103] School of Physics and Astronomy, University of Manchester, Manchester, UK
[104] CPPM, CNRS/IN2P3, Aix-Marseille Université, Marseille, France
[105] Department of Physics, University of Massachusetts, Amherst, MA, USA
[106] Department of Physics, McGill University, Montreal, QC, Canada
[107] School of Physics, University of Melbourne, Victoria, Australia
[108] Department of Physics, University of Michigan, Ann Arbor, MI, USA
[109] Department of Physics and Astronomy, Michigan State University, East Lansing, MI, USA
[110] Group of Particle Physics, University of Montreal, Montreal, QC, Canada
[111] Fakultät für Physik, Ludwig-Maximilians-Universität München, Munich, Germany
[112] Max-Planck-Institut für Physik (Werner-Heisenberg-Institut), Munich, Germany
[113] Graduate School of Science and Kobayashi-Maskawa Institute, Nagoya University, Nagoya, Japan
[114] [(a)]Department of Physics, Nanjing University, Nanjing, China; [(b)]School of Science, Shenzhen Campus of Sun Yat-sen University, Guangzhou, China; [(c)]University of Chinese Academy of Science (UCAS), Beijing, China
[115] Department of Physics and Astronomy, University of New Mexico, Albuquerque, NM, USA
[116] Institute for Mathematics, Astrophysics and Particle Physics, Radboud University/Nikhef, Nijmegen, Netherlands

[117] Nikhef National Institute for Subatomic Physics and University of Amsterdam, Amsterdam, Netherlands
[118] Department of Physics, Northern Illinois University, DeKalb, IL, USA
[119] [(a)]New York University Abu Dhabi, Abu Dhabi, United Arab Emirates; [(b)]United Arab Emirates University, Al Ain, United Arab Emirates
[120] Department of Physics, New York University, New York, NY, USA
[121] Ochanomizu University, Otsuka, Bunkyo-ku, Tokyo, Japan
[122] Ohio State University, Columbus, OH, USA
[123] Homer L. Dodge Department of Physics and Astronomy, University of Oklahoma, Norman, OK, USA
[124] Department of Physics, Oklahoma State University, Stillwater, OK, USA
[125] Joint Laboratory of Optics, Palacký University, Olomouc, Czech Republic
[126] Institute for Fundamental Science, University of Oregon, Eugene, OR, USA
[127] Graduate School of Science, Osaka University, Osaka, Japan
[128] Department of Physics, University of Oslo, Oslo, Norway
[129] Department of Physics, Oxford University, Oxford, UK
[130] LPNHE, CNRS/IN2P3, Sorbonne Université, Université Paris Cité, Paris, France
[131] Department of Physics, University of Pennsylvania, Philadelphia, PA, USA
[132] Department of Physics and Astronomy, University of Pittsburgh, Pittsburgh, PA, USA
[133] [(a)]Laboratório de Instrumentação e Física Experimental de Partículas-LIP, Lisbon, Portugal; [(b)]Departamento de Física, Faculdade de Ciências, Universidade de Lisboa, Lisbon, Portugal; [(c)]Departamento de Física, Universidade de Coimbra, Coimbra, Portugal; [(d)]Centro de Física Nuclear da Universidade de Lisboa, Lisbon, Portugal; [(e)]Departamento de Física, Universidade do Minho, Braga, Portugal; [(f)]Departamento de Física Teórica y del Cosmos, Universidad de Granada, Granada, Spain; [(g)]Departamento de Física, Instituto Superior Técnico, Universidade de Lisboa, Lisbon, Portugal
[134] Institute of Physics of the Czech Academy of Sciences, Prague, Czech Republic
[135] Czech Technical University in Prague, Prague, Czech Republic
[136] Charles University, Faculty of Mathematics and Physics, Prague, Czech Republic
[137] Particle Physics Department, Rutherford Appleton Laboratory, Didcot, UK
[138] IRFU, CEA, Université Paris-Saclay, Gif-sur-Yvette, France
[139] Santa Cruz Institute for Particle Physics, University of California Santa Cruz, Santa Cruz, CA, USA
[140] [(a)]Departamento de Física, Pontificia Universidad Católica de Chile, Santiago, Chile; [(b)]Millennium Institute for Subatomic physics at high energy frontier (SAPHIR), Santiago, Chile; [(c)]Instituto de Investigación Multidisciplinario en Ciencia y Tecnología y Departamento de Física, Universidad de La Serena, La Serena, Chile; [(d)]Department of Physics, Universidad Andres Bello, Santiago, Chile; [(e)]Instituto de Alta Investigación, Universidad de Tarapacá, Arica, Chile; [(f)]Departamento de Física, Universidad Técnica Federico Santa María, Valparaiso, Chile
[141] Department of Physics, Institute of Science, Tokyo, Japan
[142] Department of Physics, University of Washington, Seattle, WA, USA
[143] Department of Physics and Astronomy, University of Sheffield, Sheffield, UK
[144] Department of Physics, Shinshu University, Nagano, Japan
[145] Department Physik, Universität Siegen, Siegen, Germany
[146] Department of Physics, Simon Fraser University, Burnaby, BC, Canada
[147] SLAC National Accelerator Laboratory, Stanford, CA, USA
[148] Department of Physics, Royal Institute of Technology, Stockholm, Sweden
[149] Departments of Physics and Astronomy, Stony Brook University, Stony Brook, NY, USA
[150] Department of Physics and Astronomy, University of Sussex, Brighton, UK
[151] School of Physics, University of Sydney, Sydney, Australia
[152] Institute of Physics, Academia Sinica, Taipei, Taiwan
[153] [(a)]E. Andronikashvili Institute of Physics, Iv. Javakhishvili Tbilisi State University, Tbilisi, Georgia; [(b)]High Energy Physics Institute, Tbilisi State University, Tbilisi, Georgia; [(c)]University of Georgia, Tbilisi, Georgia
[154] Department of Physics, Technion, Israel Institute of Technology, Haifa, Israel
[155] Raymond and Beverly Sackler School of Physics and Astronomy, Tel Aviv University, Tel Aviv, Israel
[156] Department of Physics, Aristotle University of Thessaloniki, Thessaloníki, Greece
[157] International Center for Elementary Particle Physics and Department of Physics, University of Tokyo, Tokyo, Japan
[158] Department of Physics, University of Toronto, Toronto, ON, Canada
[159] [(a)]TRIUMF, Vancouver, BC, Canada; [(b)]Department of Physics and Astronomy, York University, Toronto, ON, Canada

[160] Division of Physics and Tomonaga Center for the History of the Universe, Faculty of Pure and Applied Sciences, University of Tsukuba, Tsukuba, Japan
[161] Department of Physics and Astronomy, Tufts University, Medford, MA, USA
[162] Department of Physics and Astronomy, University of California Irvine, Irvine, CA, USA
[163] University of Sharjah, Sharjah, United Arab Emirates
[164] Department of Physics and Astronomy, University of Uppsala, Uppsala, Sweden
[165] Department of Physics, University of Illinois, Urbana, IL, USA
[166] Instituto de Física Corpuscular (IFIC), Centro Mixto Universidad de Valencia-CSIC, Valencia, Spain
[167] Department of Physics, University of British Columbia, Vancouver, BC, Canada
[168] Department of Physics and Astronomy, University of Victoria, Victoria, BC, Canada
[169] Fakultät für Physik und Astronomie, Julius-Maximilians-Universität Würzburg, Würzburg, Germany
[170] Department of Physics, University of Warwick, Coventry, UK
[171] Waseda University, Tokyo, Japan
[172] Department of Particle Physics and Astrophysics, Weizmann Institute of Science, Rehovot, Israel
[173] Department of Physics, University of Wisconsin, Madison, WI, USA
[174] Fakultät für Mathematik und Naturwissenschaften, Fachgruppe Physik, Bergische Universität Wuppertal, Wuppertal, Germany
[175] Department of Physics, Yale University, New Haven, CT, USA
[176] Yerevan Physics Institute, Yerevan, Armenia

[a] Also Affiliated with an Institute Covered by a Cooperation Agreement with CERN, Geneva, Switzerland
[b] Also at An-Najah National University, Nablus, Palestine
[c] Also at Borough of Manhattan Community College, City University of New York, New York, NY, USA
[d] Also at Center for Interdisciplinary Research and Innovation (CIRI-AUTH), Thessaloníki, Greece
[e] Also at CERN, Geneva, Switzerland
[f] Also at CMD-AC UNEC Research Center, Azerbaijan State University of Economics (UNEC), Baku, Azerbaijan
[g] Also at Département de Physique Nucléaire et Corpusculaire, Université de Genève, Geneva, Switzerland
[h] Also at Departament de Fisica de la Universitat Autonoma de Barcelona, Barcelona, Spain
[i] Also at Department of Financial and Management Engineering, University of the Aegean, Chios, Greece
[j] Also at Department of Physics, California State University, Sacramento, USA
[k] Also at Department of Physics, King's College London, London, UK
[l] Also at Department of Physics, Stanford University, Stanford, CA, USA
[m] Also at Department of Physics, Stellenbosch University, Stellenbosch, South Africa
[n] Also at Department of Physics, University of Fribourg, Fribourg, Switzerland
[o] Also at Department of Physics, University of Thessaly, Thessaly, Greece
[p] Also at Department of Physics, Westmont College, Santa Barbara, USA
[q] Also at Faculty of Physics, Sofia University, 'St. Kliment Ohridski', Sofia, Bulgaria
[r] Also at Hellenic Open University, Patras, Greece
[s] Also at Imam Mohammad Ibn Saud Islamic University, Riyadh, Saudi Arabia
[t] Also at Institucio Catalana de Recerca i Estudis Avancats, ICREA, Barcelona, Spain
[u] Also at Institut für Experimentalphysik, Universität Hamburg, Hamburg, Germany
[v] Also at Institute for Nuclear Research and Nuclear Energy (INRNE) of the Bulgarian Academy of Sciences, Sofia, Bulgaria
[w] Also at Institute of Applied Physics, Mohammed VI Polytechnic University, Ben Guerir, Morocco
[x] Also at Institute of Particle Physics (IPP), Ottawa, Canada
[y] Also at Institute of Physics, Azerbaijan Academy of Sciences, Baku, Azerbaijan
[z] Also at Institute of Theoretical Physics, Ilia State University, Tbilisi, Georgia
[aa] Also at National Institute of Physics, University of the Philippines Diliman (Philippines), Quezon City, Philippines
[ab] Also at Technical University of Munich, Munich, Germany
[ac] Also at The Collaborative Innovation Center of Quantum Matter (CICQM), Beijing, China
[ad] Also at TRIUMF, Vancouver, BC, Canada
[ae] Also at Università di Napoli Parthenope, Naples, Italy
[af] Also at Department of Physics, University of Colorado Boulder, Colorado, USA

[ag] Also at Washington College, Chestertown, MD, USA
[ah] Also at Physics Department, Yeditepe University, Istanbul, Türkiye
* Deceased